FINAL REPORT

for Grant No. NB82 NADA 3008

DYNAMIC RESPONSE OF COMPLIANT STRUCTURES

to

Center for Building Technology
National Bureau of Standards

by

John W. Leonard, Professor
Department of Civil Engineering
Oregon State University
Corvallis, Oregon 97331

May 23, 1984

FINAL REPORT

for Grant No. NB82 NADA 3008

DYNAMIC RESPONSE OF COMPLIANT STRUCTURES

to

Center for Building Technology
National Bureau of Standards

by

John W. Leonard, Professor
Department of Civil Engineering
Oregon State University
Corvallis, Oregon 97331

May 23, 1984

Introduction

Work has been completed on the development of methods to predict the behavior of compliant structures in deep water. The responses of such structures as a whole interacting with dynamic loads due to waves and currents were studied. The following tasks related to analyses in both the frequency and time domains of compliant platforms were addressed:

1) evaluation of existing procedures for predicting dynamic response
2) evaluation of applicability of structural identification techniques of compliant structures
3) review of effects of added mass and fluid damping on compliant structures
4) evaluation of effects of large displacements and deformation

In the following sections, results of each task are summarized. These results were obtained by the principal and associate investigators (J. Leonard and R. Hudspeth) in collaboration with two graduate students (R. Young and B. Kruchoski) in Ocean Engineering, of whom only R. Young was directly supported by the grant.

Task 1 Results

Existing procedures for predicting the dynamic response of compliant platforms were evaluated. There is extensive background on techniques for use in the frequency domain. Unfortunately, compliant platforms exhibit significant nonlinearities and solutions in the time domain are needed for analysis of extreme loads. Of that class of methods, the implicit methods are recommended. Such a method was used by R. Young in his M. S. thesis, "Coupled Analyses of Compliant Offshore Platforms," a copy of which is attached as Appendix A.

In Young's work a three-dimensional, large-deflection finite element program was developed which is capable of simulating the static and dynamic behavior of large compliant ocean structures. The structures are assumed to be in the Morison regime and to be composed of cable and beam-column elements. No vortex shedding, diffraction effects, nor material nonlinearities are considered. Linear wave theory is used and multidirectional irregular seas may be simulated by a series of regular waves. Current may be included as an arbitrary current profile varying in magnitude and direction with depth. Concentrated masses and loads as well as foundation properties may also be modeled.

The iterative Newmark method was shown to provide good solutions in the time domain to nonlinear dynamic problems even at time steps and convergence tolerances which are large compared to those often suggested in the literature. The solution algorithm was shown to give reasonable results for hydrodynamic solutions. However, although these results are similar to published results, there is enough disparity to warrant investigation of the performance of this and other algorithms compared to experimental results.

The starting procedure of assuming zero initial velocity and acceleration was shown to be an acceptable method for problems in which the steady state dynamic response is sought. In fact, it is actually a superior method for those problems in which some of the response periods of the structure are much smaller than the selected time step of the numerical integration. When an initial acceleration vector is calculated for the system, the system responds as it would respond to an impact load. If this response has high accelerations at a period shorter than the time step, the inertial loads overpower the other loads in the system and convergence is hampered. When a solution is started from zero velocity and acceleration, the net effect of the constant average acceleration scheme of Newmark is to apply the load as a ramp function over one time step. For the higher frequencies, the loading appears as a static load and the large structural accelerations at high frequencies are not present. The convergence of the iterative solution is smoother and more rapid in this case.

The tension leg structure problem demonstrated that the algorithms developed in this work are capable of handling tension-leg structures and that the solution is stable over a long time history.

In general, the algorithms selected and used in Young's work perform in a manner which is satisfactory for their intended function. The techniques require a considerable amount of computer time to obtain solutions compared to the computer time usually required by linear analyses. As the nonlinearities increase in strength, the computer time for similar problems increases greatly but there is no apparent degradation in the accuracy of the results for the test problems considered.

Task 2 Results

Structural identification techniques were examined for applicability to compliant structures in deep waters. The proper design of many land-based and sea-based structural systems requires the ability to accurately predict their response to dynamic disturbances. These disturbances may originate from such sources as earthquake ground motions, fluctuating wind loads, vibrating machinery, or wave-induced hydrodynamic effects. Oftentimes a (mathematical) computer model of the structure is generated and is used to predict the response to a variety of expected load conditions. For certain complex or critical structures, scale models or prototypes are constructed and subjected to tests. Results from these tests can be used to provide data for validating the computer model, which can then be used for evaluating and refining the preliminary design.

Presented in a Ph. D. dissertation by B. Kruchoski (in press) are statistically-based estimation techniques which make use of structural test data for purposes of improving dynamic finite element models. Techniques are developed to identify optimum values of the parameters of finite element models describing land-based and sea-based structures. The parameters to be identified are those which constitute the elements of the structural mass, damping, and stiffness matrices. Included in the study are the effects of element mass, area and moment of inertia; the effects of lumped mass and stiffness; and the effects of hydrodymamic loading on the mass and damping characteristics of the structure.

Techniques for parameter identification are investigated which use test data for either free vibrations or for forced response in the time domain. Data from free vibration tests can be combinations of natural frequencies and mode shapes. Data from forced response tests can be combinations of selected displacements, velocities and accelerations.

Sensitivity matrices relating the change in structural response to changes in the structural parameters are presented for the free vibration problem, and are derived for the forced vibration problem assuming kinematic relationships in the form of the Wilson-Theta equations. A weighting matrix, constructed from the sensitivity matrices and relating the change in the structural parameters to the error between test data and predicted response, is presented for each of three estimation theories: Least Squares, Weighted Least Squares, and Bayes.

Numerical examples are included to demonstrate the validity and capabilities of the identification procedures presented. It was found that the values of the parameters being identified converge rapidly, resulting in good agreement between specified and predicted response. For structures experiencing hydrodynamic loads described by Morison's equation, it was found that relative velocity effects and uncertainties in drag and mass coefficient values may be accounted for by modifying the structural mass and damping matrices.

Task 3 Results

The effects of added mass and fluid damping on compliant platforms were studied. Pressure forces on ocean structures result from the interaction of the structure with the weakly nonlinear and slightly non-Gaussian surface water waves. For fixed space frame structures with structural members that are small compared to the dimensions of the incident wave length, the Morison equation is used to provide a static-equivalent wave force loading. For fixed, but compliant, space-frame structures, a wave-structure interaction type of Morison equation has been developed that employs the relative motion between the compliant structure and the water particles in the oscillatory wave field. The Morison equation method assumes that the effect of the structure on the wave field is negligible and that no waves may be observed radiating away from the structure despite the motions that result from the wave-structure interaction.

In the analysis of compliant platforms the tethering elements (guys or tension legs) can be considered to be in the Morison regime. In many analysis techniques, the hydrodynamic behavior of the tethering elements is decoupled from that of the platform: the tethers are first treated as massless, loadless springs when the platform motions are determined and then as hydrodynamically loaded segments with prescribed end motions. Young showed that this can be over-conservative. Results of the guyed tower test problems showed that for the examples presented, the use of static spring models of the guys, the quasistatic cables, leads to an overprediction of the tower motion and also of the guy

tensions. There is also a large difference in the time phase of the cable tensions and in the form of the tension versus time plots.

For fixed structures, such as gravity platforms in the North Sea, which have characteristic member dimensions that are no longer negligible compared to the incident wave length, the Morison equation assumption that the structure has no observable effect on the incident wave field is no longer valid. A linear diffraction theory has been developed to account for the additional pressure field that is developed around a large structure due to the no longer negligible wave-structure interaction. Because this theory is a linear approximation, it is not capable of including in a rigorous manner the nonlinear drag force effects which dominate the wave force loading when the ratio of pile diameter/wave length becomes small.

For the case of a large floating body, such as a TLP, the wave-induced motion of the structure creates an additional reaction force of the water on the structure. The present method of analyzing this interaction is to linearly decompose the wave-induced pressure forces on the structure into two components: a diffraction force on a fixed structure that is termed an exciting force; and a reaction force on an oscillating structure in otherwise still water that is termed a restoring force. A computationally efficient algorithm was developed in the course of this study for TLP's with large buoyant members and small Morison members. A copy of a paper by Hudspeth and Leonard is attached as Appendix B.

In that study it is assumed that smaller diameter circular cylinders connect vertical buoyant leg s. Because of the vertical axes

of symmetry in the vertical legs and because there are no larger horizontal buoyant members between these vertical members, a computationally efficient numerical algorithm was developed which incorporated an eigenfunction expansion for the Green's function for axisymmetric bodies of revolution and a linearized hydroelastic Morison equation for the hydrodynamic pressure forces on the small member cross bracing. A sample calculation and comparison with experimental results were included.

Task 4 Results

The effect of large displacements on the behavior of compliant platforms was studied. In Young's work, the use of updated Lagrangian coordinates and a residual feedback solution scheme was shown to be a valid technique for solving the geometrically nonlinear problem. Static test problems indicate that the scheme yields excellent results. Furthermore, these results were obtained with liberal convergence tolerances and large element discretizations.

It was confirmed that the viscous relaxation method is an excellent method to start the static solution of hardening nonlinear problems with little or no initial stiffness in one or more degrees of freedom. It was demonstrated that the method is particularly efficient when used on articulated structures which use buoyancy for stability. More iterations are required when the method is used on cable problems and on problems using both cables and beams, but the technique is still superior to dynamic relaxation for the examples considered.

The selection of the coefficients used in the relaxation process depends largely upon the experience of the analyst. However, some observations can be made to determine if the selected coefficients are adequate and if they can be improved. If insufficient initial stiffness is added to the nodes, the model of the structure remains unstable. If the decrement factor is too small, a similar situation will occur during subsequent iteration. Conversely, if the decrement factor is large and the initial stiffness is large, the convergence plot will appear like the dynamic free response of an overdamped system subject to a step load and

the solution will converge monotonically to the proper values. An optimum solution appears like the dynamic free response of an underdamped system and exhibits some overshoot, but a heavily damped solution resulting from large initial artificial stiffness and a large decrement factor will permit a solution to be obtained only at the expense of additional iteration cycles.

Publication of Results

As a result of this study, four papers have been submitted for publication:

"Identification of Structural and Hydrodynamic Parameters for Free and Forced Vibrations," B. L. Kruchoski and J. W. Leonard, to appear in Proceedings of OSDS '84, Oregon State University, Corvallis, September 1984.

"Dynamic Wave-Platform-Restraint Interaction for Tension Leg Platforms," J. W. Leonard and R. T. Hudspeth, Proceedings, OSDS '82, Oregon State University, Corvallis, September 1982.

"Dynamic Response of Tension Leg Platforms with Axisymmetric Members," R. T. Hudspeth and J. W. Leonard, in review by Engineering Structures.

"Coupled Response of Compliant Offshore Platforms," J. W. Leonard and R. Young, in review by Engineering Structures.

APPENDIX A

COUPLED RESPONSE OF COMPLIANT OFFSHORE PLATFORMS

by

Raymond A. Young

A THESIS

submitted to

Oregon State University

in partial fulfillment of
the requirements for the
degree of

Master of Science

Completed October 6, 1983

Commencement June 1984

ACKNOWLEDGEMENTS

This investigation was funded by the National Bureau of Standards and by the Minerals Management Service through Grant No. NB82NADA3008. I wish to thank both the National Bureau of Standards and the Minerals Management Service for their financial support without which this work would not have been possible. Computer funds were supplied by the Oregon State University Computer Center, and their support is also gratefully acknowledged. I also wish to thank Dr. John Leonard, my major professor, for his guidance and invaluable suggestions in my hours of need and throughout the course of this work.

Many of the details of the analysis were developed after long, often animated, discussions with my fellow graduate students and I am indebted to them for their assistance. I would especially like to thank those members of the graveyard computer shift: soon to be Dr. Brian Kruchoski, Dr. Min-Chih Huang, Dr. Hang Tuah, and Mike Zimmerman. Who else would be willing to discuss engineering problems in the middle of the night?

Finally, I would like to thank all the members of the Chicago Bridge and Iron Company Marine Research Group, 1973-1979, who instilled my initial interest, and especially William A. Tam, former Director of Marine Research, who showed me the unity of the engineering disciplines and the real value of being more than another specialist. Guys, we were good at our craft.

TABLE OF CONTENTS

		Page
1.0	INTRODUCTION	1
1.1	Compliant Tower Concept	2
1.2	Review of Compliant Tower Concepts and Previous Research	5
1.2.1	Articulated Towers	8
1.2.2	Guyed Towers	10
1.2.3	Tension Leg Platforms	12
1.2.4	Floating Production Facilities	14
1.2.5	Comparison	14
1.3	Objectives of the Work	16
1.4	Scope of the Work	19
2.0	BASIC CONCEPTS AND ASSUMPTIONS	21
2.1	Structure	21
2.1.1	Beam-Column Element	21
2.1.2	Cable Element	24
2.1.3	Foundation Element	25
2.2	Loads	26
2.2.1	Gravity	26
2.2.2	Buoyancy	26
2.2.3	Wave Loads	27
2.2.4	Current Loads without Waves	29
2.2.5	Combined Wave and Current Loads	30
2.2.6	Concentrated Loads and Masses	35
2.3	Equations of Motion	35
3.0	FINITE ELEMENT FORMULATION	37
3.1	Static Solution Techniques	39
3.2	Dynamic Solution Techniques	44
3.3	General Derivation of Element Stiffness and Mass Matrices	49

TABLE OF CONTENTS (Continued)

		Page
3.4	Beam-Column Element	55
3.5	Cable Element	74
3.6	Foundation Element	79
3.7	Load Discretization	81
4.0	VALIDATION PROBLEMS AND RESULTS	89
4.1	Problem 1: Static Point Load on a Cantilever Beam	90
4.2	Problem 2: Lumped Mass Pendulum	92
4.3	Problem 3: Point Load on a Taut String	94
4.4	Problem 4: Point Mass on a Taut String	96
4.5	Problem 5: Steady Current on an Articulated Tower	98
4.6	Problem 6: Steady Tow of a Cable with Spherical Weight	100
4.7	Problem 7: Articulated Tower in Waves	102
4.8	Problem 8: Two Dimensional Guyed Tower in Waves	109
4.9	Problem 9: Tension Leg Structure in Waves	112
5.0	SUMMARY AND RECOMMENDATIONS	119
	REFERENCES	125

LIST OF FIGURES

Figure		Page
1.1-1	Dynamic behavior of platforms	4
1.1-2	Sea spectrum diagrams	6
2.0-1	General definition sketch	22
2.2-1	Definition sketch for waves and current	32
3.4-1	Definition sketch for beam-column element	59
3.4-2	Two dimensional large-deflection rotation schematic	66
3.4-3	Three dimensional large-deflection rotation schematic	67
3.5-1	Definition sketch for the cable element	75
3.6-1	Foundation element schematic	80
3.7-1	Fixed-end forces due to distributed load	84
3.7-2	Hydrodynamic load and fixed end force discretization	86
4.1-1	Cantilever beam with concentrated transverse tip load	91
4.2-1	Free oscillation of a simple pendulum with concentrated mass	93
4.3-1	Point load on a taut string	95
4.4-1	Point mass on a taut string	97
4.5-1	Elevation of articulated tower	99
4.5-2	Viscous relaxation solution performance for an articulated tower	101
4.6-1	Steady tow of a cable with a spherical end mass	103
4.7-1	Motion of an articulated tower in waves only	105

NOTATION

Latin Symbols

A	Cross-sectional Area
a_i	Constants in Newmark Integration Method
B_{ij}	Strain-Displacement Relation
C_{ij}	Damping Matrix
C_a	Added Mass Coefficient
C_D	Drag Coefficient
C_I	Inertia Coefficient
c	Wave Phase Velocity
d	Water Depth
D	Cylinder Diameter or Drag Width or Dynamic Magnification Factor
D_{ij}	Stress-Strain Relation
E	Elastic Modulus
F_i	Nodal Loads
g	Acceleration of Gravity
K_c	Keulegan Carpenter Number
K_{ij}	Stiffness Matrix
k	Wave Number
M_{ij}	Mass Matrix
N_{ij}	Element Shape Function Matrix
P_i^I	Non-nodal Inertia Force
q_i	Structure Displacement Vector
R_i	Internal Nodal Load Vector
R_e	Reynolds Number

NOTATION (Continued)

T	Period of Harmonic Oscillation, Cable Tension
t	Time
u_i	Water Particle Displacement Due to Waves
v_i	Water Particle Displacement Due to Current
w_i	Distributed Non-nodal Load Intensity
x_i	Cartesian Coordinates ($i = 1,2,3$)

Greek Symbols

α	Angle Between Wave and Current Directions Newmark Integration Parameter
β	Frequency Ratio. Rigid Body Rotation Angle. Viscous Relaxation Damping Factor
Δ	Small Change Operator
δ	Virtual Operator
ε	Strain
ζ	Newmark Integration Parameter
Θ	Azimuth for Wave or Current
μ	Viscous Relaxation Decrement Factor
ν	Poissons Ratio, Kinematic Viscosity
π	3.1415 .....
ξ_j	Element Displacement Between Nodes
ρ	Mass Density of Water
ρ_{ij}	Mass Density Matrix
σ	Stress
ϕ	Wave Potential Function
ω	Harmonic Frequency

Superscripts

Left lower case:	Time of the configuration in which the quantity occurs
Right lower case:	Iteration number
Right upper case:	Subspecies identifiers (e.g. F^I is the nodal force, F, due to inertia, superscript I)

Subscripts

Right lower case:	i, j, k, l and numeric
	Indices of a vector or matrix
	All others are subspecies identifiers (e.g. ω_n is natural frequency)

COUPLED RESPONSE OF COMPLIANT OFFSHORE PLATFORMS

1.0 Introduction

As long as there is a demand for petroleum products and by-products, there will be a need to exploit the world's undersea petroleum and natural gas deposits. In April of 1982 some 22 percent of the world oil production was pumped from wellheads surrounded by water (Ellers, 1982). As known reserves from wells located on dry land are depleted, this percentage will increase necessitating production from wells in ever increasing water depths and steadily more severe environments.

The economic production of petroleum in deep water requires innovative structures which often test the limits of existing design technology. The compliant production platforms are a large class of deepwater structures which have challenged designers for years. The combination of structural intricacy and load complexity which must be dealt with often obscures a rational design approach. Since they are compliant, these structures must be designed dynamically. Also, since they are exposed to loads which vary in a nonlinear way and are themselves mechanisms which behave in a nonlinear manner, their analysis is highly complex. Simplified design methods are required by practical considerations, but the method of simplification and its range of validity may not be entirely lucid. In this study a finite element model is developed which is capable of dealing with nonlinear dynamic problems of

compliant platforms. This model can be used to test the limits of validity of some of the commonly made design simplifications.

1.1 Compliant Tower Concept

As water depths approach 300 meters, fixed offshore structures which rely upon bending and shear to transmit loads to the seafloor become inefficient forms. The large overturning moments of these structures when they are subjected to wave action require massive foundations and the increased natural periods of the properly designed structures approach the range of wave periods which contains significant energy. To safely build such structures in increasing depths requires enormous designs and, as a result, enormous costs.

To make drilling and production economically feasible in deep water, designers have developed several different structural concepts which rely upon compliance to reduce loading transmitted to the anchorage and which use anchorages different from the cantilever beam-column concept of the traditional fixed structure.

A compliant ocean structure is one which moves laterally significant distances when subject to wave and wind loadings. It relies upon its dynamic softness to reduce maximum transmitted anchorage loads, unlike the fixed structure where structural velocities and accelerations are small and the time varying wind and wave loads may be treated as a time series of static problems, the compliant structure has significant kinematics and the role of structural mass, added mass, and damping must be considered. This

is best illustrated by Figure 1.1-1 (after Nair and Duval, 1982) which is a plot of the dynamic amplification factor versus frequency ratio for a single degree of freedom spring-mass-damper system. The dynamic amplification factor, D, is the ratio of maximum dynamic deflection of a system to the static deflection under a static load of identical amplitude. The frequency ratio, β, is the ratio of the frequency of the dynamic load to the natural frequency of oscillation of the system. A rigid structure is designed so that its natural periods yield low β ratios so that its response may be treated as static. A compliant structure is designed so that the reduced motion as high values of β is obtained.

As water depth increases, the frequency ratio β for a fixed ocean structure is shifted toward significant dynamic mangnification. Region I of Figure 1.1-1 represents shallow water fixed structures while Region II represents deep water fixed structures. As water depth increases past the 450 meter depth, the dynamic magnification of practical forms of a fixed structure may be found in Region III, where dynamic loads are extreme. Compliant structures lie in Region IV, a region of attenuated dynamic response. A tremendous design advantage is gained in this region, but the penalty is that the design must now be a dynamic one.

In the ocean the loading frequency range due to waves is large, ranging from capillary wave frequencies of as much as 100 Hz to tidal and transtidal waves with frequencies of the order of 10^{-5} to 10^{-6} Hz. (SPM, 1977). Fortunately, only a narrow band of wave

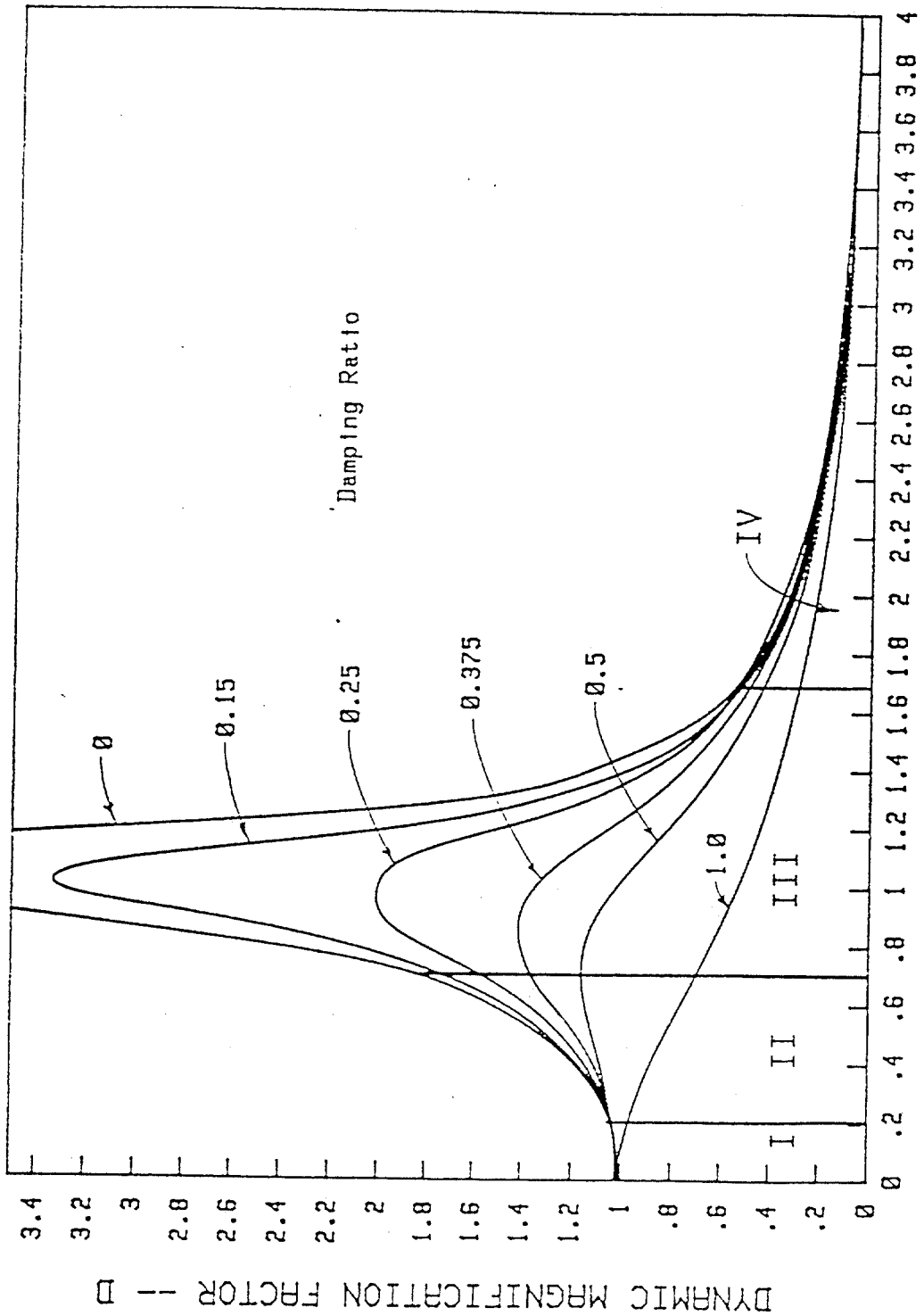

Figure 1.1-1 Dynamic behavior of platforms

frequencies possess the energy to significantly affect offshore structures. The waves in this band are the gravity waves with periods of 5 to 25 seconds (0.2 to 0.04 Hz), and one must try to design structures with natural frequencies outside this range. The period distribution, or spectrum, of this wave energy is shown in Figure 1.1-2 (Ellers, 1982) for two different geographical regions, the Gulf of Mexico and the North Sea. The significant wave height is the average height of the highest one-third waves in a given sea state and is an indicator of sea surface roughness. Also shown in the figure are the relative locations of structure periods for both fixed and compliant offshore structures.

1.2 Review of Compliant Tower Concepts and Previous Research Work

Ocean engineers have used structural compliance as a means to reduce environmental loads on structures for many years in the case of single point mooring systems (SPMs). With the success of these simple systems, it was a natural development to extrapolate the technology to larger, more complex structures. When increased water depths made traditional fixed structures economically unattractive, the fundamental ideas of the SPM were applied on a larger scale to offshore oil production platforms for ocean depths greater than about 600 ft.

Compliant structure concepts may be classified in one of four categories:

1. Articulated towers (ATs);
2. Guyed towers (GTs);

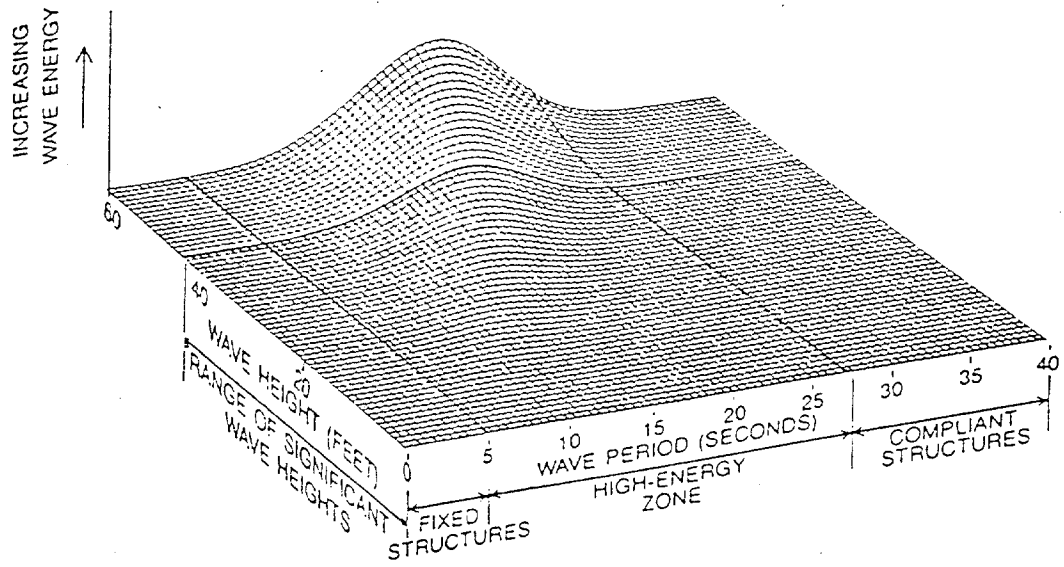

Gulf of Mexico

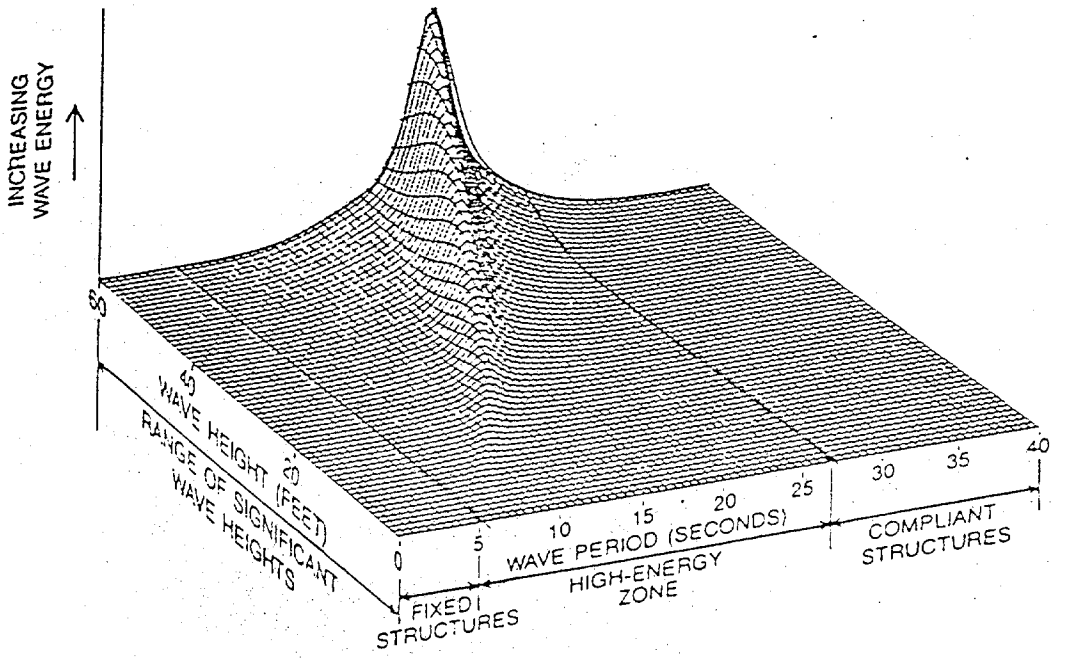

North Sea

Figure 1.1-2 Sea spectrum diagrams

3. Tension leg platforms (TLPs), also known as tethered buoyant platforms (TBPs); and
4. Floating production facilities (FPFs)

Each reduces maximum stresses by complying (moving) with the dynamic loads as they act on the structure and, hence, each experiences motions that are large compared to those of fixed structures. The concepts differ mainly in the means by which the loadings are transmitted to the seabed and in the form of the anchorage to the sea floor. They all resemble inverted pendulums, with excess buoyancy replacing gravity loads.

The relative advantages of a compliant structure over a fixed-base structure include:

1. Reduced structure to connect platform to sea floor for large water depths;
2. Lateral structural response at periods longer, and vertical response at periods shorter than the predominant incident wave periods;
3. They are potentially more mobile and reusable in new fields;
4. Increased fabrication and outfitting in construction yards reduces weather-sensitive offshore work periods;
5. Separate installation of foundations and/or installation over previously drilled wells; and
6. Enhanced "tunability" of periods of the system for a particular site.

Some of the relative disadvantages or difficulties of compliant structures relative to fixed-based structures include:

1. Structure must be designed to resist an enlarged spectrum of wave loads due to enhanced responses at both low and high frequencies;
2. Increased concern about nonlinearities and stability of dynamic motion;
3. Crew discomfort during motions;
4. Foundation and riser connection design;
5. Possible greater sensitivity to fatigue effects; and
6. Lack of experience to date with respect to design and in-service behavior.

1.2.1 Articulated Towers (ATs)

The articulated tower consists of a vertical column to which buoyancy has been attached near the water surface and to which ballast is usually added near the bottom. The tower is connected to the sea floor through an articulated hinge joint to a base which may be of either piled or gravity type. The articulated hinge generally is either a ball and socket or a Cardan type of joint. The tower itself may be either a tubular column or a trussed steel latticework.

The structure is dynamically tuned to have a natural period removed from periods of high wave energy, usually longer than the wind-wave period range. This is accomplished by adjusting the size and location of buoyancy and ballast on the tower. In the process

of tuning, consideration is also given to hinge loads, for it is desirable to keep the loads to a minimum from both a foundation design and hinge design viewpoint.

The articulated tower was among the first of the more elaborate compliant designs to see ocean service. It serves as the first link between the sea-keeping analysis of the free body, traditionally the domain of the naval architect, and the environmental load analysis of the permanent structure, the traditional task of the ocean engineer. The scale of the structure in its region of applicability warrants a more elaborate analysis than is commonly the case for a SPM.

Articulated towers are presently being used as single point mooring and loading terminals, control tower and flare structures and, coupled to a resident tanker, as early production facilities in the North Sea and in the Atlantic Ocean. They also have been studied for use as production platforms in marginal fields where reserve size does not warrant large facilities. The structures are typically designed for water depths of 200 to 600 ft but concepts have been developed for water depths in excess of 1200 ft. Also recently proposed are facilities which consist of multiple articulated columns connected in parallelogram fashion to a foundation and to a deck structure. Such an arrangement permits larger deck loads and virtually eliminates roll and pitch motions of the deck.

Both in the United States (Chakrabarti and Cotter, 1980) and in Great Britain (Kirk and Jain, 1977, 1981) the dynamics of these

structures in two and three dimensions have been thoroughly explored. Kirk and Jain employed a time step technique to solve the nonlinear differential equation of motion using linear wave theory and noncollinear current. Chakrabarti and Cotter's work initially dealt with a closed form solution of the two-dimensional problem but was later extended to include transverse tower motion. More recently, Kirk and Jain have extended their work to include the analysis of a double articulated structure in noncollinear wave and current.

1.2.2 Guyed Towers (GTs)

The guyed tower is a rectangular lattice column connected to the sea floor by either a piled foundation or a "spud can" gravity type foundation. The tower is long and slender and depends upon a group of catenary guy lines for lateral stability in resisting wave and wind loads. Essentially it is an extension of the guyed radio tower to the water environment. An important distinctive feature of the guys is the clump weights which are attached to the cable guys and which initially are at rest on the sea floor some distance from both the tower and the cable anchors.

The guyed tower is designed, as are the other compliant structures, to have a natural period longer than the wave periods of significant energy. This is accomplished largely by selection of number of guy lines and control of guy line tension. Since it is desired from operating requirements to have a relatively stiff system for normal sea conditions the tower is tensioned to be

fairly rigid. In these circumstances the clump weights are sized to remain on the bottom. In survival sea conditions, it is desirable to allow the system to become more compliant. This occurs when the clump weights leave the bottom. Not only does the guy system become softer but also, since the natural period is on the high end of the wave periods, the natural period of the structure increases and the dynamic amplification factor for the driving wave frequencies decreases.

A guyed tower, the concept of which is attributed to L.D. Finn, was first constructed as a one-fifth scale instrumented model test structure in 293 feet of water in the Gulf of Mexico in 1978 (Finn and Young, 1978). Results of the model test confirmed the adequacy of Finn's original linearized analysis (Finn, 1976) of this complex structure as a means of obtaining peak loads. However, test data showed that such a simplified analysis would not adequately describe the kinematic and dynamic response of the structure as a function of time, an important concern in fatigue analysis. Recent work (Mes, 1981, 1982) has begun to consider the nonlinearities of the combined analysis problem of tower and guys in a hydrodynamic loading environment. A nonlinear stochastic analysis of a guyed tower using spring idealizations for guys has been performed using the Fokker-Planck equation (Smith et al., 1980). Currently, simplified tower-guy models are being developed that are suitable for parametric study (Triantafyllou et al., 1982).

The only guyed tower in service to date is the above-mentioned test structure installed in the Gulf of Mexico. Plans are under way, however, for installation of a more than 1000 foot tower in the Gulf of Mexico in 1983.

1.2.3 Tension Leg Platforms (TLPs)

The tension leg platform (TLP) is essentially a semisubmersible vessel which is moored to the sea floor by a number of pretensioned tendons. The tendons are connected at the sea floor to a template which is piled in place. It is significant to note that unlike the case of normal pile foundations, the piles experience tension rather than compression. The tendons in early concepts were often splayed out from the platform at significant batter but model testing showed that such an arrangement led to large dynamic loads in individual tethers, and now almost all TLPs have vertical tendons which have larger pretension, a smaller dynamic load and a net reduction in peak loading. Like the articulated towers, these structures are free to move in surge and sway. They also have a more limited freedom in yaw, while roll, pitch, and heave are severely restricted by the pretensioned tendons. The structure is sized by adjusting tendon tension and platform buoyancy so that requirements concerning surge, sway, and yaw periods and "setdown", are satisfied. Setdown, the change in water line location on the buoyancy chambers as the platform moves to maximum surge and sway, must not be so large as to permit waves to strike the deck structure. The natural periods of the structure in surge, sway and yaw

must be greater than the wave priods of significant energy. The heave, roll and pitch natural periods, on the other hand, being much shorter, must be less than the significant wave energy periods. Further, amplitudes of motion must be sufficiently small to prevent flexural yielding of the drilling risers which connect the platform to the subsea completion template.

A tension leg platform (TLP), also referred to as a tethered buoyant platform (TBP), first saw ocean service with the field testing of the Triton platform in 1974 (MacDonald, 1974 and Pauling and Horton, 1970). The dynamics of the TLP have been considered (Rainey, 1978, 1980) in terms of a Mathieu-Hill type nonlinear differential equation of motion. This equation resulted from the nonlinear restoring force of the TLP structural system. The former of these two papers is believed to be the first to demonstrate the possibility of the existence of both subharmonic and superharmonic instabilities of the tower motion. Much subsequent literature deals with this problem (Albrecht et al., 1978; DeZoysa, 1978; McIver, 1981; Yoshida et al., 1981; and Jefferys and Patel, 1981).

While many investigators were examining the nonlinear instabilities of the TLP, others (Natvig and Pendered, 1980; and Ashford and Wood, 1978) were examining optimized computational techniques for both linearized frequency-domain analyses and time-domain solutions of the equations of motion. Three-dimensional potential theory has been used in the analysis of the motion of the TLP in irregular seas (Gie and de Boom, 1981). Their work reveals the particular effect of unsteady drift force on the structure.

Presently no TLPs are in service but one is scheduled to be in service in the Hutton field of the North Sea in 1984 (Tetlow and Leece, 1982; Mercier et al., 1980, 1982; Mercier and Marshall, 1981; and Mercier, 1982). Located at a site with 480 feet water depth, it will serve as a test structure for comparison to fixed structures, and also for extrapolation of the concept to deeper water.

1.2.4 Floating Production Facilities (FPFs)

Floating production facilities (FPFs) are similar to TLPs in that they both use a semisubmersible type of vessel as a platform. They differ by having a catenary-type of anchoring system rather than the tendons of the TLP. As such, the structure is free to move with relatively large amplitudes in the roll-pitch-heave modes compared to the TLP. It is required that natural periods in all modes be removed from significant wave energy periods. Usually the periods are desired to be longer than the wave periods. Guys are selected and sized to limit surge and sway to amplitudes acceptable to the riser cluster.

FPFs have been in service since 1975 in the North Sea. Ten such units are presently in operation worldwide.

1.2.5 Comparison

Although selection of a structure is often dependent upon stringent site-specific conditions as related to the mechanical particulars of individual concepts, it is worthwhile to compare the

relative advantages and limitations of the various compliant structures.

In terms of relative payload capabilities for a fixed water depth, the TLP may be ranked as being capable of carrying the heaviest deck loads. It is followed in order by the FPF, the GT, and lastly the AT (Lewis, 1982). Water depth range is listed for the FPF as 250 to 6000 ft, for the TLP as 500 to 3000 ft and for the GT as 600 to 2000 ft (Lewis, 1982). The estimated depth range for the AT lies in the 200 to 1200 ft range and is limited by natural period. It is difficult to obtain a soft system in shallow water and the buoyancy requirements for a system stiff enough to limit deck accelerations are prohibitive in deeper waters. The TLP shallow limit is restricted by the permissible angular offset of the riser cluster and the deep limit by the natural period of the structure in heave. The GT is limited in shallow water by angular deviation of the tower structure at the base, and in deep water by the first natural mode of the tower in bending. The FPF has no such mechanical limitations but is limited solely by economic practicality.

Both the TLP and FPF offer excellent resistance to seismic loadings because of their essentially free floating nature, although some care must be exercised with regard to the heave natural frequencies of the TLP. The GT and AT have less of an advantage in this regard, with the vertical natural frequency approaching earthquake spectrum frequencies as the length of tower increases with water depth.

Total structure weight naturally increases with water depth but it increases at different rates for each structure (Lewis, 1982). The AT weight increases approximately parabolically with depth due to increased buoyancy requirements. The GT weight increases logarithmically due mainly to flexural stiffness restrictions. Both the TLP and FPF have a proportional weight increase with depth (Lewis, 1982) since both concepts require reasonably simple modifications to the tendons or guys to extend the floating structure to deeper water.

The last comparison to be made here is one of operability. These are, after all, work platforms. The major advantages of the GT and AT are that both provide continuous riser support from the sea floor and both allow deck-level completion of wells, techniques already developed and proven on fixed structures.

The TLPs and FPFs require subsea completion, a relatively new procedure, and laterally unsupported risers which are held in tension to prevent buckling. Both structures require riser string tensions which permit vertical motion of the platform to take place without significant fluctuation in riser tension. The FPF, with significantly more heave amplitude than the TLP, requires a much larger tensioning system which adds considerable equipment cost and loading to the deck structure.

1.3 Objectives of the Work

The objective of this work is to develop a computer tool suitable for the nonlinear coupled analysis of a compliant guy-

structure system in an ocean environment. There exists in the literature a significant volume of work dealing with separate components of the compliant ocean structure. The dynamic response of the platform, generally governed by the Morison equation, with cables modelled as springs has been treated by a variety of authors (Penzien, 1976; Taudin, 1978; Fish, Dean, and Heaf, 1980; Fish and Rainey, 1979). Likewise, many investigators (Ansari, 1978; Suhara, et al., 1981; Peyrot, 1980; De Zoysa, 1978; Wilhelmy, et al., 1981) have contributed to the analysis of catenary moorings using either finite element or finite difference approaches.

Generally the motions of the guy-structure system are determined in a decoupled analysis procedure. In this procedure, the guys are first represented by springs with load deflection characteristics similar to those of the static guy system. The platform is then dynamically analysed using these spring representations. The resulting motions of the platform analysis are then applied to a dynamic model of the guy cluster and the resulting loads in the cable to tower connection are compared to those of the spring-platform analysis to see if they compare reasonably.

There is a subtle problem in this form of analysis that is disconcerting. By performing this solution procedure, it is presupposed that the procedure is valid and the results are forced to fit an assumed character. Since the general coupled dynamic problem involves numerous nonlinearities, the normal intuitive feel for the proper response is quickly lost and it is difficult to

assess the validity of the assumptions of decoupled analysis in a qualitative manner.

Model guy tests and theoretical guy calculations indicate that there is a need for a coupled analysis which incorporates the nonlinear behavior of the total system (Mes, 1981). One main reason is that theoretical work indicates that there is hysteretic energy dissipation in the guy system. Certainly hydrodynamic drag loads on the cables are energy dissipators, and they are spatially and directionally dependent. In a wave or current field, not only are the drag loads dependent upon the spatial orientation of the cable but also they are dependent upon the directionality of the wave or current, drag loads being greater when moving against the wave or current than when moving with it.

A nonlinear coupled analysis program which can deal with phenomena such as the spatially and directionally dependent drag forces will provide a means to quantitatively assess the validity of decoupling assumptions and also the range of that validity. It is doubtful that the nonlinear coupled analysis will supplant more simplified procedures since such analyses are usually by nature too expensive and time consuming for all but perhaps the final phases of design. They do, however, provide insight to the complicated physical phenomena and with judicious model selection, such an analysis will contribute greatly to physical understanding of a complex problem and to design confidence.

1.4 Scope of the Work

The computer program developed in this work is a nonlinear finite element program capable of solving large displacement problems, both statically and dynamically in the time domain. The solution procedure is formulated using the updated Lagrangrian coordinate reference frame. The algorithm used is a residual feedback scheme which is an incremental iterative technique in which the load may be applied in steps with a full Newton-Raphson iteration to convergence at each step. The linearized matrix equations are solved using Gauss elimination. Static problems with low initial stiffness are considered using a viscous relaxation procedure incorporated into the residual feedback algorithm. An implicit scheme, Newmark's method, is used for the numerical integration in time.

The particular elements developed include a cubic subparametric beam element with geometric stiffness, a two node isoparametric cable element and a foundation element. The beam element has a consistent mass matrix which is adjusted for added mass over all, or any portion, of the element. The cable element is a straight element also with a consistent mass matrix. The cable element mass matrix is formed assuming the cable is always submerged. The foundation element incorporates viscous damping in addition to spring stiffness in the six nodal degrees of freedom. All element materials are assumed to be linearly elastic.

Hydrodynamic loads are calculated from linear wave theory using a form of the Morison equatin modified to account for element orientation and element velocities and accelerations. Irregular waves may be simulated by a series of wave components of varying period, height, phase, and direction. Current is specified as a current profile which may vary in magnitude and direction with depth.

Additional loadings may be specified as concentrated masses or concentrated forces. The concentrated masses participate in the dynamic solution and are assigned weight. The concentrated loads are static.

No interference, proximity or diffraction effects of the flow are considered. Values of drag and inertia coefficients are specified at problem outset and remain constant. Wind and seismic dynamic loads are not considered.

Chapter 2 includes a discussion of the concepts and assumptions which form the basis of the mathematical description of the physical problem. Chapter 3 gives the derivation of the solution algorithms, of the element formulations, and of the load calculation scheme. Chapter 4 contains a selection of program validation problems and sample problems of compliant structures. Chapter 5 is a summary of the results with recommendations for additional work.

2.0 Basic Concepts and Assumptions

The compliant structure is, in general, a complex one. Composed of many different elements, chain, cable, rope, tubulars, structural sections, plate, etc., it presents a more than modest challenge for the designer. In additional to the structural intricacies, the loadings are a complex interaction of gravity, buoyancy, waves, current, wind and seismic activity. In order to deal practically with either the design or analysis problem it is necessary to make certain simplifying assumptions. It is the purpose of this chapter to set the ground rules and assumptions that were made concerning the physical idealization (see Figure 2.0-1 for a general definition sketch).

The mathematical derivations for the finite element model are given in Chapter 3. Both static and dynamic solution algorithms as well as the individual element stiffness and mass matrices are developed there. The method of distributed load discretization is also explained.

2.1 Structure

2.1.1 Beam-column Element

The primary structural components of the compliant offshore platform are the beam-column elements which form the rigid support frame for such deck components as living quarters, helipads, drilling tables, etc. The beam-column elements in this analysis are subject to the following restrictions:

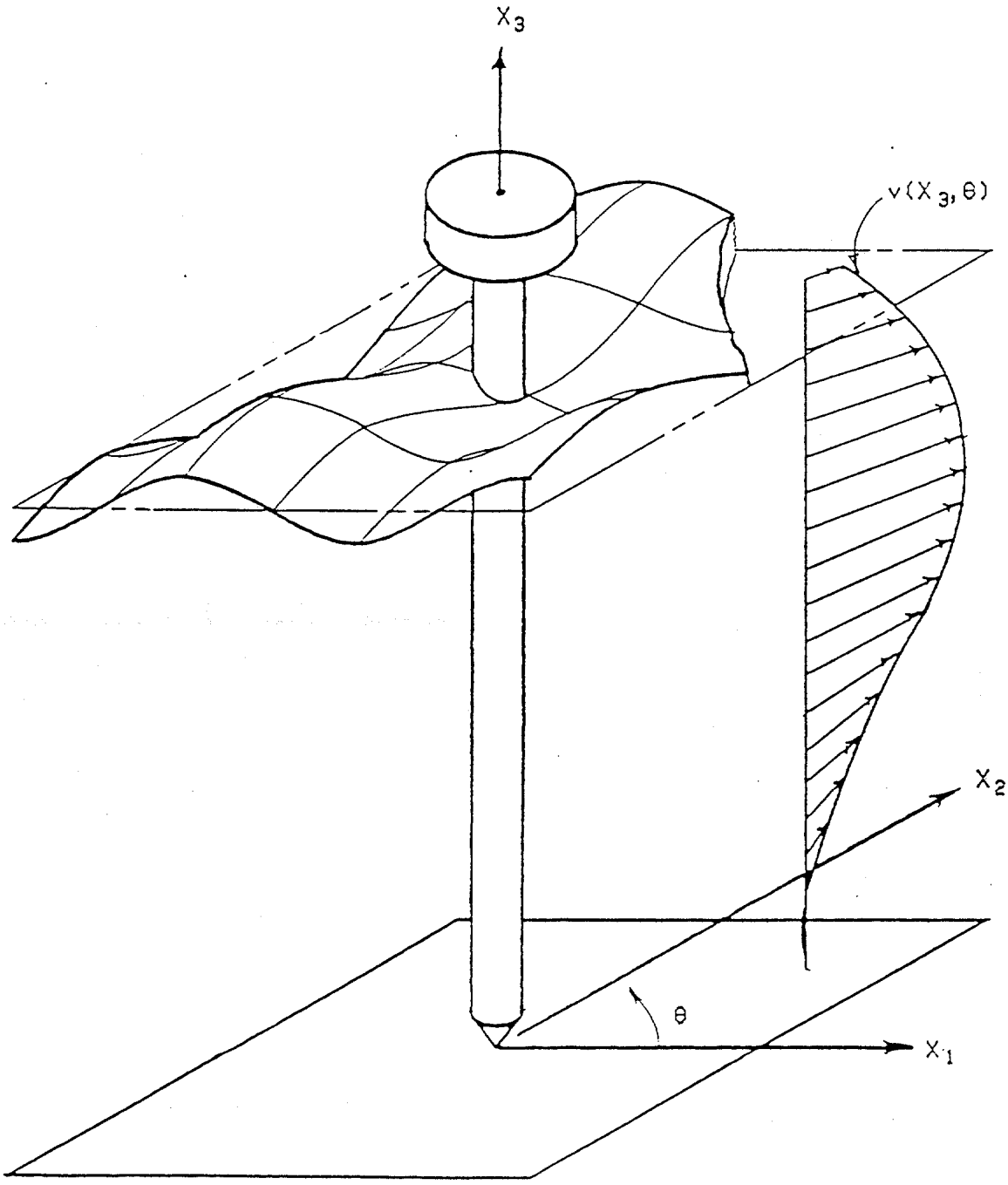

Figure 2.0-1 General definition sketch

1. The elements are composed of a linearly elastic material. Significant deviation from linearity of modulus of elasticity in such elements is usually an indication of yielding, a condition undesirable for a practical design.
2. Although the beam-column elements may undergo large displacements elastic deformations are assumed to be small enough that small deflection beam theory is valid within the elements.
3. Shear deformations are neglected. The elements are considered to be long enough that transverse deformations due to shear are negligible compared to those due to bending.
4. Bending moments of inertia about the major and minor axes need not be the same. This permits modelling of standard structural shapes used in deck framing.
5. Polar moments of inertia may be independent of bending moments of inertia to permit the use of experimentally determined torsional constants.
6. Element weight density may be specified independently of element mass density so that the quasistatic solutions, i.e. solutions in which inertia forces are neglected, of dynamic problems may be performed for comparison with dynamic solutions including inertia.
7. Hydrodynamic load coefficients are assumed to be independent of the orientation of the beam. No account is taken of variation in Reynolds number or Keulegan-Carpenter number within the flow field.

8. The hydrodynamic load coefficients are assumed to apply to an axisymmetric body. Since most submerged members are tubulars, and in light of the scarcity of information concerning hydrodynamic coefficients of nonaxisymmetric shapes, the assumption is a reasonable approximation.

2.1.2 Cable Element

The second essential structural element found on most compliant structures is the guy or cable element which provides lateral stability to the structure. Cables behave in an inherently geometrically nonlinear fashion and linear approximations are sufficient for only small deflection, low cable sag to span ratio problems. The cable elements of this analysis are subject to the following assumptions.

1. The cable elements are composed of a linearly elastic material. Most chains and steel wire ropes may be successfully modelled under this restriction. Synthetic ropes do not generally satisfy this restriction, exhibiting highly nonlinear elastic curves as well as hysteresis over much of their working load range.
2. The cable elements are assumed to possess negligible flexural and torsional stiffnesses. This assumption adequately describes chain and most cable. Large diameter wire rope however may have significant flexural and torsional stiffnesses if the length to diameter ratio is sufficiently small.

3. In the slack condition, determined by the absence of tension, zero structural stiffness is assumed.
4. In the slack condition, inertia loads due to cable mass and added mass are transmitted to the connecting structure.
5. Element weight density may be specified independently of element mass density so that quasistatic solutions of dynamic problems are easily implemented.
6. The cables are assumed to be cylindrical in shape and hydrodynamic load coefficients are assumed to be independent of cable orientation and local water particle kinematics. These assumptions are reasonable for all ropes and, if a sufficient length is considered, they are also valid on the average for chain.

2.1.3 Foundation Element

The compliant platform is eventually anchored to the seafloor by one or more of a variety of foundation devices such as piles, fluke anchors, or gravity foundations. There is, of course, interaction between the seafloor and the structural anchorage. To account for this interaction a simple foundation element is used. It is subject to the following restrictions:

1. The foundation stiffness is linear over the range of applied loads.
2. The foundation may have different stiffnesses in each of the six degrees of freedom.

3. Energy dissipation by the soil is assumed to occur as equivalent viscous damping.
4. The damping parameter, like the stiffness parameter, may be specified separately for each of the six degrees of freedom.
5. Any effective mass of the foundation must be represented as a lumped mass at the foundation to structure connection.
6. Hydrodynamic loads on the foundation are ignored.

2.2 Loads

In addition to dead loads due to gravity the compliant structure is influenced by buoyancy, waves, currents, tides, wind loads, seismic loads and a variety of live loads peculiar to the purpose of the structure. Only loads due to gravity, buoyancy, waves and currents are considered in this work.

2.2.1 Gravity

For the purpose of this study gravity is specified to act only on members for which a weight density is specified and also on all concentrated masses.

2.2.2 Buoyancy

The buoyancy force is assumed to act in opposition to the forces due to gravity. It is applied to all members for which displaced volume is specified and is applied only to those elements or portions of elements which lie below the still water level.

2.2.3 Wave Loads

Wave loads are calculated using a generalized form of the Morison equation. The Morison equation as originally proposed (Morison et al., 1950) for a fixed vertical pile is expressed as

$$dF^w = [\frac{1}{2} \rho C_D D \mid \dot{u}_1 \mid \dot{u}_1 + \frac{\Pi}{4} \rho C_I D^2 \ddot{u}_1] dx_3 \qquad (2.2.1)$$

where ρ is the fluid density, D is the pile diameter. The horizontal fluid particle velocity $\dot{u}_1$, and the horizontal particle acceleration $\ddot{u}_1$ are determined using an appropriate wave theory. The parameter C_D is the empirical drag coefficient and C_I is the inertia coefficient. Both coefficients are determined from governing design rules or from experimental data.

To calculate the forces on an inclined cylinder the Morison equation needs to be modified to account for the orientation of the cylinder axis relative to the water particle velocity and acceleration vectors. Although there are at least four different methods of calculating forces on inclined cylinders using the Morrison equation (Wade and Dwyer, 1976), the method recommended by Sarpkaya and Isaacson, 1981 is used in this work. The resultant water particle velocity and acceleration vectors are decomposed into components tangent to and normal to the cylinder. The normal components are used to calculate the wave loads. Forces due to the tangential components are neglected. That it is acceptable to neglect the tangential component has been shown by Berteaux, 1976. The equation may thus be written in vector component form as

$$dF_i^W = [\frac{1}{2} \rho C_D D |\dot{u}_i^N| \dot{u}_i^N + \frac{\pi}{4} \rho C_I D^2 \ddot{u}_i^N] dx_i' \qquad (2.2.2)$$

where the superscript N indicates flow normal to the cylinder axis and dx_i' is the differential distance along the cylinder axis.

The equation (2.2.2) may be further modified to account for the motion of the cylinder in the fluid. The inertia coefficient, C_I, may be considered to be made up of two components, the added mass coefficient, C_a, and a term due to the pressure gradient of the accelerating fluid. The added mass term is the value of fluid mass which must be accelerated at the same rate around the cylinder to preserve a uniform flow field both ahead of and behind the cylinder. In ideal flow its value can be shown to be unity for a cylinder, but real fluid effect usually reduce this value to less than unity. The term due to the pressure gradient of the accelerating fluid may be calculated from the Bernoulli equation and is found to be unity. Thus,

$$C_I = C_a + 1.0 \qquad (2.2.3)$$

when the fluid is uniformly accelerating past the cylinder. When the cylinder is accelerating in a fluid at rest

$$C_I = C_a \qquad (2.2.4)$$

After the velocity and acceleration terms for both fluid and cylinder are substituted into Equation (2.2.2), we obtain

$$dF^{w}_{i} = [\tfrac{1}{2} \rho C_D D \mid \dot{u}^{N}_{i} - \dot{q}^{N}_{i} \mid (\dot{u}^{N}_{i} - \dot{q}^{N}_{i}) + \tfrac{\pi}{4} \rho (C_a + 1) D^2 \ddot{u}^{N}_{i} - \tfrac{\pi}{4} \rho C_a D^2 \ddot{q}^{N}_{i}] \, dx'_i \qquad (2.2.5)$$

where $\dot{q}^{N}_{i}$ and $\ddot{q}^{N}_{i}$ are the components of cylinder velocity and acceleration normal to its axis.

2.2.4 Current Loads Without Waves

In the ocean, current direction need not coincide with wave direction and may vary with depth. The current speed may also change with depth. To permit a realistic current description, a current profile which may vary in both magnitude and direction with depth is considered. The current is assumed to be steady and it is assumed to have no vertical component.

The hydrodynamic load due to current only is calculated using the drag term of the generalized Morison equation

$$dF_i^{c} = \tfrac{1}{2} [\rho C_D D \mid \dot{v}^{N}_{i} - \dot{q}^{N}_{i} \mid (\dot{v}^{N}_{i} - \dot{q}^{N}_{i})] \, dx'_i \qquad (2.2.6)$$

where $\dot{v}^{N}_{i}$ is the current velocity component normal to the cylinder and F^{c}_{i} is the hydrodynamic drag force due to current.

2.2.5 Combined Wave and Current Loads

Wave and current loadings naturally occur simultaneously. An exact treatment of the combined wave and current kinematics for other than a uniform current is a complicated problem and is unsuitable for the purpose at hand. Fortunately, a simple superposition scheme has been shown to be adequate when the Morison equation is used for most situations of engineering interest (Dalrymple, 1974). Provided that the particle velocities are summed before calculating the drag load rather than calculating the drag loads individually and then summing (the result being underprediction of the drag load) the nonlinear effects due to the interaction of current and wave are negligible (Leonard and Hudspeth, 1979). When the drag force is properly accounted for the combined force equations becomes

$$F_i^H = \int_L (dF_i^{w+c})$$

$$= \int_L \left[\frac{1}{2} \rho C_D D \left| \dot{u}_i^N + \dot{v}_i^N - \dot{q}_i^N \right| (\dot{u}_i^N + \dot{v}_i^N - \dot{q}_i^N)\right.$$

$$\left. + \frac{\pi}{4} \rho (C_a + 1) D^2 \ddot{u}_i^N - \frac{\pi}{4} \rho C_a D^2 \ddot{q}_i^N \right] dx_i' \qquad (2.2.7)$$

In this final form of the equation, C_D and C_a values determined from experimental data should be selected using the Reynolds number of Keulegan-Carpenter number calculated using $\left|(\dot{u}_n)_{max} + \dot{v}_n - \dot{q}_n\right|$,

where $(\dot{u}_n)_{max}$ is the maximum normal water particle velocity due to wave. That is,

$$R_e = \frac{|(\dot{u}^N)_{max} + \dot{v}^N - \dot{q}^N|D}{\nu} \tag{2.2.8}$$

and

$$K_c = \frac{|(\dot{u}^N)_{max} + \dot{v}^N - \dot{q}^N| T}{D} \tag{2.2.9}$$

where Re is the Reynolds number, K_C is the Keulegan Carpenter number, ν is the kinematic viscosity of the fluid, and T is the wave period.

Water particle kinematics due to waves are calculated using linear wave theory with no adjustment for free surface effects. When a current is present, the wave characteristics need to be modified to reflect the current upon which the wave is superimposed. Figure 2.2-1 shows a sketch of the wave-current field. If the current is uniform, one may derive the wave particle kinematics in a reference frame moving at a constant velocity which freezes the wave form with respect to time (Sarpkaya and Isaacson, 1981). The current is assumed to move at a uniform velocity, $\dot{v}$. The wave celerity, c, in a reference frame moving at velocity, $\dot{v}$, is defined as $c = \omega/k$ where ω is the angular frequency ($\omega = 2\pi/T$) and k is the wave number ($k = 2\pi/L$; L = wave length). The reference frame which freezes the waveform thus moves at

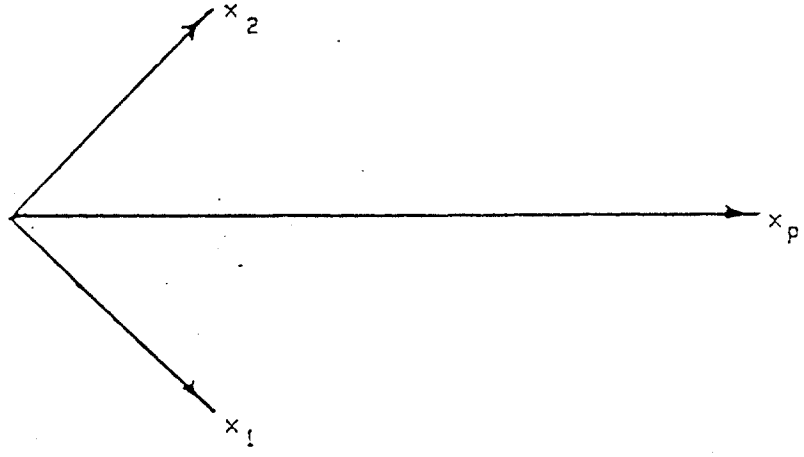

PLAN

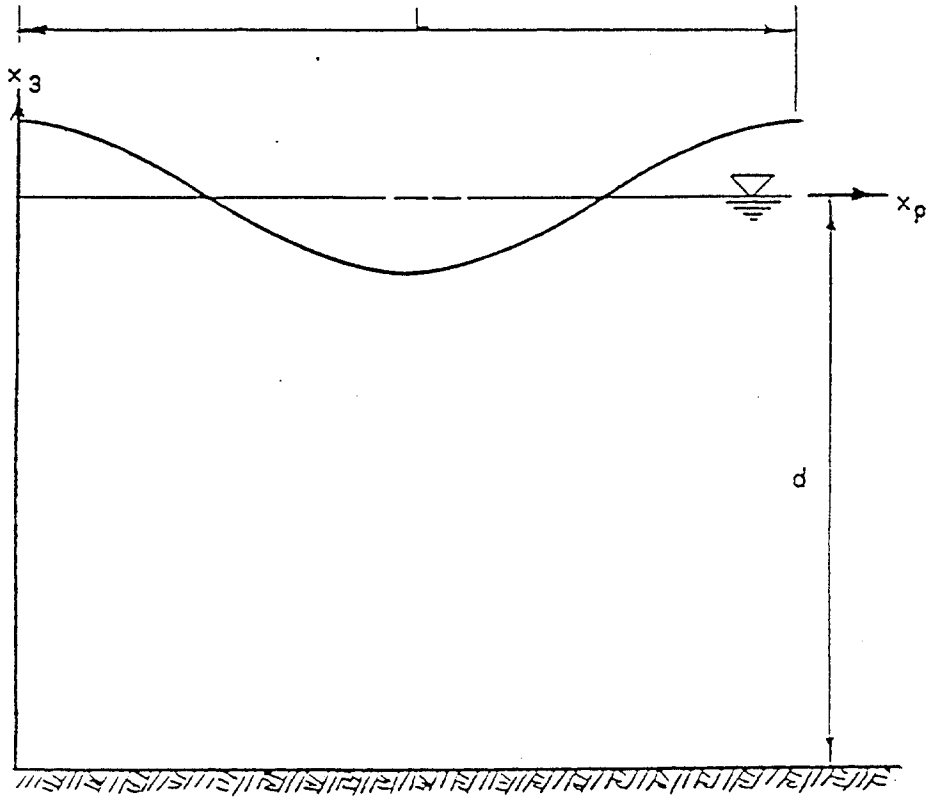

ELEVATION

Figure 2.2-1 Definition sketch for waves and current

velocity $c + \dot{v}$. If $\dot{u}'$ is defined as the water particle velocity observed in the reference frame moving at $c + \dot{v}$ then $\dot{u}' = \dot{u} - \dot{v} - c$, where $\dot{u}$ is the water particle velocity observed in the fixed reference frame. Using the standard small amplitude wave theory boundary conditions, one may solve the Laplace equation, $\nabla^2 \phi' = 0$, where $\phi' = \phi - (c + \dot{v})\, x_p$ and x_p is a horizontal distance measured in the direction of wave propagation. The dispersion relation obtained is $c = \{\frac{g}{k} \tanh kd\}^{1/2}$ where g is the acceleration of gravity and d is the water depth. This relation is identical to that derived for waves in no current, i.e. if the reference frame is moving with the current, the wave appears identical to the wave that would be observed if there were no current. It has the same wavelength and period. This implies that in the fixed reference frame the presence of uniform current is observed as an apparent change in period of the wave, i.e. a Doppler effect.

The wave celerity with respect to the fixed reference frame may be expressed as $c_c = c + \dot{v}$ and the wave frequency with respect to the fixed frame may be expressed as $\omega_c = \omega + k\,\dot{v}$. For currents oblique to the direction of wave propagation, only the component of current parallel to the direction of wave propagation alters the wave kinematics so that the wave frequency may be defined as

$$\omega_c = \omega + k\,|\dot{v}|\cos\alpha \qquad (2.2.10)$$

where α is the angle between current direction and wave direction.

If the current profile varies with depth the problem is more complicated and a simple solution is no longer possible. Although Biesel, (1950) has solved the problem for a triangular steady current profile, more general solutions are unknown. As a consequence, an ad hoc procedure is used here to account for the apparent wave frequency shift. A weighted average current in the wave direction is calculated according to the relation

$$\langle \dot{v} \rangle = \frac{\int_{-d}^{o} \dot{v}\,(x_3)\cos\alpha\,(x_3)\,\cosh\,(k\,(x_3 + d))\,dx_3}{\int_{-d}^{o} \cosh\,(k\,(x_3 + d))\,dx_3} \qquad (2.2.11)$$

where d is the water depth and $\langle \dot{v} \rangle$ indicates the weighted average current velocity in the direction of the wave. The frequency ω_L is then calculated from the relation

$$\omega_c = \omega + k\,\langle \dot{v} \rangle \qquad (2.2.13)$$

There is an ambiguity as to which wave frequency value is specified in the design wave or wave spectrum. In situ recordings obviously yield values for ω_c . Hindcasts based on wind data give values for ω. If one has values for ω_c, it is necessary to calculate an adjusted wavelength which reflects the frequency of the wave in still water. If one has values of ω, it is necessary to compute ω_c. Rarely in the conceptual or design phase of most offshore structures is in situ information available for design and hindcasts are often the only source of loading information. For

this reason, the wave period that is assumed given is that corresponding to ω. The value of ω_c is calculated.

2.2.6 Concentrated Loads and Masses

To permit some versatility in loading, provision is made for the use of both concentrated loads and concentrated masses. The concentrated loads are time invariant in the dynamic solution. The concentrated masses possess time invariant weight due to gravity in static calculations and they have both time invariant weight and inertia which are effective in the dynamic solution.

2.3 Equations of Motion

Newton's second law for a multiple degree of freedom system may be written in vector component notation as

$$F_i = M_{ij} \ddot{q}_j \tag{2.3.1}$$

where the force vector, F_i, is composed of the restoring force $K_{ij} q_j$, the structural damping force, $C_{ij} \dot{q}_j$, the forcing function $F_i^H(t)$, and any steady loads F_i^s. M_{ij} is the mass matrix, K_{ij} is the structural stiffness matrix, C_{ij} is the structural damping matrix and q_j is the vector of structure displacements. By inserting the expressions for F_i into Equation (2.3.1), one obtains

$$M_{ij} \ddot{q}_j + C_{ij} \dot{q}_j + K_{ij} q_j = F_i^H(t) + F_i^s \tag{2.3.2}$$

which is recognized as the equation of motion of an oscillating system.

Since structural damping is generally assumed small with respect to hydrodynamic damping, the second term in Equation (2.3.2) is neglected in this work. Integration of Equation (2.2.7) over the length of the member, L, and substitution of the result into Equation (2.3.2) lead to the relation

$$M_{ij}\,\ddot{q}_j + K_{ij}\,q_j = [\tfrac{1}{2}\,\rho\,C_D D\,|V_i^N|\,(\dot{u}_i^N + \dot{v}_i^N - \dot{q}_i^N) + \tfrac{\pi}{4}\,\rho\,(C_a + 1)\,D^2\,\ddot{u}_i^N - \tfrac{\pi}{4}\,\rho\,C_a\,D^2\,\ddot{q}_i^N]\,L + F_i^s \qquad (2.3.3)$$

where

$$|V_i^N| = \left(\sum_{j=1}^{3} (\dot{u}_j^N + \dot{v}_j^N - \dot{q}_j^N)^2{}_i\right)^{1/2} \qquad (2.3.4)$$

is the resultant relative velocity of node i. This set of simultaneous second order differentral equations must be solved numerically for all but the most trivial structures. Chapter 3 describes the numerical techniques used in this work.

3.0 Finite Element Formulation

The mathematical model of the compliant structure is based on the stiffness method of finite element analysis. The load-deformation characteristics of a number of discrete elements comprising the structure are described in approximate fashion by the load-deformation characteristics of the nodes to which the elements are connected.

In the case of static linear structural analysis, the discretization leads to a set of simultaneous linear equations which may be written in indicial notation as

$$F_i = K_{ij}\, q_j \tag{3.0.1}$$

where repeated subscripts imply summation over the range 1, N; N = number of degrees of freedom, F_i are components of the nodal load vector, K_{ij} are invariant stiffness coefficients due to the connecting elements, and q_j are components of the vector of nodal displacement.

For large-deflection statical problems, the stiffness matrix becomes a function of the displacement vector,

$$F_i = K_{ij}\,(q_k)\, q_j \tag{3.0.2}$$

and the solution of the nonlinear simultaneous equations becomes more difficult. Generally the nonlinear problem is solved by first linearizing the nonlinear relationship and then performing some form of incremental, or iterative, or combined incremental-iterative solution.

No matter which solution scheme is selected for the nonlinear problem, it is required to analyze the structure in a consistent reference frame so that the true loads and displacements and the true strains can be calculated. Small deflection analyses are performed using a Lagrangian reference frame in which the new position of the structure after loading is measured from the original position. For such analyses the small strain relationship between deformation and displacement is valid and the strain-displacement relationship is linear. When combined with a linearly elastic stress-strain relationship such as has been assumed for this work, the resultant load-deflection relationship is a linear one, i.e. Equation (3.0.1).

The rigid body translational components of the nodal displacements become important relative to deformation when displacements are large. In structural analysis there are two generally used methods of dealing with these large displacements, the total Lagrangrian formulation and the updated Lagrangian formulation (Cook, 1981). The former uses the Green-Lagrange strain tensor, which contains nonlinear terms, to account for large displacements in the element formulation. The latter permits the use of the

small displacement strain tensor by updating the nodal coordinates in a manner that accounts for the large displacements. The updated Lagrangian formulation was selected for this work because of the availability of a large variety of possible elements for use in the program element library.

In the updated Lagrangian technique the coordinates in which the elements deform are local coordinates for which the use of the small deformation strain tensor is valid. The orientation of these local coordinate systems is determined from the current nodal coordinates which are calculated from the displacement results of the most recent increment or iteration. The deformations of the elements due to previous loads are converted to equivalent internal nodal forces and are treated as preload. This preload cancels that part of the applied external load which would cause the existing deformation and leaves only the difference between the external and internal load to cause additional deformation.

3.1 Static Solution Techniques

The simplest solution to the static equations of equilibrium occurs when the stiffness matrix as invariant, the force displacement relation thus being linear. In this case a Gauss elimination scheme will obtain the unknown displacement, given the stiffness and the nodal loads. The LDL^T decomposition and back-substitution variant of the basic Gauss elimination technique (Bathe, 1981) was chosen as the fundamental equation solver for this class of problems. It was selected primarily because of the

wealth of available program procedures which have been developed for it (Bathe, 1981, Zienkiewicz, 1977).

If, as discussed in Section 3.0, the calculated nodal displacements are large, the stiffness matrix becomes a function of the displacements. To solve the nonlinear relations, a residual feedback technique is used (Tuah, 1982). This technique is a combined incremental-iterative solution of the linearized load-displacement relations.

The iterative part of the algorithm may be derived by expanding the nonlinear matrix equation (3.0.2) in a Taylor series about the displacement vector, q_j, evaluated at an approximate displacement, q_j^{n-1},

$$F_i(q_k^{n-1} + \Delta q_k^n) = [F_i\ (q_k)]^{n-1} + [\frac{\partial F_i(q)}{\partial q_j}]^{n-1}\ \Delta q_j^n + 0\ [\Delta q_j^n]^2 \quad (3.1.1)$$

with n = 1,2,3.... A following lower case superscript denotes iteration number and Δq_j^n is a correction to q_j^{n-1}. The displacement vector, q_j^o is defined as the initial structure displacement. When only first order terms in the Taylor Expansion are retained and when it is recognized that

$$[\frac{\partial F_i\ (q_k)}{\partial q_j}]^{n-1} = K_{ij}^{n-1} \quad (3.1.2)$$

where K_{ij}^{n-1} is the tangent stiffness matrix, the equation becomes

$$F_i\ (q_k^{n-1} + \Delta q_k^n) = F_i\ (q)^{n-1} + K_{ij}^{n-1}\ \ \Delta q_j^n \tag{3.1.3}$$

The load vector $F_i\ (q_k)^{n-1}$ is the load vector required to keep the structure in the shape represented by the displacements q_k^{n-1} and it is equivalent to the internal load vector R_i^{n-1} caused by these displacements. The expression may then be rearranged as

$$K_{ij}^{n-1}\ \ \Delta q_j^n = F_i^n - R_i^{n-1} \tag{3.1.4}$$

and successive iterations are given by,

$$q_j^n = q_j^{n-1}\ \ + \Delta q_j^n \tag{3.1.5}$$

The algorithm can be converted to an incremental-iterative scheme by simply defining the first iterations to the stiffness matrix, K_{ij}^o, and to the internal load vector, R_i^o, at time, $t + \Delta t$, as those determined at the previous time, t. That is,

$${}^{t+\Delta t}K_{ij}^{n-1}\ \Delta q_j^n = {}^{t+\Delta t}F_i^n\ - {}^{t+\Delta t}R_i^{n-1} \tag{3.1.6}$$

where a leading superscript denotes increment number; the initial value of the internal load is the internal load determined from the previous convergent load step,

$${}^{t+\Delta t}R_i^o = {}^tR_i^n \tag{3.1.7}$$

and the initial value of the tangent stiffness matrix is also determined from the configuration of the previous convergent load step,

$$ {}^{t+\Delta t}K_{ij}^{o} = {}^{t}K_{ij}^{n} \tag{3.1.8} $$

Convergence to the proper solution during iteration is determined by calculation of the norms of the displacement vectors q_j and Δq_j. When

$$ \frac{\| \Delta q_j \|}{\| q_j \|} = \frac{(\sum_{j=1}^{N} \Delta q_j^{\,2})^{1/2}}{(\sum_{j=1}^{N} q_j^{\,2})^{1/2}} < \text{Tol} \tag{3.1.9} $$

where Tol is a specified convergence tolerance and N is the order of the vector, convergence is assumed to have been reached.

Many compliant structures possess an initially low, or zero, stiffness with respect to transverse loads when in their still water equilibrium configurations. Attempting to solve the stiffness equation without some sort of starting modification results in either a singular matrix for which a solution is not possible or in extremely large initial displacement estimates and the probability of slow or no convergence to a solution.

In order to accommodate low initial stiffness, the residual feedback scheme has been modified to use a technique known as

viscous relaxation (Webster, 1980). The procedure has been shown to give excellent convergence characteristics in cable problems (Webster, 1980; Lo, 1981; Tuah, 1982). It is implemented by the addition of a viscous drag term to the iterative part of the residual feedback solution algorithm,

$$C_{ij}^{n}\ \dot{q}_j + K_{ij}^{n-1}\ \Delta q_j^{n} = F_i^{n} - R_i^{n} \tag{3.1.10}$$

where $\dot{q}_j$ is a vector representing the rate of displacement and C_{ij} is an arbitrary damping matrix usually selected as a constant multiplying the identity matrix, i.e. $C_{ij} = C\ \delta_{ij}$, where δ_{ij} = (=1 if i = j; = 0 if i ≠ j) is the Kronecker delta. Since the rate of displacement may be expressed as the change in displacement with respect to two iteration steps,

$$\dot{q}_j = \frac{\Delta q_j^{n}}{n - (n-1)} = \Delta q_j^{n}, \tag{3.1.11}$$

Equation (3.1.10) may be written as

$$[C^{n}\ \delta_{ij} + K_{ij}^{n-1}]\ \Delta q_j^{n} = F_i^{n} - R_i^{n} \tag{3.1.12}$$

which is the modified form of the iterative part of the residual feedback scheme.

To eliminate the artificial stiffness as the iteration proceeds, the value of C is decreased each iteration by the alogrithm.

$$C^n = \mu\, C^{n-1} \tag{3.1.13}$$

where μ is a decrement parameter specified to give effective rapid convergence. The selection of the best value of μ is problem dependent and should be chosen by trial and error. The selection of an initial value for C also affects convergence and is adjustable by use of a damping factor, β. In this work C is initially calculated as

$$C^o = \beta\ \text{Min}\langle K_{axial}\rangle_{elem} \tag{3.1.14}$$

where $\langle K_{axial}\rangle_{elem}$ is the average of the axial stiffness for all the elements of a particular element type, e.g. beam or cable. The symbol Min indicates that the least average stiffness among the element types is used. The selection scheme is purely arbitrary, but it has been shown to give acceptable results.

3.2 Dynamic Solution Techniques

Because of the potentially strong nonlinearity of both the hydrodynamic loading and the structural response, solution of the equation of motion, Equation (3.2.3), is performed in the time domain. The solution algorithm selected is the Newmark method. This method is an implicit self-starting scheme which has been used with success for several nonlinear problems (Bathe, et. al., 1975; Lo, 1981; Tuah, 1982).

The method is based upon the assumption that the acceleration varies according to some known function during each time step. In the incremental form,

$$ {}^{t+\Delta t}\dot{q}_i = {}^{t}\dot{q}_i + [(1-\zeta)\,{}^{t}\ddot{q}_i + \zeta\,{}^{t+\Delta t}\ddot{q}_i]\,\Delta t \qquad (3.2.1) $$

and

$$ {}^{t+\Delta t}q_i = {}^{t}q_i + {}^{t}\dot{q}_i\Delta t + [(\tfrac{1}{2}-\alpha)\,{}^{t}\ddot{q}_i + \alpha\,{}^{t+\Delta t}\ddot{q}_i]\,\Delta t^2 \qquad (3.2.2) $$

where ζ and α are parameters which must be chosen. Substituting Equations (3.2.1) and (3.2.2) into the equation of motion

$$ M_{ij}\,{}^{t+\Delta t}\ddot{q}_j + C_{ij}\,{}^{t+\Delta t}\dot{q}_j + K_{ij}\,{}^{t+\Delta t}q_j = {}^{t+\Delta t}F_i \qquad (3.2.3) $$

and solving for ${}^{t+\Delta t}q_j$, one obtains

$$ \hat{K}_{ij}\,{}^{t+\Delta t}q_j = {}^{t+\Delta t}\hat{F}_j \qquad (3.2.4) $$

where

$$ \hat{K}_{ij} = a_o\,M_{ij} + a_1\,C_{ij} + K_{ij} $$

$$ {}^{t+\Delta t}\hat{F}_{ij} = {}^{t+\Delta t}F_{ij} + M_{ij}\,(a_o\,{}^{t}q_j + a_2\,{}^{t}\dot{q}_j + a_3\,{}^{t}\ddot{q}_j) \qquad (3.2.5) $$

$$ + C_{ij}\,(a_1\,{}^{t}q_j + a_4\,{}^{t}\dot{q}_j + a_5\,{}^{t}\ddot{q}_j) $$

and

$$a_o = \frac{1}{\alpha\ \Delta t^2} \qquad a_1 = \frac{\zeta}{\alpha\ \Delta t} \qquad a_2 = \frac{1}{\alpha\ \Delta t}$$

$$a_3 = \frac{1}{2\alpha} - 1 \qquad a_4 = \frac{\zeta}{a} - 1 \qquad a_5 = \frac{\Delta t}{2}\left(\frac{\zeta}{\alpha} - 2\right) \qquad (3.2.6)$$

Equation (3.2.4) constitutes an equivalent static problem from which q_j can be determined. Recommended values of the α and ζ parameters are 0.25 and 0.5, respectively (Bathe, 1981). These values provide an unconditionally stable integration scheme for the linear problem and generally provide good stability characteristics for the nonlinear scheme although unconditional stability is no longer guaranteed (Bathe, 1981). The scheme has not been proven unconditionally stable for all nonlinear problems, but proofs of its unconditional stability for specific problems have been obtained (Belytschko and Schoeberle, 1975).

Once ${}^{t+\Delta t}q$ is determined, new values for ${}^{t+\Delta t}\ddot{q}$ and ${}^{t+\Delta t}\dot{q}$ for the next time increment are calculated by Equations (3.2.1) and (3.2.2). The resultant expressions are

$${}^{t+\Delta t}\ddot{q} = a_o\ ({}^{t+\Delta t}q - {}^{t}q) - a_2\ {}^{t}\dot{q} - a_3\ {}^{t}\ddot{q} \qquad (3.2.7)$$

$${}^{t+\Delta t}\dot{q} = {}^{t}\dot{q} + a_6\ {}^{t}\ddot{q} + a_7\ {}^{t+\Delta t}\ddot{q} \qquad (3.2.8)$$

where

$$a_6 = \Delta t\ (1-\zeta) \qquad a_7 = \zeta\ \Delta t \tag{3.2.9}$$

The solution for q_j from Equation (3.2.4) is strictly incremental and is not particularly accurate for nonlinear problems unless a very short time step is used.

An improved nonlinear integration scheme can be formulated by adopting a residual feedback iteration scheme at each time step. Integration at each instant in time proceeds until dynamic equilibrium is achieved. If the inertia and damping terms are treated as equivalent loads, the residual feedback scheme of Bathe, 1981 may be extended to include damping and may be written as

$$ {}^{t+\Delta t}M_{ij}^{n-1}\ {}^{t+\Delta t}\ddot{q}_j^{n} + {}^{t+\Delta t}C_{ij}^{n-1}\ {}^{t+\Delta t}\dot{q}_j^{n} + {}^{t+\Delta t}K_{ij}^{n-1}\ \Delta q_j^{n} $$

$$ = {}^{t+\Delta t}F_i^{n} - {}^{t+\Delta t}R_i^{n-1} \tag{3.2.10}$$

where

$$ {}^{t+\Delta t}q_j^{n} = {}^{t+\Delta t}q_j^{n-1} + \Delta q_j^{n} \tag{3.2.11}$$

In a manner similar to the derivation of the purely incremental scheme with Equation (3.2.11) substituted for ${}^{t+\Delta t}q_j$, Equation (3.2.10) is solved for ${}^{t+\Delta t}\Delta q_j^{n}$ to obtain

$$ {}^{t+\Delta t}\hat{K}_{ij}\,\Delta\, q_j^n = {}^{t+\Delta t}\hat{F}_i^n - {}^{t+\Delta t}R_i^{n-1} - {}^{t+\Delta t}M_{ij}^n\,(a_o\,{}^{t+\Delta t}q_j^{n-1}) $$

$$ - {}^{t+\Delta t}C_{ij}^n\,(a_1\,{}^{t+\Delta t}q_j^{n-1}) \qquad (3.2.12) $$

which is the desired recursive formula for an equivalent static problem. The solution to Equation (3.2.12) then proceeds as was described in Section 3.1 for the combined incremental and iterative statical problem.

The external force F_j^H in Equation (2.3.2) contains the hydrodynamic drag term

$$ F_j^D = \frac{1}{2}\,\rho\, C_D D\, |V_j^N|\, (\dot{u}_j^N + \dot{v}_j^N - \dot{q}_j^N) \qquad (3.2.13) $$

However, $\dot{q}_j^N$ at time $t+\Delta t$ is as yet unknown. If this nonlinear drag term in the external force is moved to the left side of Equation (3.2.10) leads to a nonlinear set of simultaneous equations. This problem is avoided in this work by using a scheme patterned after Anagnostopoulos, 1982. The value for $\dot{q}_j^N$ is the value calculated from the last time step, ${}^t\dot{q}_j^N$. The force F^D is thus calculated as

$$ {}^{t+\Delta t}F_i^{Dn} = \frac{1}{2}\,\rho\, C_D D\, |V_i^{Nn}|\,[{}^{t+\Delta t}(\dot{u}_i^{Nn} + \dot{v}_i^{Nn}) - {}^t\dot{q}_i^N] \qquad (3.2.14) $$

where

$$|V_i^N| = \left(\sum_{j=1}^{3} \left({}^{t+\Delta t}(\dot{u}_j^{Nn} + \dot{v}_j^{Nn}) - {}^{t}\dot{q}_j^{N(n-1)} \right)_i^2 \right)^{1/2} \qquad (3.2.15)$$

The drag component of the hydrodynamic force is thus approximated at the beginning of each iteration but the approximation is upgraded with each subsequent iteration.

3.3 General Derivation of Element Stiffness and Mass Matrices.

The derivation of the element stiffness matrices for use in Equations (3.1.12) and (3.2.12) may be carried out using the principle of virtual displacements and the Rayleigh-Ritz method of approximate solution. The principle of virtual displacements states that:

> "For a deformable structure in equilibrium under the action of a system of applied (external) forces, the external virtual work due to an admissible virtual displaced state is equal to the virtual strain energy due to the same displacement."
> (McGuire and Gallagher, 1979)

This principle may be expressed in indicial notation as

$$\int_V \delta\varepsilon_i \, \sigma_i \, dV - \delta q_i \, F_i = 0 \qquad (3.3.1)$$

where $\delta\varepsilon_i$ are the virtual strains, δq_i are the virtual displacements, F_i are the real loads applied to the structure, and σ_i are the real stresses resulting from the loads F_i.

The strains are related to the stresses by a constitutive relation of the form

$$\sigma_i = \sigma_{oi} + D_{ij}\ \varepsilon_j \tag{3.3.2}$$

where σ_{oi} is the initial stress and D_{ij} is the constitutive matrix which for linearly elastic isotropic materials takes the form

$$D = \frac{E\ (1-\nu)}{(1+\nu)\ (1-2\nu)} \begin{bmatrix} 1 & \frac{\nu}{1-\nu} & \frac{\nu}{1-\nu} & 0 & 0 & 0 \\ & 1 & \frac{\nu}{1-\nu} & 0 & 0 & 0 \\ & & 1 & 0 & 0 & 0 \\ & & & \frac{1-2\nu}{2(1-\nu)} & 0 & 0 \\ & \text{Sym} & & & \frac{1-2\nu}{2(1-\nu)} & 0 \\ & & & & & \frac{1-2\nu}{2(1-\nu)} \end{bmatrix} \tag{3.3.3}$$

in which E is the elastic modulus and ν is Poisson's ratio. When Equation (3.3.2) is substituted into Equation (3.3.1), the relation becomes

$$\int_V \delta\varepsilon_i\ \sigma_{oi}\ dV + \int_V \delta\varepsilon_i\ D_{ij}\ \varepsilon_j\ dV - \delta q_i\ F_i = 0 \tag{3.3.4}$$

The virtual strains are related to the virtual displacements by the relation

$$\delta\varepsilon_i = \frac{\partial\varepsilon_i}{\partial q_k}\,\delta\, q_k \tag{3.3.5}$$

which, when substituted into Equation (3.3.4) yields

$$\int_V \frac{\partial\varepsilon_i}{\partial q_k}\,\delta q_k\,\sigma_{oi}\,dV + \int_V \frac{\partial\varepsilon_i}{\partial q_k}\,\delta\, q_k\, D_{ij}\,\varepsilon_j\,dV$$

$$-\,\delta\, q_k\, F_k = 0 \tag{3.3.6}$$

Since δq_k is independent of V,

$$\delta q_k \left[\int_V \frac{\partial\varepsilon_i}{\partial q_k}\,\sigma_{oi}\,dV + \int_V \frac{\partial\varepsilon_i}{\partial q_k}\,D_{ij}\,\varepsilon_j\,dV - F_k\right] = 0 \tag{3.3.7}$$

With δq_k nonzero for nontrivial cases,

$$\int_V \frac{\partial\varepsilon_i}{\partial q_k}\,\sigma_{oi}\,dV + \int_V \frac{\partial\varepsilon_i}{\partial q_k}\,D_{ij}\,\varepsilon_j\,dV - F_k = 0 \tag{3.3.8}$$

which is the basic virtual work expression for element stiffness relations.

It remains to specify the strain-displacement relation between ε_i and q_k. The relationship between strain at a point on the element and displacement at that point is given by

$$\varepsilon_i\,(x_k) = f_{ij}\,\xi_j\,(x_k) \tag{3.3.9}$$

where ξ_j is a vector of displacement functions which describe the

deflected shape of the element. In Lagrangian coordinates f_{ij} is the Green Lagrange strain tensor for large deflection and the small displacement strain tensor for small deflection. In the finite element method, the displacements, q_k are calculated at the nodes of the elements. The displacements within the element, ξ_j are expressed in terms of the nodal displacements by means of the shape function matrix, N_{jk},

$$\xi_j = N_{jk}\, q_k \tag{3.3.10}$$

Equation (3.3.9) then becomes

$$\varepsilon_i = f_{ij}\, N_{jk} q_k \tag{3.3.11}$$

The expression $f_{ij}N_{jk}$ describes the relation between nodal displacements and the strains at any point within the element. Cook, 1981 has defined this matrix as the strain-displacement matrix

$$B_{ik} = f_{ij}N_{jk} \tag{3.3.12}$$

The strain displacement relation thus becomes

$$\varepsilon_i = B_{ik}\, q_k \tag{3.3.13}$$

When Equation (3.3.13) is substituted into Equation (3.3.8),

$$\int_V B_{ik}\,\sigma_{oi}\,dv + \int_V B_{ik}\,D_{ij}\,B_{j\ell}\,q_{j\ell}\,dV - F_k = 0 \qquad (3.3.14)$$

The values of q_k are not functions of V, and thus

$$\int_V B_{ij}\,D_{ij}\,B_{j\ell}\,dV\,q_\ell = F_k - \int_v B_{ik}\,\sigma_{oi}\,dV \qquad (3.3.15)$$

Comparing Equation (3.3.15) to Equation (3.1.4) and noting that q_ℓ is equivalent to Δq_j^n, we see that the stiffness matrix is

$$K_{k\ell} = \int_V B_{ik}\,D_{ij}\,B_{j\ell}\,dV \qquad (3.3.16)$$

and that the initial structure prestress is

$$F_k^o = \int B_{ik}\,\sigma_{oi}\,dV \qquad (3.3.17)$$

and Equation (3.3.15) may then be rewritten as

$$K_{k\ell}\,q_\ell = F_k - F_k^o \qquad (3.3.18)$$

Mass matrices may be derived in a manner analogous to the stiffness matrices. By D'Alembert's principle, $M_{ij}\,\ddot{q}_j$ may be treated as an inertia force. The terms in M_{ij} are equivalent masses. They are the mass and inertia values which when subjected to nodal accelerations apply inertia forces to the node which are the same as the inertia forces applied to the node by the continuous element undergoing the same nodal accelerations.

The kinematics of any point in an element may be expressed in terms of nodal displacements by again using the shape functions. The displacements are given by Equation (3.3.10) and the corresponding velocities and accelerations are given by

$$\dot{\xi}_k = N_{ki}\ \dot{q}_i \tag{3.3.19}$$

$$\ddot{\xi}_k = N_{ki}\ \ddot{q}_i \tag{3.3.20}$$

The inertia force at any point may be expressed by

$$P_k{}^I = N_{ki}\ \rho_{ij}\ \ddot{q}_j \tag{3.3.21}$$

where ρ_{ij} is a matrix of directionally dependent mass density terms and P_k^I is the inertia force at any point within the element. The density terms are dependent upon the directional characteristics of the effective mass and moments of inertia of the particular element.

To relate the inertia load of each P_k^I to the nodal inertia loads, again use the principle of virtual displacement.

$$F_k^I\ \delta q_k = \int_V P_k^I\ \delta\ \xi_k\ dV \tag{3.3.22}$$

When Equation (3.3.10) is substituted into Equation (3.3.22)

$$F_k^I \, \delta q_k = \int_V P_\ell^I \, N_{\ell k} \, \delta q_k \, dV \tag{3.3.23}$$

For nonzero values of δq_k, this equation may be rewritten as

$$F_k^I = \int_V N_{\ell k} \, P_\ell^I \, dV \tag{3.3.24}$$

If Equation (3.3.21) is substituted into Equation (3.3.24)

$$F_k^I = \int_V N_{\ell k} \, N_{\ell i} \, \rho_{ij} \, dV \, \ddot{q}_j \tag{3.3.25}$$

is obtained. The integral is termed the consistent mass matrix, M_{kj}, and Equation (3.3.25) becomes

$$F_k^I = M_{kj} \, \ddot{q}_j \tag{3.3.26}$$

where

$$M_{kj} = \int_V N_{\ell k} \, N_{\ell i} \, \rho_{ij} \, dV \tag{3.3.27}$$

3.4 Beam-Column Element

The beam-column element selected is a two-noded straight element. Strain deformation of the element is described by three translational and three rotational degrees of freedom at each node. The displacement, or geometric location of the element is described solely by the three translational degrees of freedom. The beam-column is thus a subparametric element. It is derived using small deflection approximations but it accounts for the non-linear effect of axial load on bending stiffness.

The stiffness matrix may be derived from Equation (3.3.16). To permit the use of reasonably large elements and still account for the effects of axial loading on bending stiffness, the element will be formulated to include the change in bending stiffness due to axial loads. Small-displacement approximations will still be made.

To deal with the axial load effects, the Green Lagrange strain tensor, F_{ij}^{GL}, must be used. This strain tensor is written as

$$
F^{GL} = \begin{bmatrix}
\frac{\partial}{\partial x_1} + \frac{1}{2}\left(\frac{\partial}{\partial x_1}\right)^2 & \frac{1}{2}\left(\frac{\partial}{2x_1}\right)^2 & \frac{1}{2}\left(\frac{\partial}{\partial x_1}\right)^2 \\
\frac{1}{2}\left(\frac{\partial}{\partial x_2}\right)^2 & \frac{\partial}{\partial x_2} + \frac{1}{2}\left(\frac{\partial}{\partial x_2}\right)^2 & \frac{1}{2}\left(\frac{\partial}{\partial x_2}\right)^2 \\
\frac{1}{2}\left(\frac{\partial}{\partial x_3}\right)^2 & \frac{1}{2}\left(\frac{\partial}{\partial x_3}\right)^2 & \frac{\partial}{\partial x_3} + \frac{1}{2}\left(\frac{\partial}{\partial x_3}\right)^2 \\
\frac{\partial}{\partial x_2} + \frac{\partial}{\partial x_1}\frac{\partial}{\partial x_2} & \frac{\partial}{\partial x_1} + \frac{\partial}{\partial x_1}\frac{\partial}{\partial x_2} & \frac{\partial}{\partial x_1}\frac{\partial}{\partial x_2} \\
\frac{\partial}{\partial x_2}\frac{\partial}{\partial x_3} & \frac{\partial}{\partial x_3} + \frac{\partial}{\partial x_2}\frac{\partial}{\partial x_3} & \frac{\partial}{\partial x_2} + \frac{\partial}{\partial x_2}\frac{\partial}{\partial x_3} \\
\frac{\partial}{\partial x_3} + \frac{\partial}{\partial x_3}\frac{\partial}{\partial x_1} & \frac{\partial}{\partial x_3}\frac{\partial}{\partial x_1} & \frac{\partial}{\partial x_1} + \frac{\partial}{\partial x_3}\frac{\partial}{\partial x_1}
\end{bmatrix}
\tag{3.4.1}
$$

It may be rewritten as the sum of the linear small displacement strain tensor, F_{ij}^{L} , and a tensor of nonlinear terms, F_{ij}^{NL} ,

$$F_{ij}^{GL} = F_{ij}^{L} + F_{ij}^{NL} \tag{3.4.2}$$

or,

$$F^{GL} = \begin{bmatrix} \frac{\partial}{\partial x_1} & & \\ & \frac{\partial}{\partial x_2} & \\ & & \frac{\partial}{\partial x_3} \\ \frac{\partial}{\partial x_2} & \frac{\partial}{\partial x_1} & \\ & \frac{\partial}{\partial x_3} & \frac{\partial}{\partial x_2} \\ \frac{\partial}{\partial x_3} & & \frac{\partial}{\partial x_1} \end{bmatrix} + \begin{bmatrix} \frac{1}{2}\left(\frac{\partial}{\partial x_1}\right)^2 & \frac{1}{2}\left(\frac{\partial}{\partial x_1}\right)^2 & \frac{1}{2}\left(\frac{\partial}{\partial x_1}\right)^2 \\ \frac{1}{2}\left(\frac{\partial}{\partial x_2}\right)^2 & \frac{1}{2}\left(\frac{\partial}{\partial x_2}\right)^2 & \frac{1}{2}\left(\frac{\partial}{\partial x_2}\right)^2 \\ \frac{1}{2}\left(\frac{\partial}{\partial x_3}\right)^2 & \frac{1}{2}\left(\frac{\partial}{\partial x_3}\right)^2 & \frac{1}{2}\left(\frac{\partial}{\partial x_3}\right)^2 \\ \frac{\partial}{\partial x_1}\frac{\partial}{\partial x_2} & \frac{\partial}{\partial x_1}\frac{\partial}{\partial x_2} & \frac{\partial}{\partial x_1}\frac{\partial}{\partial x_2} \\ \frac{\partial}{\partial x_2}\frac{\partial}{\partial x_3} & \frac{\partial}{\partial x_2}\frac{\partial}{\partial x_3} & \frac{\partial}{\partial x_2}\frac{\partial}{\partial x_3} \\ \frac{\partial}{\partial x_3}\frac{\partial}{\partial x_1} & \frac{\partial}{\partial x_3}\frac{\partial}{\partial x_1} & \frac{\partial}{\partial x_3}\frac{\partial}{\partial x_1} \end{bmatrix} \tag{3.4.3}$$

If it is assumed that:

1) torsional and shear contributions are small with respect to bending contributions for strain in the x_1' direction
2) normal strains in the x_2' and x_3' directions are negligible

3) bending deformation contributes little to torsional strain

4) the contribution of nonlinear axial deformations are small with respect to nonlinear bending deformation

5) rotational deformations are sufficiently small in bending such that the normal strain in the x_1' direction may be expressed as

$$\varepsilon_1 = \frac{\partial \xi_1}{\partial x_1'} + x_2' \frac{\partial^2 \xi_2}{\partial x_1'^2} + x_3' \frac{\partial^2 \xi_3}{\partial x_1'^2} \tag{3.4.4}$$

where $\frac{\partial^2 \xi_2}{\partial x_1'^2}$ and $\frac{2^2 \xi_3}{\partial x_1'^2}$ are the radius of curvature then Equation (3.4.3) becomes

$$f^L + f^{NL} = \begin{bmatrix} \frac{\partial}{\partial x_1'} & -x_2' \frac{\partial^2}{\partial x_1'^2} & -x_3' \frac{\partial^2}{\partial x_1'^2} \\ 0 & 0 & 0 \\ 0 & 0 & 0 \\ 0 & 0 & 0 \\ 0 & \frac{\partial}{\partial x_3} & \frac{\partial}{\partial x_2} \\ 0 & 0 & 0 \end{bmatrix} + \begin{bmatrix} 0 & \frac{1}{2}\left(\frac{\partial}{\partial x_1'}\right)^2 & \frac{1}{2}\left(\frac{\partial}{\partial x_1'}\right)^2 \\ 0 & 0 & 0 \\ 0 & 0 & 0 \\ 0 & 0 & 0 \\ 0 & 0 & 0 \\ 0 & 0 & 0 \end{bmatrix} \tag{3.4.5}$$

The shape functions, N_{jk}, assumed for the element are cubic polynomials. In local coordinates x_i' , as shown in Figure 3.4-1,

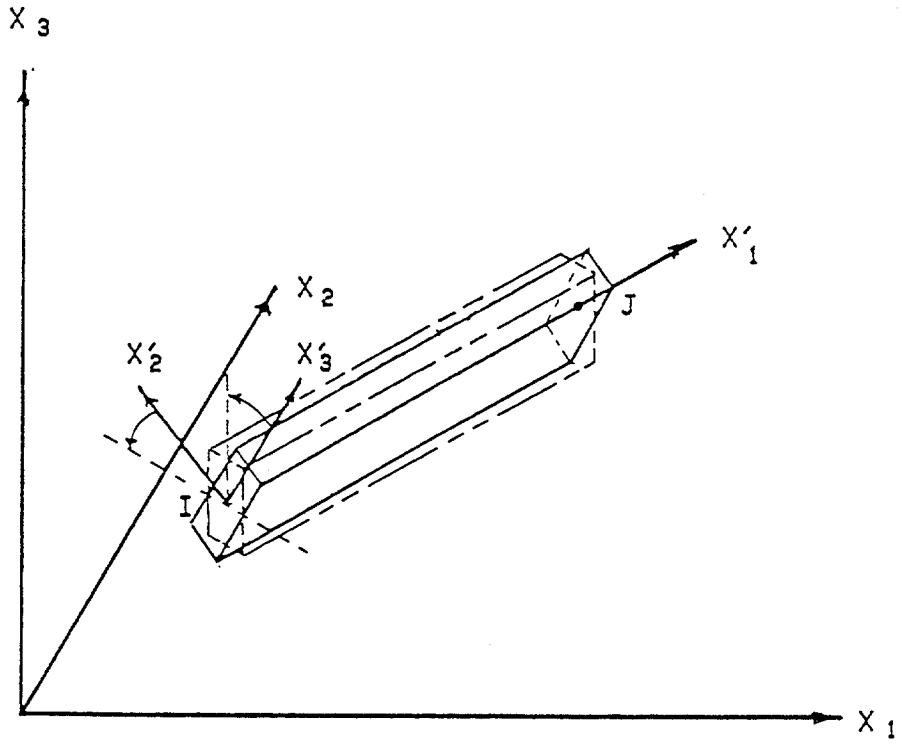

Figure 3.4-1 Definition sketch for beam-column element

the assumed shape functions for the beam-column element are

$$N = \begin{bmatrix} A & & & & B & & & \\ & C & & -D & & E & & -F \\ & & C & D & & & E & F \\ & & & A & & & B & \\ & & G & D & & & -G & F \\ & G & & & D & -G & & F \end{bmatrix} \qquad (3.4.6)$$

where

$$A = \frac{L - x_1'}{L}$$

$$B = \frac{x_1'}{L}$$

$$C = \frac{L^3 - 3L\, x_1'^2 + 2\, x_1'^3}{L^2}$$

$$D = \frac{L^2\, x_1' - 2\, L\, x_1'^2 + x_1'^3}{L^3}$$

$$E = \frac{3\, L\, x_1'^2 - 2\, x_1'^3}{L^3}$$

$$F = \frac{x_1'^3 - L\, x_1'^2}{L^3}$$

$$G = \frac{-6\, L\, x_1' + 6\, x_1'^2}{L^3}$$

When Equation (3.4.2) is substituted into Equation (3.3.12),

$$B_{ik} = (f_{ij}^{L} + F_{ij}^{NL})\ N_{jk} \tag{3.4.7}$$

is obtained. This may be rewritten as

$$B_{ik} = B_{ik}^{L} + B_{ik}^{NL} \tag{3.4.8}$$

If the symmetry of Equation (3.3.3) is recognized, Equation (3.3.16) becomes upon substitution of Equation (3.4.8),

$$K_{kl} = \int_V (B_{ik}^{L}\ D_{ij}\ B_{jl}^{L} + 2\ (B_{ik}^{L}\ D_{ij}\ B_{jl}^{NL}) + B_{ik}^{NL}\ D_{ij}\ B_{jl}^{NL})\ dV \tag{3.4.9}$$

For a beam of constant cross-section, this equation may be rewritten

$$K_{kl} = \int_L \int_A (B_{ik}^{L}\ D_{ij}\ B_{jl}^{L} + 2\ B_{ik}^{L}\ D_{ij}\ B_{jl}^{NL} + B_{ik}^{NL}\ D_{ij}\ B_{jl}^{NL})\ dA\ dx_1' \tag{3.4.10}$$

where A is the cross-sectional area of the beam and L is its length.

Integration of the first term in Equation (3.4.10) yields the linear stiffness matrix, where A is the cross-sectional area, E is the elastic modulus, J is the torsional constant, I_y and I_z are the

$$K^{BNL} = -\frac{F_1 L}{30}\begin{bmatrix}
0 & & & & & & & & & & & \\
0 & \frac{36}{L^2} & & & & & & & & & & \\
\frac{3}{L} & 0 & 4L & & & & & & & & & \\
-\frac{36}{L^2} & 0 & -\frac{3}{L} & \frac{36}{L^2} & & & & & & & & \\
\frac{3}{L} & 0 & -L & -\frac{3}{L} & 0 & 4L & & & & & & \\
0 & -\frac{36}{L^2} & -\frac{3}{L} & 0 & \frac{3}{L} & 0 & \frac{36}{L^2} & & & & & \\
0 & \frac{3}{L} & -L & -\frac{3}{L} & 0 & 2L & -\frac{3}{L} & 4L & & & & \\
-\frac{36}{L^2} & 0 & \frac{3}{L} & \frac{36}{L^2} & 0 & -\frac{3}{L} & -\frac{36}{L^2} & 0 & \frac{36}{L^2} & & & \\
\frac{3}{L} & 0 & -L & -\frac{3}{L} & 0 & 4L & -\frac{3}{L} & 2L & \frac{3}{L} & 4L & & \\
0 & -\frac{36}{L^2} & -\frac{3}{L} & 0 & \frac{3}{L} & 0 & \frac{36}{L^2} & 0 & -\frac{3}{L} & 0 & \frac{36}{L^2} & \\
0 & \frac{3}{L} & -L & -\frac{3}{L} & 0 & 2L & -\frac{3}{L} & 4L & \frac{3}{L} & 2L & -\frac{3}{L} & 4L
\end{bmatrix} \qquad (3.4.11)$$

$$
K^{BL} = E\begin{bmatrix}
\frac{A}{L} & & & & & & -\frac{A}{L} & & & & & \\
 & \frac{12I_z}{L^3} & & & \frac{6I_z}{L} & & & -\frac{12I_z}{L^3} & & & \frac{6I_z}{L^2} & \\
 & & \frac{12I_y}{L^3} & & \frac{-6I_y}{L^2} & & & & -\frac{12I_y}{L^3} & & \frac{-6I_y}{L^2} & \\
 & & & \frac{J}{2(1+\nu)L} & & & & & & \frac{-J}{2(1+\nu)L} & & \\
 & & \frac{-6I_y}{L^2} & & \frac{4I_y}{L} & & & \frac{6I_y}{L^2} & & & \frac{2I_y}{L} & \\
 & \frac{6I_z}{L} & & & & \frac{4I_z}{L} & & & -\frac{6I_z}{L^2} & & & \frac{2I_z}{L} \\
-\frac{A}{L} & & & & & & \frac{A}{L} & & & & & \\
 & -\frac{12I_z}{L^3} & & & -\frac{6I_z}{L^2} & & & \frac{12I_z}{L^3} & & & \frac{6I_z}{L^2} & \\
 & & -\frac{12I_y}{L^3} & & \frac{6I_y}{L^2} & & & & \frac{12I_y}{L^3} & & \frac{6I_y}{L^2} & \\
 & & & \frac{-J}{2(1+\nu)L} & & & & & & \frac{J}{2(1+\nu)L} & & \\
 & & \frac{-6I_y}{L^2} & & \frac{2I_y}{L} & & & \frac{6I_y}{L^2} & & & \frac{4I_y}{L} & \\
 & \frac{6I_z}{L^2} & & & & \frac{2I_z}{L} & & & \frac{6I_z}{L^2} & & & \frac{4I_z}{L}
\end{bmatrix} \qquad (3.4.12)
$$

moments of inertia about the x_2' and x_3' axes respectively and ν is Poisson's ratio.

Integration of the last two terms in Equation (3.4.10) yields the nonlinear, or geometric, stiffness matrix, where F_1 is the axial compressive force on the element.

Conversion of the derived local stiffness matrix to global coordinates for assembly into the global stiffness matrix is performed using standard transformation techniques (see Cook, 1981).

The calculation of the internal load vector for the beam element is complicated by the fact that the nodes have rotational degrees of freedom. Implicit in the assumption of small deflection beam theory is the use of small angle trigonometric function approximations. The internal loads are calculated from Equation (3.0.1) using the current element stiffness matrix and the current nodal displacements. When the element undergoes large rigid body rotations, the use of the total rotational displacement angle in Equation (3.0.1) will lead to erroneous results since the small angle approximations which were used in the development of the element are no longer valid.

In order to correctly calculate the large deflection internal load vector using updated Lagrangian coordinates and the small deflection beam element, it is necessary to calculate the relatively large rigid body rotation angle and to subtract it from the total nodal rotations. The resultant relative angles of rotation are small, provided the structure is initially well-proportioned or

provided there is a sufficiently fine discretization to keep the relative angle small. Figure 3.4-2 (after Cook, 1981) illustrates the problem in a two dimensional space. The element in its initial configuration has a chord oriented at some angle $\beta°$. After the beam undergoes large rigid body displacement and deformation, the element chord lies at a new angle β^N described by $\tan^{-1} \frac{s_2^N}{s_1^N}$. The relative angles of rotation of the deformed element in its displaced configuration are the rotation angles of the nodes minus the rotation angle of the chord. These relative angles are the ones used in calculating the internal load vector for the element.

In a three-dimensional space the procedure becomes more involved. Figure 3.4-3 shows the scheme extended to a three dimensional space. For the arbitrarily oriented element as shown in the figure, this extension requires more computation, but it is straightforward. A problem arises, however when the element happens to lie along a coordinate axis. Its projection into the plane normal to that axis is a point and β is consequently undefined.

The method used in this analysis to permit a member to lie on an axis is to always work in the current local coordinate element reference frame when calculating the internal load vector. In this reference frame the element always lies along the x_1' axis and the current β angle in the $x_2' - x_3'$ plane is undefined. The rigid body rotation about the chord is set to zero. Since linear torsional theory does not require small angle trigonometric approximations and since the torsion was assumed uncoupled in developing the

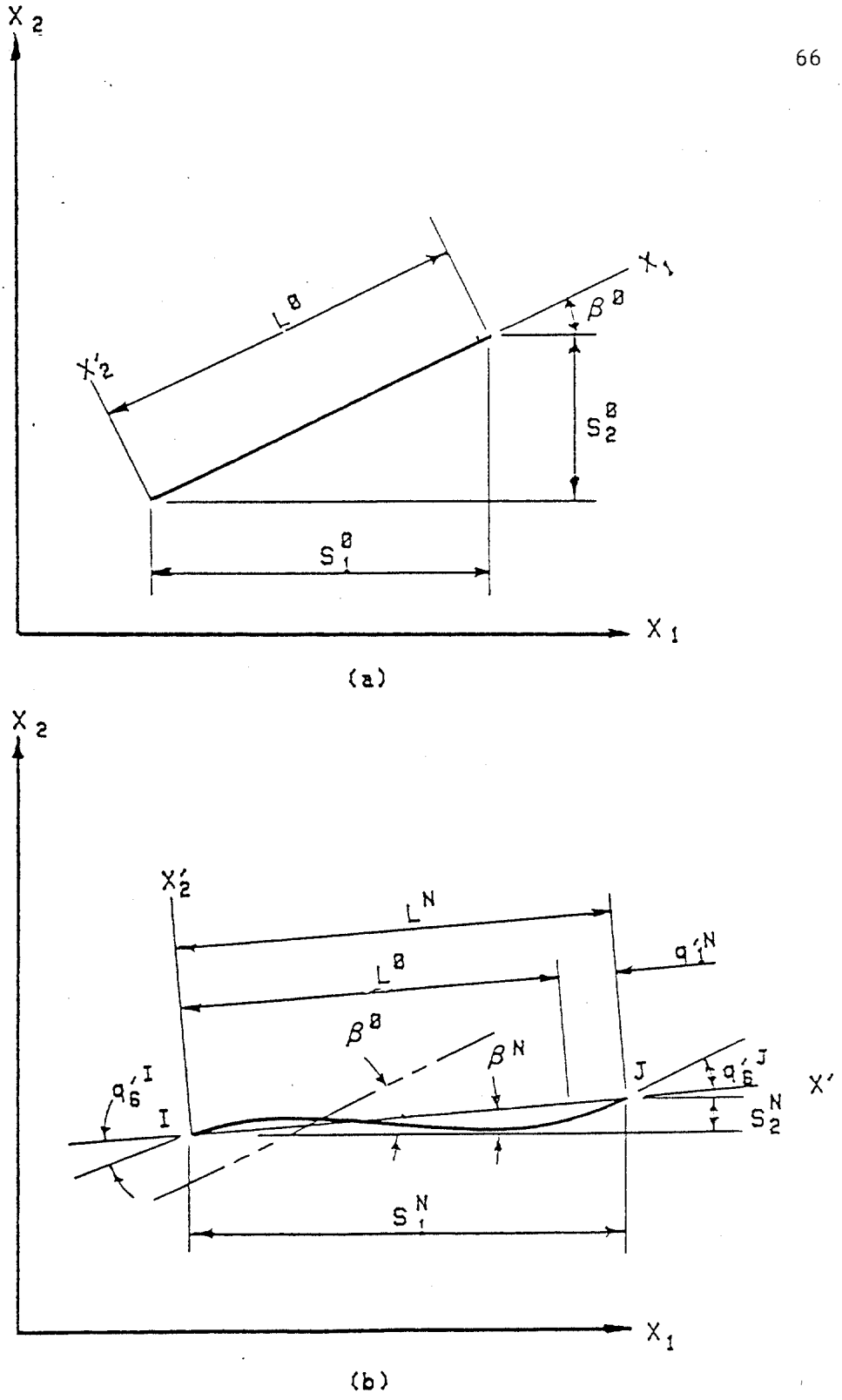

Figure 3.4-2 Two dimensional large-deflection rotation schematic

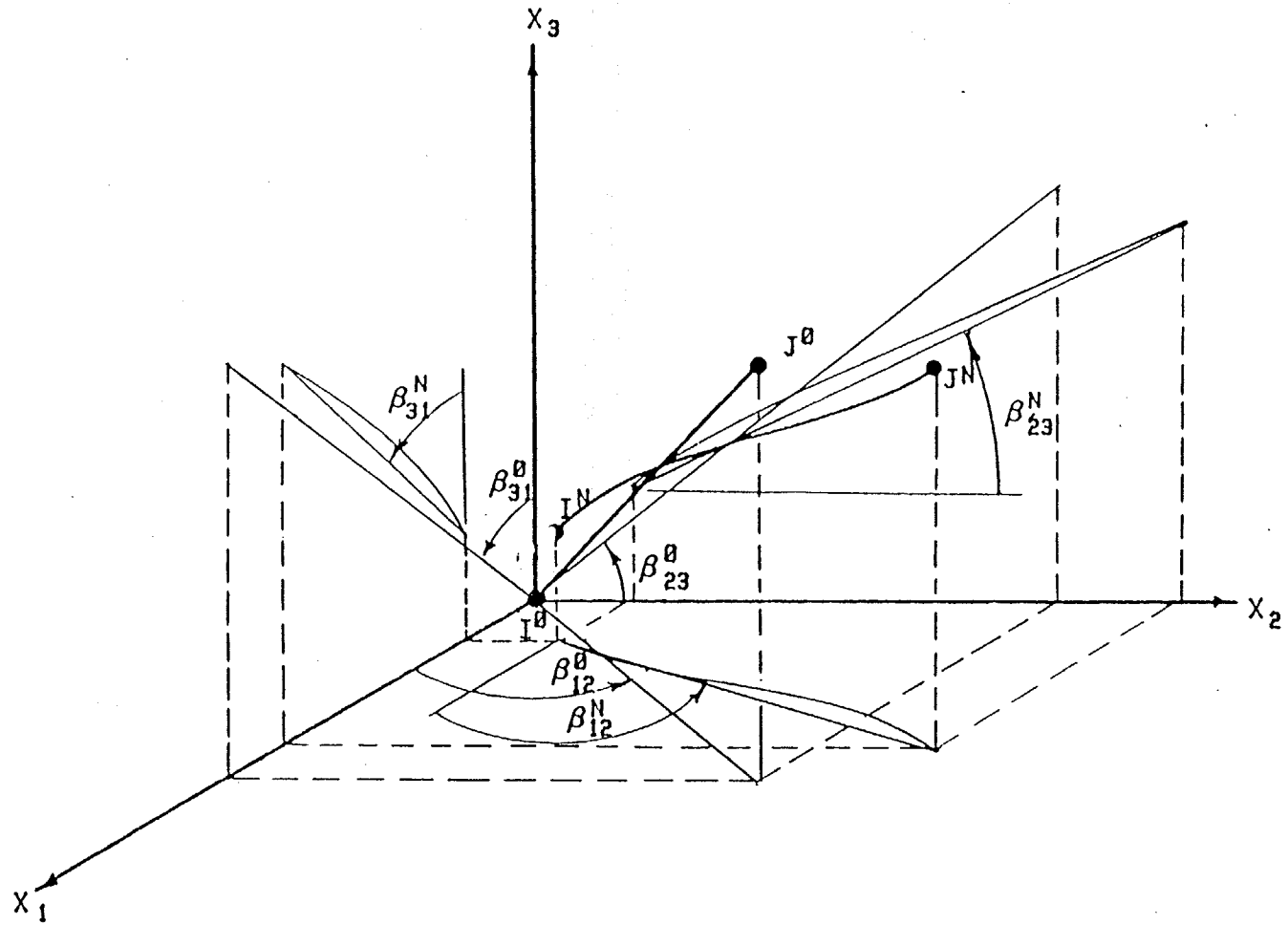

Figure 3.4-3 Three dimensional large-deflection rotation schematic

stiffness matrix, setting β_{23} to zero is consistent with previous assumptions. To calculate the β_{12} and β_{13} angles, the original position global nodal coordinates are transformed to the local nodal coordinates in the current position and the rotation angles are calculated as in the two dimensional case of Figure 3.4-2. Now the x_1' axis points out of the plane of the figure and the deformed shape shown in the figure is the projection of the deformed shape into the appropriate plane. The angles obtained are the negatives of the desired β angles since they were obtained in the current reference frame rather than in the Lagrangian reference frame.

The consistent mass matrix for the beam element may be derived using the assumed shape functions of Equation (3.4.6) and the mass density matrix

$$\rho = \begin{bmatrix} \rho^b & 0 & 0 \\ 0 & \rho^b + \rho^{am} & 0 \\ 0 & 0 & \rho^b + \rho^{am} \end{bmatrix} \qquad (3.4.13)$$

where ρ^b is the beam mass density and ρ^{am} is the equivalent added mass density due to hydrodynamic flow.

When the integration is performed in the x_2' and x_3' directions, Equation (3.3.27) becomes

$$M_{kj} = A \int_L N_{1k} N_{1i} \rho_{ij} dx'_1 \qquad (3.4.14)$$

where ρ_{ij} is a discontinuous function of x'_1 for the general case of an element piercing the water surface. The integral may be written as the sum of two integrals

$$M_{kj} = A \left[\int_o^a N_{1k} N_{1i} \rho_{ij}^{(1)} dx'_1 + \int_a^L N_{1k} N_{ki} \rho_{ij}^{(2)} dx'_1 \right] \qquad (3.4.15)$$

where a is the location of the water line on the element x'_1 axis, and in the discontinuous density, $\rho_{ij}^{(n)}$, the added mass contributions, ρ^{am}, is a nonzero constant for the submerged portion of the member and zero for the portion of the member above the water surface. If the inertia terms resulting from rotations of the beam cross sections are neglected, the mass matrix becomes

$$
M = \begin{bmatrix}
M_1 & & & & M_7 & & & & \\
 & M_2 & & & M_6 & M_9 & & & M_{17} \\
 & & M_3 & M_5 & & & M_{11} & M_{16} & \\
 & & M_4 & & & & M_{15} & & \\
 & & & M_8 & & & M_{14} & M_{19} & \\
 & & & & M_{10} & M_{13} & & & M_{21} \\
 & & & & & M_{12} & & & \\
 & & & & & & M_{18} & & M_{22} \\
 & & & \text{Sym} & & & M_{20} & M_{23} & \\
 & & & & & & & M_{22} & \\
 & & & & & & & & M_{25} \\
 & & & & & & & & M_{26}
\end{bmatrix} \qquad (3.4.16)
$$

where M_i are given in Table 3.4.1

Table 3.4.1 Terms in Beam-column Consistent Mass Matrix

$$M_1 = \frac{A}{L^2}\left[\rho^{(1)}\left(L^2a - La^2 + \frac{a^3}{3}\right) + \rho^{(2)}\left(\frac{L^3}{3} - L^2a - La^2 - \frac{a^3}{3}\right)\right]$$

$$M_2 = \frac{A}{L^6}\left[\rho^{(1)}\left(L^6a - 2L^4a^3 + L^3a^4 + \frac{a}{5}L^2a^5 - 2La^6 + \frac{4}{7}a^7\right)\right.$$
$$\left. + \rho^{(2)}\left(\frac{13}{35}L^7 - \left(L^6a - 2L^4a^3 + L^3a^4 + \frac{a}{5}L^2a^5 - 2La^6 + \frac{4}{7}a^7\right)\right)\right]$$

$$M_3 = M_2$$

$$M_4 = M_1$$

$$M_5 = -M_6$$

$$M_6 = \frac{A}{L^5}\left[\rho^{(1)}\left(\frac{1}{2}a^2L^5 - \frac{2}{3}a^3L^4 - \frac{1}{2}a^4L^3 + \frac{8}{5}a^5L^2 - \frac{7}{6}a^6L + \frac{2}{7}a^7\right) + \rho^{(2)}\left(\frac{11}{210}L^7 - \left(\frac{1}{2}a^2L^5 - \frac{2}{3}a^3L^4 - \frac{1}{2}a^4L^3 + \frac{8}{5}a^5L^2 - \frac{7}{6}a^6L + \frac{2}{7}a^7\right)\right)\right]$$

$$M_7 = \frac{A}{L^2}\left[\rho^{(1)}\left(\frac{La^2}{2} - \frac{a^3}{3}\right) + \rho^{(2)}\left(\frac{L^3}{6} - \frac{La^2}{2} + \frac{a^3}{3}\right)\right]$$

$$M_8 = \frac{A}{L^4}\left[\rho^{(1)}\left(\frac{1}{3}a^3L^4 - a^4L^3 + \frac{6}{5}a^5L^2 - \frac{2}{3}a^6L + \frac{1}{7}a^7\right)\right.$$
$$\left. + \rho^{(2)}\left(\frac{L^7}{105} - \left(\frac{1}{3}a^3L^4 - a^4L^3 + \frac{6}{5}a^5L^2 - \frac{2}{3}a^6L + \frac{1}{7}a^7\right)\right)\right]$$

$$M_9 = \frac{A}{L^6}\left[\rho^{(1)}\left(L^4a^3 - \frac{1}{2}L^3a^4 - \frac{9}{5}L^2a^5 + 2La^6 - \frac{4}{7}a^7\right)\right.$$
$$\left. + \rho^{(2)}\left(\frac{27}{210}L^7 - \left(L^4a^3 - \frac{1}{2}L^3a^4 - \frac{9}{5}L^2a^5 + 2La^6 - \frac{4}{7}a^7\right)\right)\right]$$

$$M_{10} = M_8$$

Table 3.4.1 Terms in Beam-column Consistent Mass Matrix (Cont.)

$$M_{11} = M_9$$

$$M_{12} = \frac{A}{L^2}\left[\rho^{(1)}\left(\frac{a^3}{3}\right) + \rho^2\left(\frac{L^3 - a^3}{3}\right)\right]$$

$$M_{13} = \frac{A}{L^5}\left[\rho^{(1)}\left(\frac{3}{4}a^4 L^3 - \frac{8}{5}a^5 L^2 + \frac{7}{6}a^6 L - \frac{2}{7}a^7\right)\right.$$

$$\left. + \rho^{(2)}\left(\frac{13}{420}L^7 - \left(\frac{3}{4}a^4 L^3 - \frac{8}{5}a^5 L^2 + \frac{7}{6}a^6 L - \frac{2}{7}a^7\right)\right)\right]$$

$$M_{14} = - M_{13}$$

$$M_{15} = M_7$$

$$M_{16} = - M_{17}$$

$$M_{17} = \frac{A}{L^5}\left[\rho^{(1)}\left(-\frac{1}{3}L^4 a^3 + \frac{1}{4}L^3 a^4 + \frac{3}{5}L^2 a^5 - \frac{5}{6}L a^6 + \frac{2}{7}a^7\right)\right.$$

$$+ \rho^{(2)}\left(-\frac{13}{420}L^7 - \left(-\frac{1}{3}L^4 a^3 + \frac{1}{4}L^3 a^4 + \frac{3}{5}L^2 a^5\right.\right.$$

$$\left.\left. - \frac{5}{6}L a^6 + \frac{2}{7}a^7\right)\right)\Bigg]$$

$$M_{18} = \frac{A}{L^6}\left[\rho^{(1)}\left(\frac{9}{5}L^2 a^5 - 2La^6 + \frac{4}{7}a^7\right) + \rho^{(2)}\left(\frac{39}{105}L^2\right.\right.$$

$$\left.\left. - \left(\frac{9}{5}L^2 a^5 - 2La^6 + \frac{4}{7}a^7\right)\right)\right]$$

$$M_{19} = M_{21}$$

$$M_{20} = M_{18}$$

$$M_{21} = \frac{A}{L^4}\left[\rho^{(1)}\left(-\frac{1}{4}L^3 a^4 + \frac{3}{5}L^2 a^5 - \frac{1}{2}L a^6 + \frac{1}{7}a^7\right)\right.$$

$$\left. + \rho^{(2)}\left(-\frac{1}{140}L^7 - \left(-\frac{1}{4}L^3 a^4 + \frac{3}{5}L^2 a^5 - \frac{1}{2}L a^6 + \frac{1}{7}a^7\right)\right)\right]$$

Table 3.4.1 Terms in Beam-column Consistent Mass Matrix (Cont.)

$$M_{22} = M_{12}$$

$$M_{23} = - M_{24}$$

$$M_{24} = \frac{A}{L^5}\left[\rho^{(1)}\left(-\frac{3}{5}a^5L^2 + \frac{5}{6}a^6L - \frac{2}{7}a^7\right) + \rho^{(2)}\left(-\frac{11}{210}L^7 - \left(-\frac{3}{5}a^5L^2 + \frac{5}{6}a^6L - \frac{2}{7}a^7\right)\right)\right]$$

$$M_{25} = \frac{A}{L^4}\left[\rho^{(1)}\left(\frac{1}{7}a^7 - \frac{1}{3}La^6 + \frac{1}{5}L^2a^5\right) + \rho^{(2)}\left(\frac{1}{105}L^7 - \left(\frac{1}{7}a^7 - \frac{1}{3}La^6 + \frac{1}{5}L^2a^5\right)\right)\right]$$

$$M_{26} = M_{25}$$

3.5 Cable Element

The cable element is a two-noded isoparametric element in which both displacement and deformation are described by nodal translations. It is a straight element (Figure 3.5-1) which uses a linear interpolating function to describe the variation in tension between nodes.

In the local coordinate system, the assumed shape functions are

$$N = \begin{bmatrix} 1 - \frac{x_1'}{L} & 0 & 0 & \frac{x_1'}{L} & 0 & 0 \\ 0 & 1 - \frac{x_1'}{L} & 0 & 0 & \frac{x_1'}{L} & 0 \\ 0 & 0 & 1 - \frac{x_1'}{L} & 0 & 0 & \frac{x_1'}{L} \end{bmatrix} \quad (3.5.1)$$

Tuah, 1982 has derived the linear and nonlinear stiffness matrices for updated Lagrangian coordinates in the global reference frame. The linear stiffness matrix is given by

$$K^{CL} = \frac{T}{L} \begin{bmatrix} 1 & 0 & 0 & -1 & 0 & 0 \\ & 1 & 0 & 0 & -1 & 0 \\ & & 1 & 0 & 0 & -1 \\ & & & 1 & 0 & 0 \\ & & \text{Sym} & & 1 & 0 \\ & & & & & 1 \end{bmatrix} \quad (3.5.2)$$

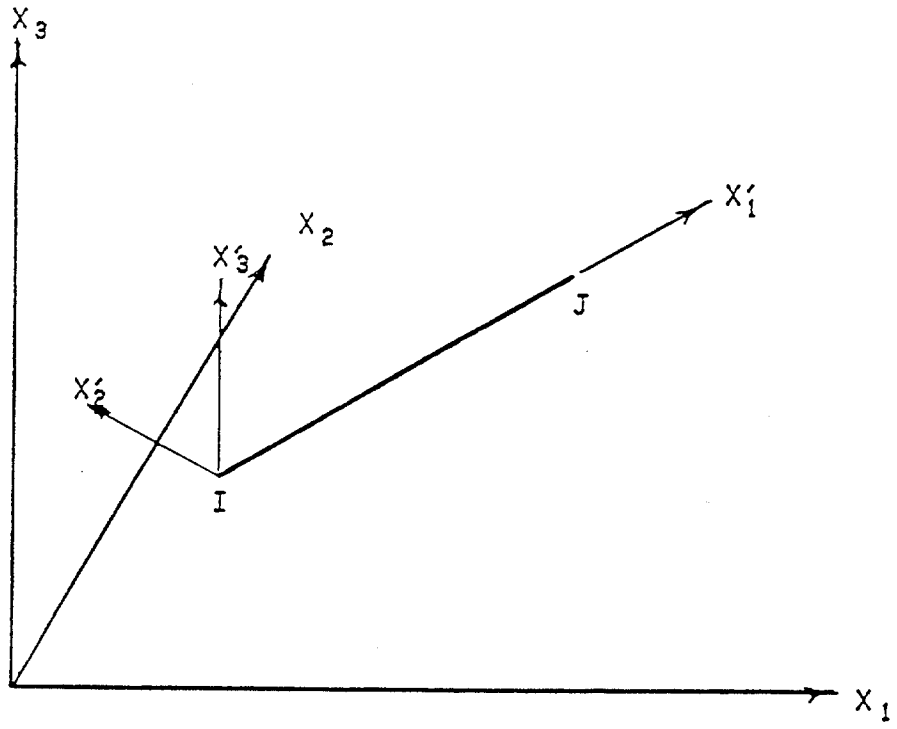

Figure 3.5-1 Definition sketch for the cable element

Here T is the cable tension and L is the element length in the updated reference configuration. The values of T and L are given by

$$T = T_o + \Delta T \tag{3.5.3}$$

$$L = L_o + \Delta L \tag{3.5.4}$$

where the subscript, o, indicates the initial value.

The nonlinear matrix is given by

$$K^{CNL} = \frac{A_o\ E}{L_o\ L^2} \begin{bmatrix} [C^{11}]_{3x3} & [C^{12}]_{3x3} \\ [C^{21}]_{3x3} & [C^{22}]_{3x3} \end{bmatrix} \tag{3.5.5}$$

where

$$C_{ij}^{11} = C_{ij}^{22} = x_i^I\ x_j^I - (x_i^I\ x_j^J + x_i^J\ x_j^I) + x_i^J\ x_j^J$$

$$C_{ij}^{12} = C_{ij}^{21} = -\ C_{ij}^{11} \tag{3.5.6}$$

The values x_i^I and x_i^J are the current global coordinates of the element I node and J node respectively.

Tuah, 1982 has shown that the internal load vector may be calculated by

$$R_i = K_{ij}^{CL} x_j \tag{3.5.7}$$

where x_j are the global coordinates of the element nodes in the current configuration.

The consistent mass matrix for the cable element may be developed in a manner similar to the beam mass matrix. It is assumed that the cable never pierces the water surface so the added mass is continuous over the entire element. Equation (3.3.24) may be evaluated using the assumed shape functions, Equation (3.5.1) and the mass density matrix

$$\rho = \begin{bmatrix} \rho^c & & & & & \\ & \rho^c + \rho^{am} & & & & \\ & & \rho^c + \rho^{am} & & & \\ & & & \rho^c & & \\ & & & & \rho^c + \rho^{am} & \\ & & & & & \rho^c + \rho^{am} \end{bmatrix} \tag{3.5.8}$$

where ρ^c is the cable mass density. Again performing the integration in the x_2' and x_3' directions, Equation (3.3.24) becomes Equa-

tion (3.4.10) where A is now the cross sectional area of the cable. Evaluating the integral, the mass matrix becomes

$$M^c = \frac{1}{6}\begin{bmatrix} 2m' & 0 & 0 & m' & 0 & 0 \\ & 0 & 0 & 0 & m & 0 \\ & 2m & 0 & 0 & 0 & m \\ & & 2m & 0 & 0 & 0 \\ & & & 2m' & 0 & 0 \\ & \text{Sym} & & & 2m & 0 \\ & & & & & 2m \end{bmatrix} \qquad (3.5.9)$$

where

$$m' = \rho^c A_o L_o$$

$$m = [\rho^c + \rho^{am}] A_o L_o \qquad (3.5.10)$$

and L_o is the initial element length. The matrix is converted from local to global coordinates using standard transformation methods.

3.6 Foundation Element

The foundation element is assumed to be oriented in global coordinates and maybe represented schematically as shown in Figure 3.6.1. Its stiffness matrix may be written by inspection as

$$K^F = \begin{bmatrix} K_{x_1} & & & & & \\ & K_{x_2} & & & & \\ & & K_{x_3} & & & \\ & & & K_{x_4} & & \\ & & & & K_{x_5} & \\ & & & & & K_{x_6} \end{bmatrix} \qquad (3.6.1)$$

The damping may likewise be written as

$$C^F = \begin{bmatrix} C_{x_1} & & & & & \\ & C_{x_2} & & & & \\ & & C_{x_3} & & & \\ & & & C_{x_4} & & \\ & & & & C_{x_5} & \\ & & & & & C_{x_6} \end{bmatrix} \qquad (3.6.2)$$

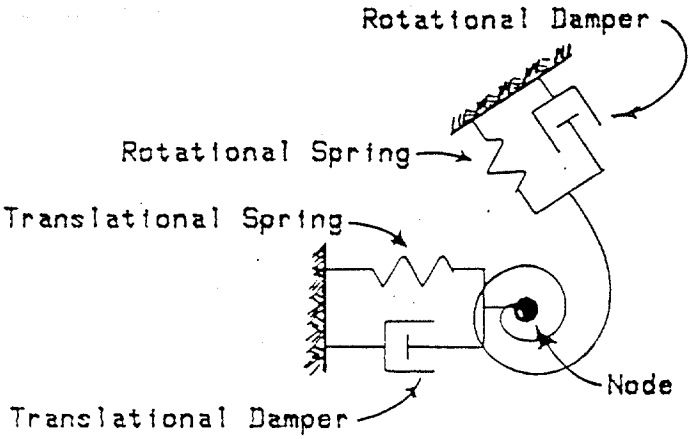

VIEW A-A

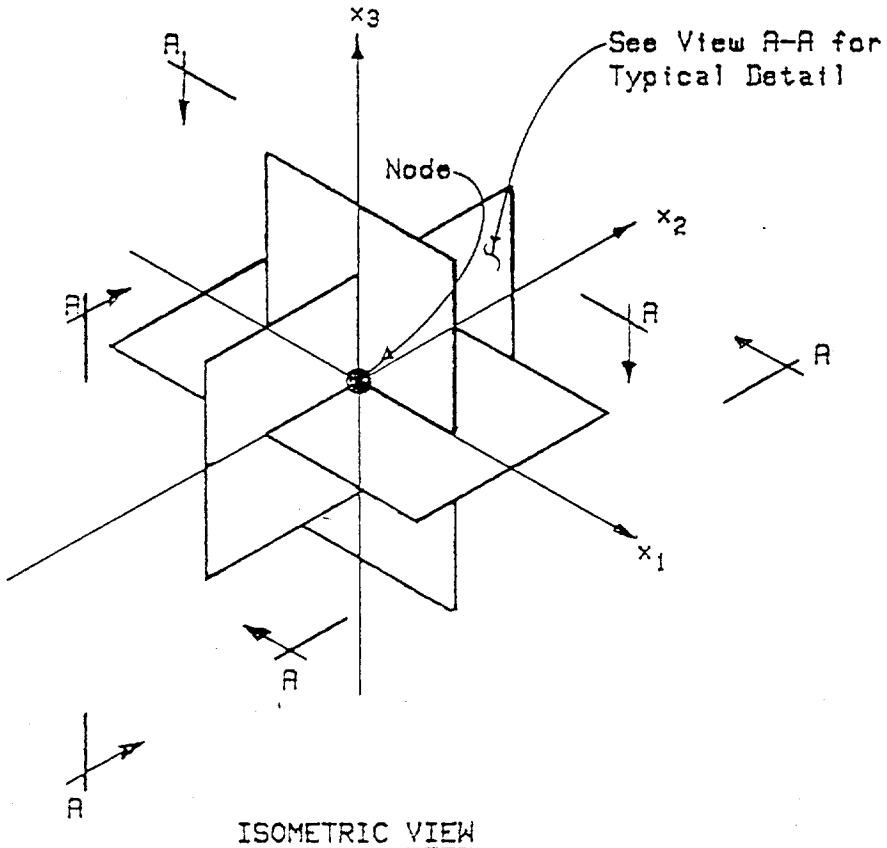

ISOMETRIC VIEW

Figure 3.6-1 Foundation element schematic

3.7 Load Discretization

Concentrated loads are applied directly to the nodes but distributed loads on elements due to gravity, buoyancy, current, and waves must be transformed to equivalent loads applied at the nodes. The nodal loads that are sought are those which, if applied to the element at the nodes, would produce the same strain energy in the element as the distributed load would when the element nodal degrees of freedom are fixed.

These fixed end forces may be derived using virtual displacement principles. Using the general statement of the principle of virtual displacements, (Section 3.3), one may express the relation between strain energy and external work as

$$\int_V \delta\varepsilon_i \, \sigma_i \, dV - \int_V \delta\xi_i \, P_i \, dV = 0 \qquad (3.7.1)$$

where P_i are the external loads and $\delta\xi_i$ are the virtual displacements. If Equation (3.3.1) is now substituted into Equation (3.7.1),

$$\int_V \delta\xi_i \, P_i \, dV = \delta q_k \, F_k \qquad (3.7.2)$$

is obtained. Substitution of Equation (3.3.10) gives

$$\int_V (N_{ik}\delta q_k) \, P_i \, dV = \delta q_k \, F_k \qquad (3.7.3)$$

Since δq_k is not a function of V and since it is an arbitrary non-zero value, Equation 3.7.3 can be written

$$\int_V N_{ik} P_i \, dV = F_k \tag{3.7.4}$$

For one-dimensional elements such as the cable and the beam, the equation simplifies to

$$\int_o^L N_{ik} P_i \, (x_1') \, dx_1' = F_k \tag{3.7.5}$$

This equation is then solved either exactly or using the Rayleigh-Ritz method for the reaction at the nodes, F_k. For beam and cable elements exact solutions are possible and the nodal forces are recognized as the fixed end forces of elementary structural analysis.

Since the orientations of the elements are varied and since the hydrodynamic loads are calculated normal to the individual element axes, all loads are calculated using local element coordinates. The loads are summed after being transformed to the global reference frame.

Gravity loads are assumed uniform along the element length. The total global gravity load is transformed into components tangential to and normal to the element and the forces are distributed to the nodes by the relations.

$$F_i^G = \frac{P_i^G}{2} \qquad i = 1,3$$

$$F_j^G = \frac{P_i^G\, L}{12} \qquad i = 2,3 \text{ and } j = i + 3 \tag{3.7.1}$$

where P_i^G is the total weight component in the x_1' direction. Since both the cable and beam elements are straight, the torsional load F_4^G is zero. Likewise $F_5^G = F_6^G = 0$ for the cable element since it possesses no bending stiffness.

Buoyancy loads are assumed to act over elements with constant cross-section and hence with uniform displaced volume. But, since elements may pierce the surface, the buoyancy load is not necessarily continuous over the entire length of the element. The hydrodynamic loading may also be discontinuous for the same reason plus the loading is generally not uniform over the submerged part of the element. Since the buoyant load may be considered as a special case of the more general hydrodynamic load, the two are handled in the same manner.

In order to allow the use of reasonably large elements and to produce an accurate load profile for arbitrarily defined combinations of wave, current, and buoyancy, a load influence function is used to calculate the fixed and forces. If the reactions due to a point load of unit magnitude on the element are known, the reactions from any load distribution may be calculated as the sum of the reactions due to a series of point loads whose magnitudes are determined by the loading function. Figure 3.7-1 shows the

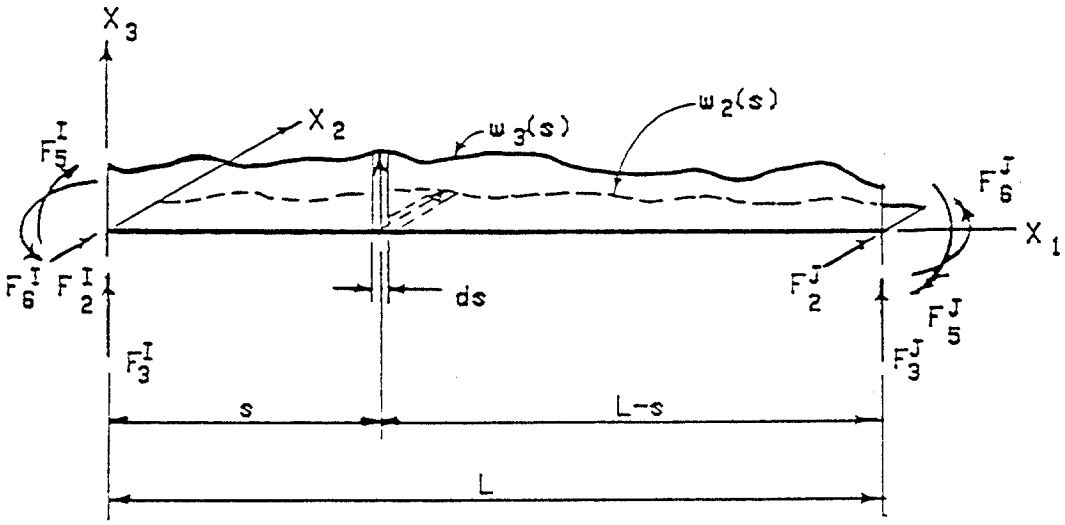

Figure 3.7-1 Fixed end forces due to distributed load

basic element with a transverse load of intensity, w (s). The total fixed end forces due to the load may be shown to be

$$F_1^I = \int_o^L \frac{w_1(s)}{L} (L-s)\, ds$$

$$F_i^I = \int_o^L \frac{w_i(s)}{L^3} (L^3 - 3\, s^2\, L + 2\, s^3)\, ds \qquad i = 2,3$$

$$F_j^I = \int_o^L \frac{w_i(s)}{L^3} (sL^2 - 2s^2\, L + s^3)\, ds \qquad i = 2,3 \;\&\; j = i + 3$$

and (3.7.2)

$$F_1^J = \int_o^L \frac{w_1(s)}{L} s\, ds$$

$$F_i^J = \int_o^L \frac{w_i(s)}{L^3} (3L\, s^2 - 2\, s^3)\, ds \qquad i = 2,3$$

$$F_j^J = \int_o^L \frac{w_i(s)}{L^2} (s^2\, L - s^3)\, ds \qquad i = 2,3 \;\&\; j = i+3$$

It is assumed that no torsional loads are applied between nodes so $F_4^I = F_4^J = 0$. Also for the cable elements, which have no rotational degrees of freedom, $F_j^I = F_j^J = 0$, $j = i + 3$.

To permit the use of an arbitrary current profile and also to reduce computational effort, the hydrodynamic load intensities are calculated at a fixed number (20) of equally spaced elevations from sea bottom to the still water line. Between each elevation load intensity is assumed to vary linearly. Figure 3.7-2 shows an

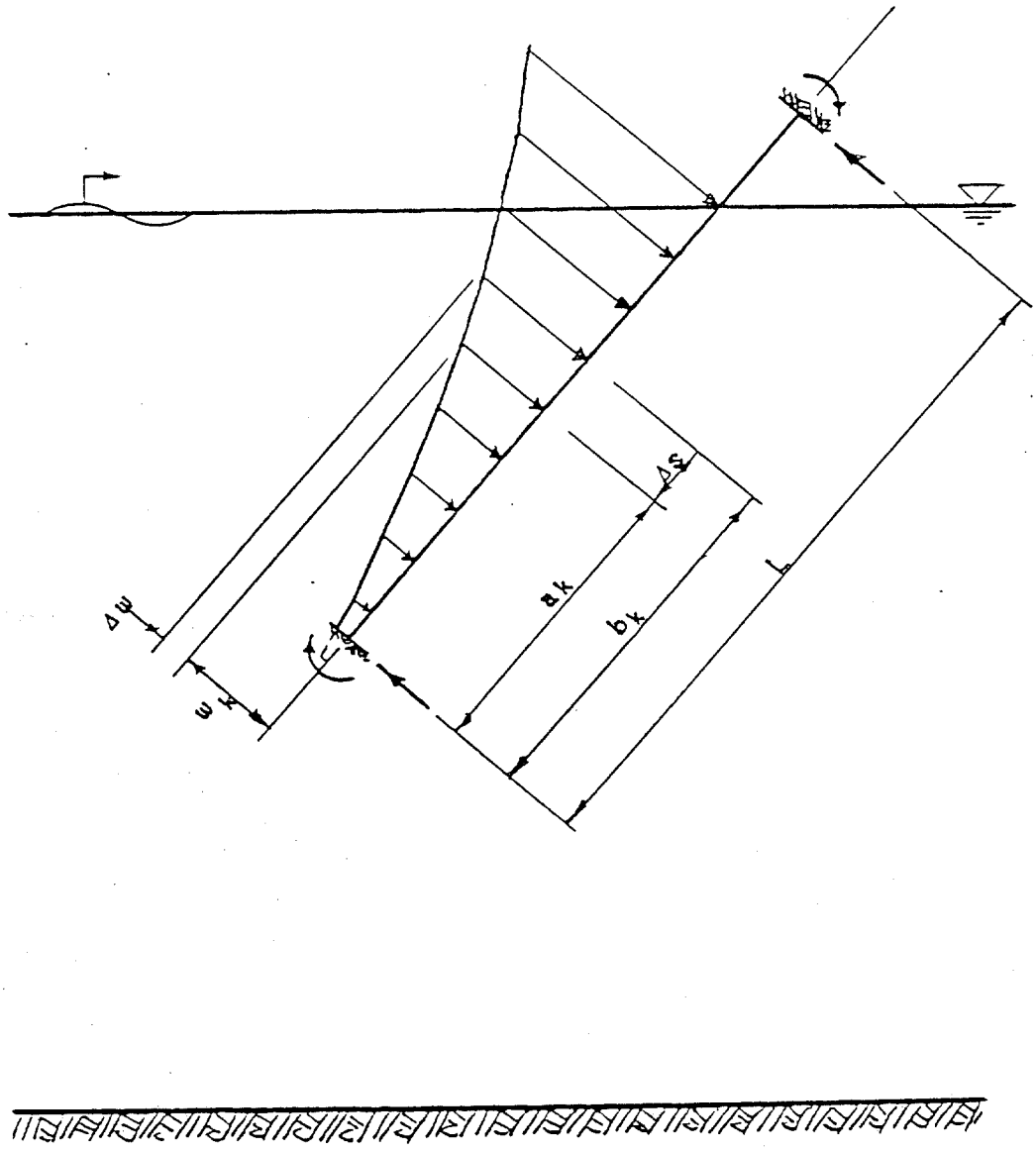

Figure 3.7-2 Hydrodynamic load and fixed end force discretization

element arbitrarily oriented in the water with the discretized load profile imposed on it.

The fixed end forces are calculated by first interpolating to find the load intensity at the submerged element end nodes and to find the location with respect to node I of the remaining calculated load intensities. Then the fixed end forces due to each trapezoidal load prism are calculated. Using Equation (3.7.2) and assuming a trapezoidal load prism, one can show that

$$F_i^I = \sum_{k=1}^{N} \frac{1}{L^3} \left[Y L^3 s + \frac{Z}{2} L^3 s^2 - Y L s^3 + \frac{2Y-3ZL}{4} s^4 + \frac{2}{5} Z s^5 \right] \Big|_{a_k}^{b_k}$$

$$F_j^I = \sum_{k=1}^{N} \frac{1}{L^2} \left[\frac{Y}{2} L^2 s^2 + \frac{ZL^2-2YL}{3} s^3 + \frac{Y-2ZL}{4} s^4 + \frac{Z}{5} s^5 \right] \Big|_{a_k}^{b_k}$$

and (3.7.3)

$$F_i^J = \sum_{k=1}^{N} \frac{1}{L^3} \left[YL s^3 - \frac{2Y - 3ZL}{4} s^4 - \frac{2}{5} Z s^5 \right] \Big|_{a_k}^{b_k}$$

$$F_j^J = \sum_{k=1}^{N} \frac{1}{L^2} \left[\frac{Y}{3} L s^3 - \frac{Y - ZL}{4} s^4 - \frac{1}{5} Z s^5 \right] \Big|_{a_k}^{b_k}$$

for $i = 2,3$ and $j = i + 3$. The constants Y and Z are given by

$$Y = w_k - \frac{\Delta w}{\Delta s} s_a$$

$$Z = \frac{\Delta w}{\Delta s} \qquad (3.7.4)$$

where w_{a_k} is the load intensity at location a_k, Δw is the change in load intensity between a_k and b_k, s_a is the distance from the origin to point a_k and Δs is the distance between the known load intensity points.

4.0 Validation Problems and Results

The computer program developed to implement the algorithms presented in the previous chapter was validated by a series of test problems. The first seven problems were used to check individual program segments and solution schemes. Known experimental or analytic solutions are used as a basis for comparison. The remaining two problems are of a more general nature and do not have direct quantitative comparison to other work although they may be compared qualitatively to other solutions.

Problem 1 is a large deflection analysis of a cantilever beam with a concentrated load at its tip. Problem 2 is a dynamic analysis of a simple pendulum in which a beam element is used as the pendulum arm. Problem 3 is a large deflection analysis of a taut string with a transverse point load applied at midspan. Problem 4 is a large deflection analysis in which a concentrated mass is supported by a taut string and allowed to vibrate freely. In Problem 5 a steady hydrodynamic loading due to current is applied to a model of an articulated tower and the angle of inclination of the tower is calculated. Problem 6 is the steady state solution of a cable with a spherical mass at its end towed at constant speed in water.

In Problem 7 the articulated tower is subjected to waves only and then to waves in the presence of a cross current. For Problem 8, the dynamic response of a two dimensional model of a guyed tower is analyzed using two differing assumptions with respect to cable

behavior: 1) with the hydrodynamic loads and the inertia loads of the cable included in the analysis; and 2) with the cables acting in a quasistatic manner as springs with load-deflection characteristics identical to the static catenary cable. The last problem is a dynamic analysis of a tension leg structure. The analysis is performed in two-dimensional space and the structure is subjected to wave loads.

4.1 Problem 1: Static Point Load on a Cantilever Beam

This problem demonstrates the acceptability 1) of the large-deflection nonlinear analysis technique, 2) of the stiffness formulation for the beam element, and 3) of the fundamental core of equation solver and bookkeeping routines in the computer program. A one element and a five element problem were considered. A load of 95,413 N. was applied in six equal load steps and a convergence tolerance of 0.01 was required. The beam has the following properties:

Elastic Modulus	$2. \times 10^{11}$ Pa
Cross-sectional Area	1.456 m^2
Second Moment of the Area	3.58 m^4
Length	150 m

The nondimensionalized deflections are plotted in Figure 4.1-1. The solid curve is a plot of the large deflection analytic solution obtained by Frisch-Fay, 1962. The data in the figure show that the element formulation and updated Lagrangian solution algorithm yield excellent results for this problem even when a coarse, one-element discretization is chosen.

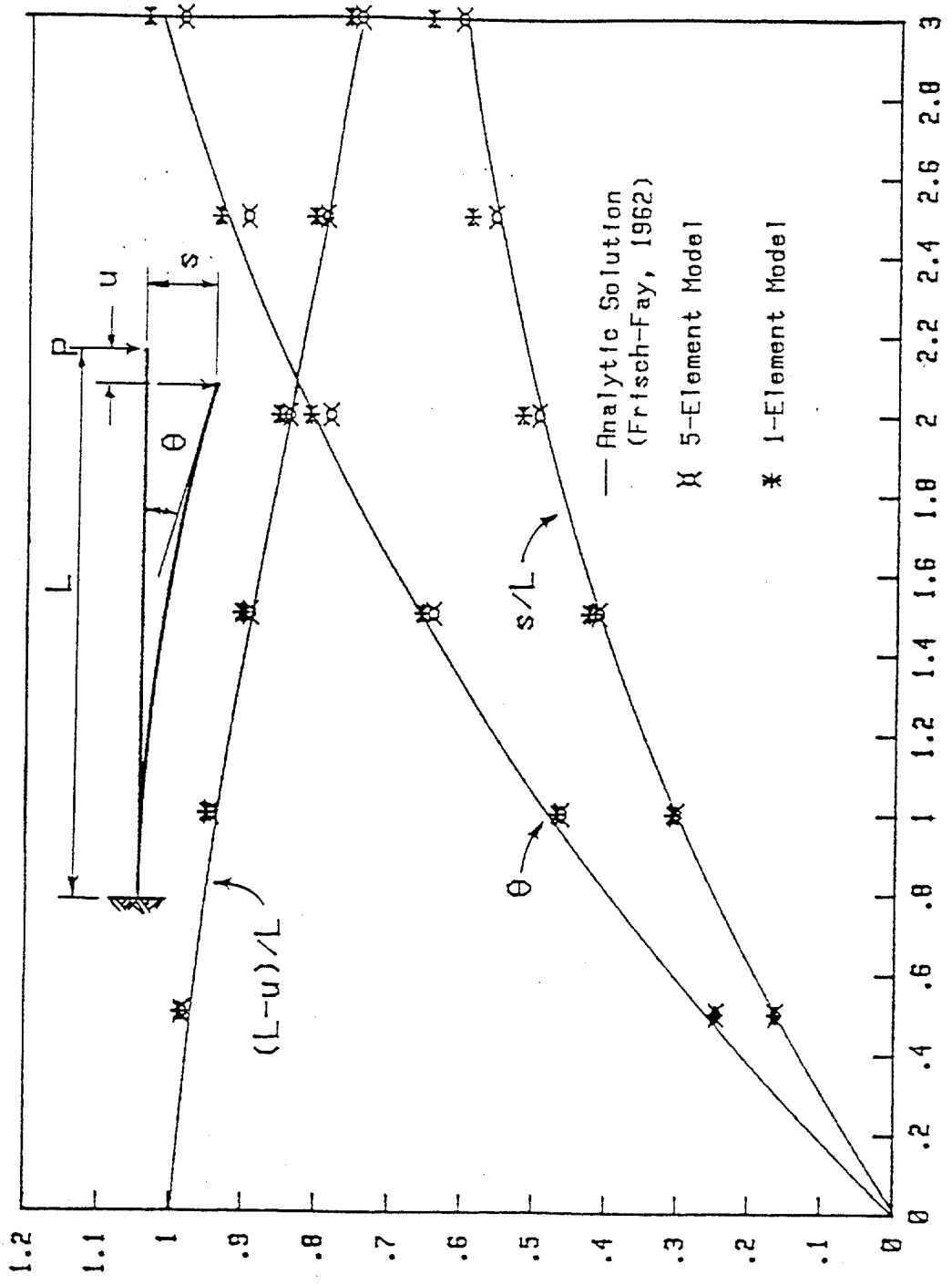

Figure 4.1-1 Cantilever beam with concentrated transverse tip load

4.2 Problem 2: Lumped Mass Pendulum

To demonstrate the accuracy of the dynamic algorithm adopted, a simple pendulum was considered. A lumped mass with no rotational inertia was located at the end of a massless beam, displaced 10 meters and released. Undamped motion was assumed. Convergence tolerance was 0.01. The time step used was 1.75 seconds. The mechanical properties were:

Beam:

	Elastic Modulus	$2. \times 10^{11}$ Pa
	Cross-Sectional Area	1.456 m^2
	Second Moment of the Area	3.580 m^4
	Length	150 m
Mass:	X_1 Magnitude	1.718×10^5 kg
	X_2 Magnitude	1.718×10^5 kg
	X_3 Magnitude	1.718×10^5 kg

Figure 4.2-1 shows the history of response. The natural period calculated analytically from the small amplitude pendulum solution (Volterra and Zachmanoglou, 1965) is 24.58 sec. The period predicted numerically by the computer program is 24.88 sec. (1.2 % error). There is no perceptible decrease in amplitude in the two complete cycles shown. The fact that the numerically calculated amplitude of motion of 9.84 meters is slightly less than the initial displacement of 10 meters (1.6 % error) is explained by the self-starting feature of the Newmark algorithm. The initial conditions used to start the algorithm were zero velocity and accelera-

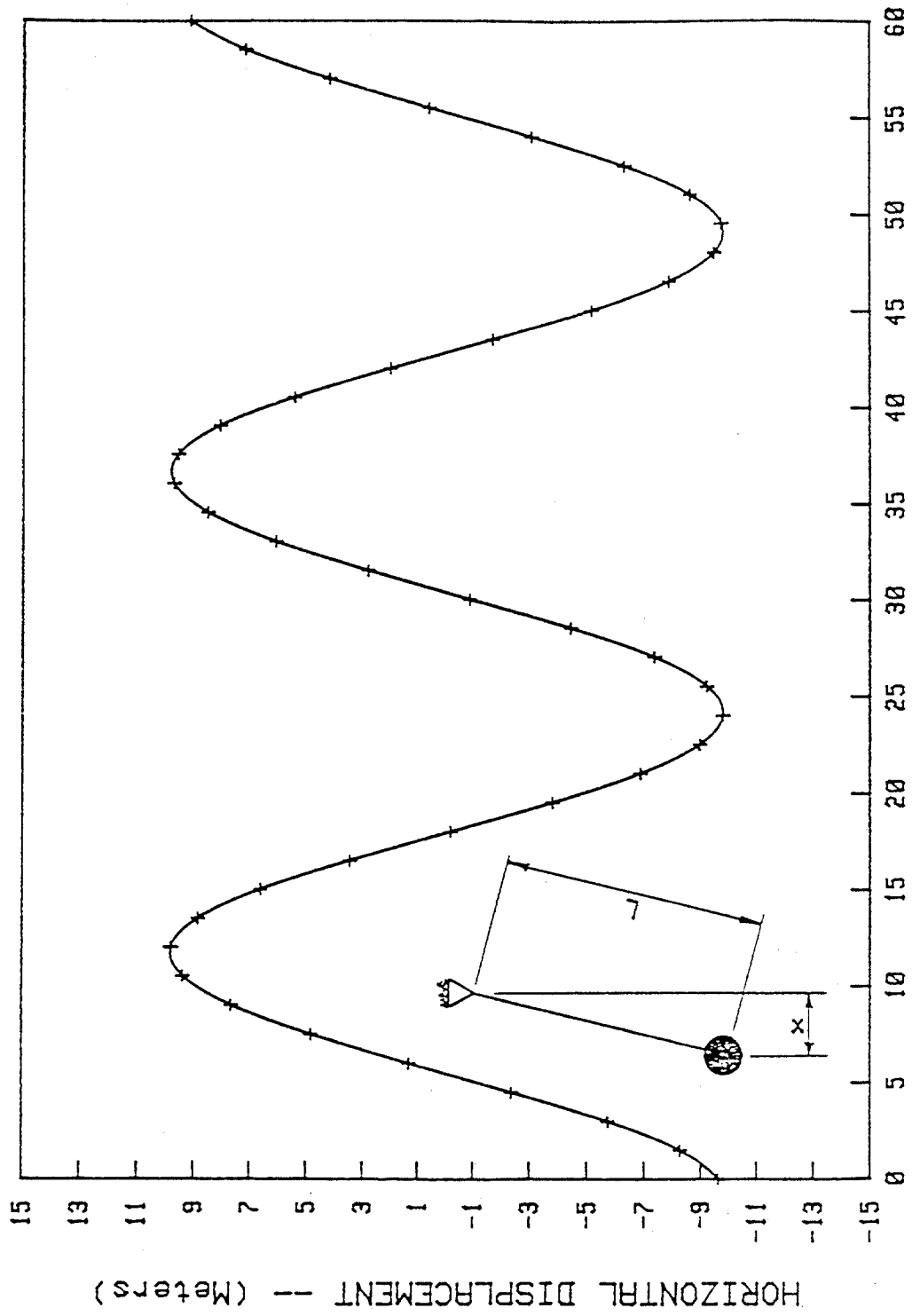

Figure 4.2-1 Free oscillation of a simple pendulum with concentrated mass

tion: the load due to gravity is applied gradually during the first time step with a consequent decrease in amplitude. The accuracy of the results could be improved by using a shorter time step or by decreasing the tolerance but the results obtained are quite satisfactory for their intended purpose.

4.3 Problem 3: Point Load on a Taut String

The purpose of this problem was to check the algorithm for calculating the stiffness matrices for the cable elements. The model consisted of two collinear cable elements with the following properties:

Elastic Modulus	1×10^7 lb/ft^2
Initial Cross-sectional Area	0.1 ft^2
Initial Tension	50 lbs
Weight Density	0.0 lb/ft^3

A transverse load located at midspan was applied in seven equal load steps. The maximum load was 7,000 lbs, and convergence was assumed when the tolerance was less than or equal to 0.01.

Since the initial cable configuration possesses no transverse stiffness, the viscous relaxation method was used to start the solution. The parameters used in the solution were:

Initial Artificial Damping Constant	2033 lb/ft
Damping Factor	0.001
Decrement Factor	0.0005

The results are shown in Figure 4.3-1. The continuous curve is an analytic solution to the problem (Tuah, 1982). Convergence

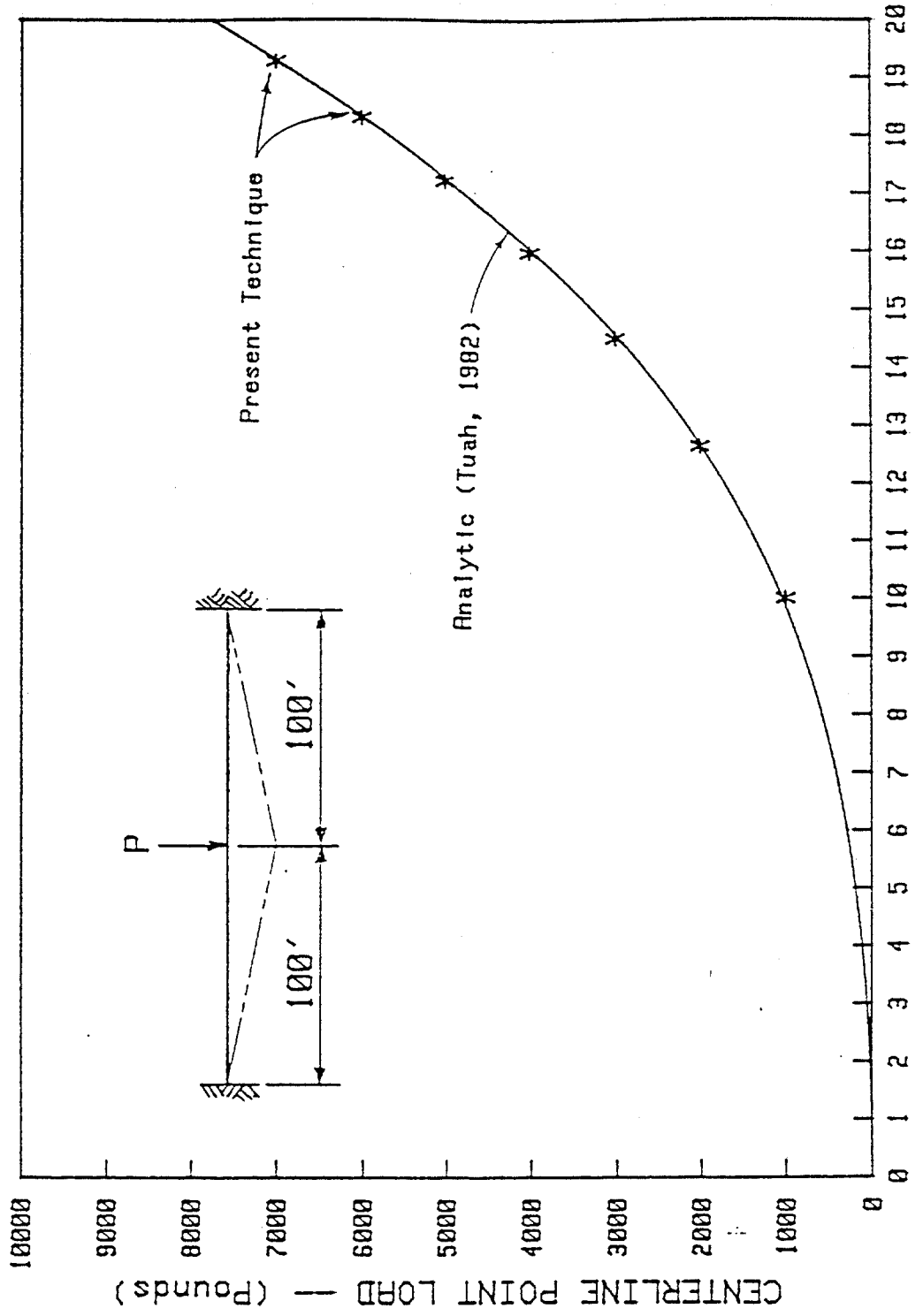

Figure 4.3-1 Point load on a taut string

to the first load step was reached in eight iterations. Convergence for the next two load steps required three iterations and the remaining four load steps required two iterations each. Webster, (1975) solved this problem two ways: 1) with a purely incremental scheme using 100 load steps; and 2) with a modified Newton Raphson scheme using 55 iterations. The viscous relaxation solution technique of this work provides a solution that converges in a total of 22 iterations. The results as can be seen for the figure compare very well with the analytic solution.

4.4 Problem 4: Point Mass on a Taut String

The purpose of this problem was to check the dynamic algorithm for cases involving cables. The cable is again stretched between two points. Its mechanical properties are as described in Section 4.3; but, instead of a concentrated load, a 5 slug concentrated mass is placed at the midpoint. The mass was displaced 2 feet and released.

Figure 4.4-1 shows the nonlinear solution. For comparison, a sine curve at the analytically calculated natural period of 0.262 seconds (see Volterra and Zachmanoglou, 1965 for procedure). The numerically calculated natural period is 0.263 seconds (0.4 % error) at a time step of 0.01 seconds and a convergence tolerance of 0.01. Also shown are the results of the same problem with a time step of 0.05 seconds. In that instance the numerically calculated natural period is 0.321 seconds (22.5 % error). This demonstrates the period lengthening effect of the Newmark integration scheme (Bathe, 1981).

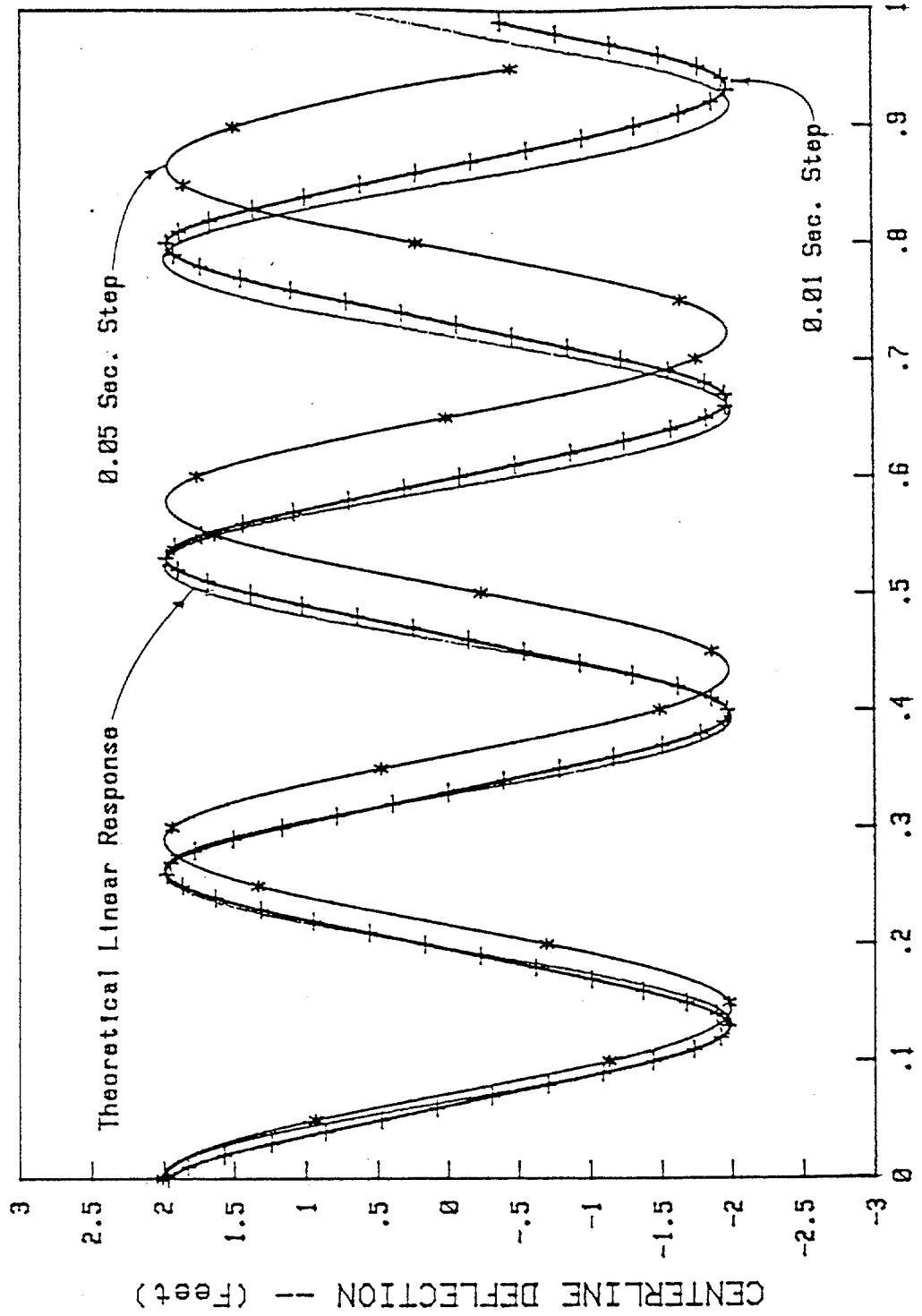

Figure 4.4-1 Point mass on a taut string

It is interesting to note that the natural period calculated by a small-deflection analysis is 4.44 seconds. If the small-deflection solution were used to estimate the time step to be used for this particular problem and fifty time steps per cycle of the estimated period were selected, there would be fewer than three time steps occurring in each cycle of the true response. The error in natural period would thus be even greater than that of the 0.05 second time period. If a time step of one-twentieth of that small-deflection natural period were selected, the analysis would completely miss the natural period of response and the analysis would show a period of response which is totally in error. This simple example demonstrates that for nonlinear problems it is highly desirable to repeat an analysis at a different time step for a length of time sufficient to determine that the original solution is valid.

4.5 Problem 5: Steady Current on an Articulated Tower

In order to check the drag force calculation algorithm, a simple articulated tower was modelled and subjected to steady current. The result for steady lean of the tower was then compared to an analytic solution in which the tower was modelled as a rigid body. The model selected was one after Kirk and Jain, 1977, and is shown in Figure 4.5-1 with geometric and dynamic particulars. The mechanical properties of the shaft are identical to those of the lumped-mass pendulum of Section 4.2. The drag coefficient used was 0.5 and the inertia coefficient was 2.0.

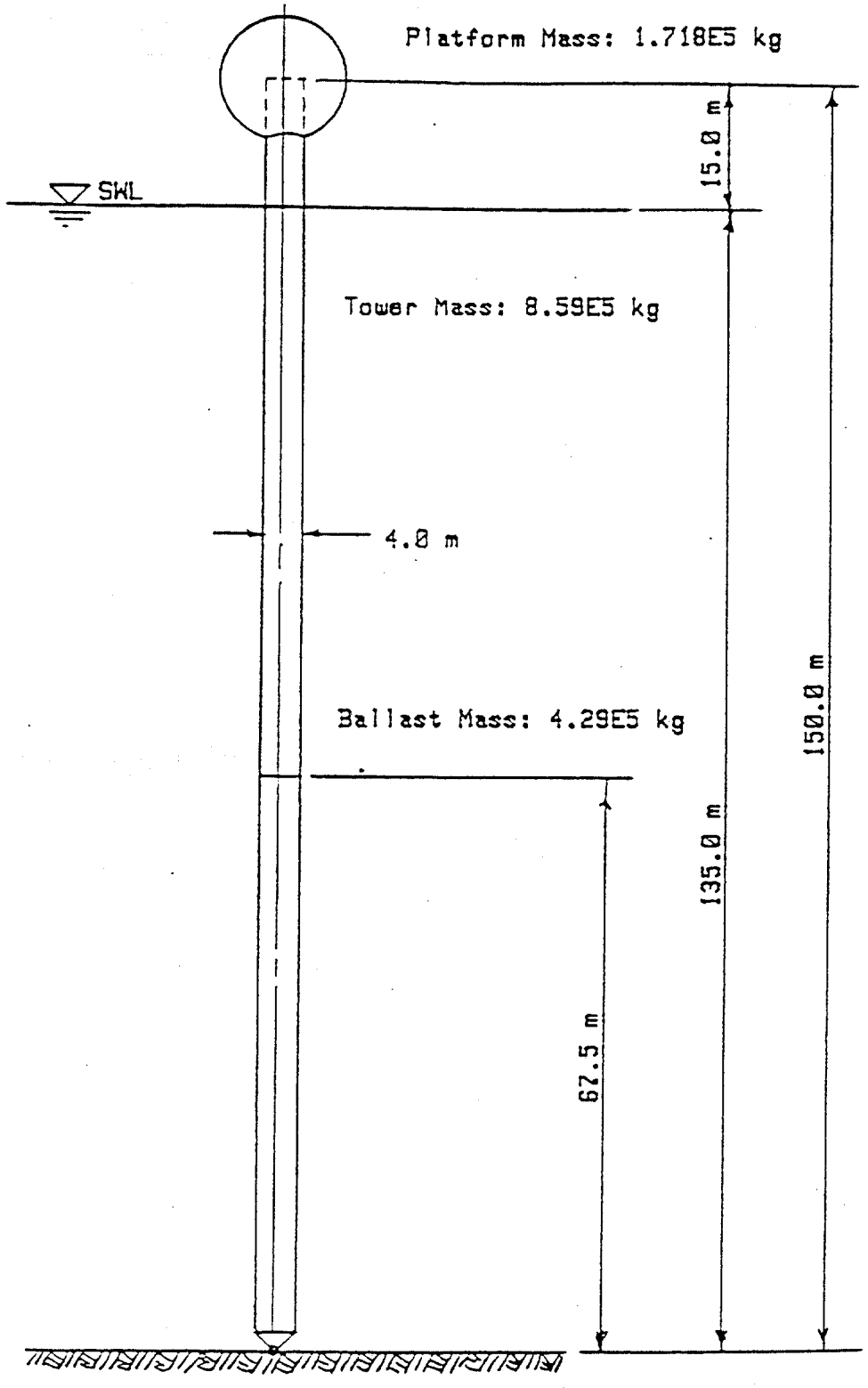

Figure 4.5-1 Elevation of articulated tower

A steady uniform current of 0.9125 m/s was applied to the tower and the steady angle of inclination was found to be 0.0205 radians. The angle of inclination calculated analytically is also 0.0205 radians. The convergence tolerance used by the program was 0.01.

Since the tower has no stiffness in the horizontal directions when in the vertical position, the viscous relaxation option was used to start the solution. The following parameters were used:

Initial Artificial Damping Constant	3.9×10^9 N/m
Damping Factor	0.00001
Decrement Factor	0.0005

Convergence was reached in five iterations. Figure 4.5-2 shows a plot of the solution convergence.

4.6 Problem 6: Steady Tow of a Cable with Sphere

This problem demonstrates the accuracy of the calculation of hydrodynamic drag forces on the cable element and confirms the validity of neglecting tangential drag forces. The problem was originally presented by Webster, 1974 and the experimental curve was determined by Gibbons and Walton, 1966. The structure consists of a long wire terminated by a spherical mass. The wire and mass are towed by a surface vessel at a steady speed of 10.5 knots. The particulars of the ten element model are as follows:

Cable Data

Diameter	0.350 in
Submerged Weight	0.169 lb/ft

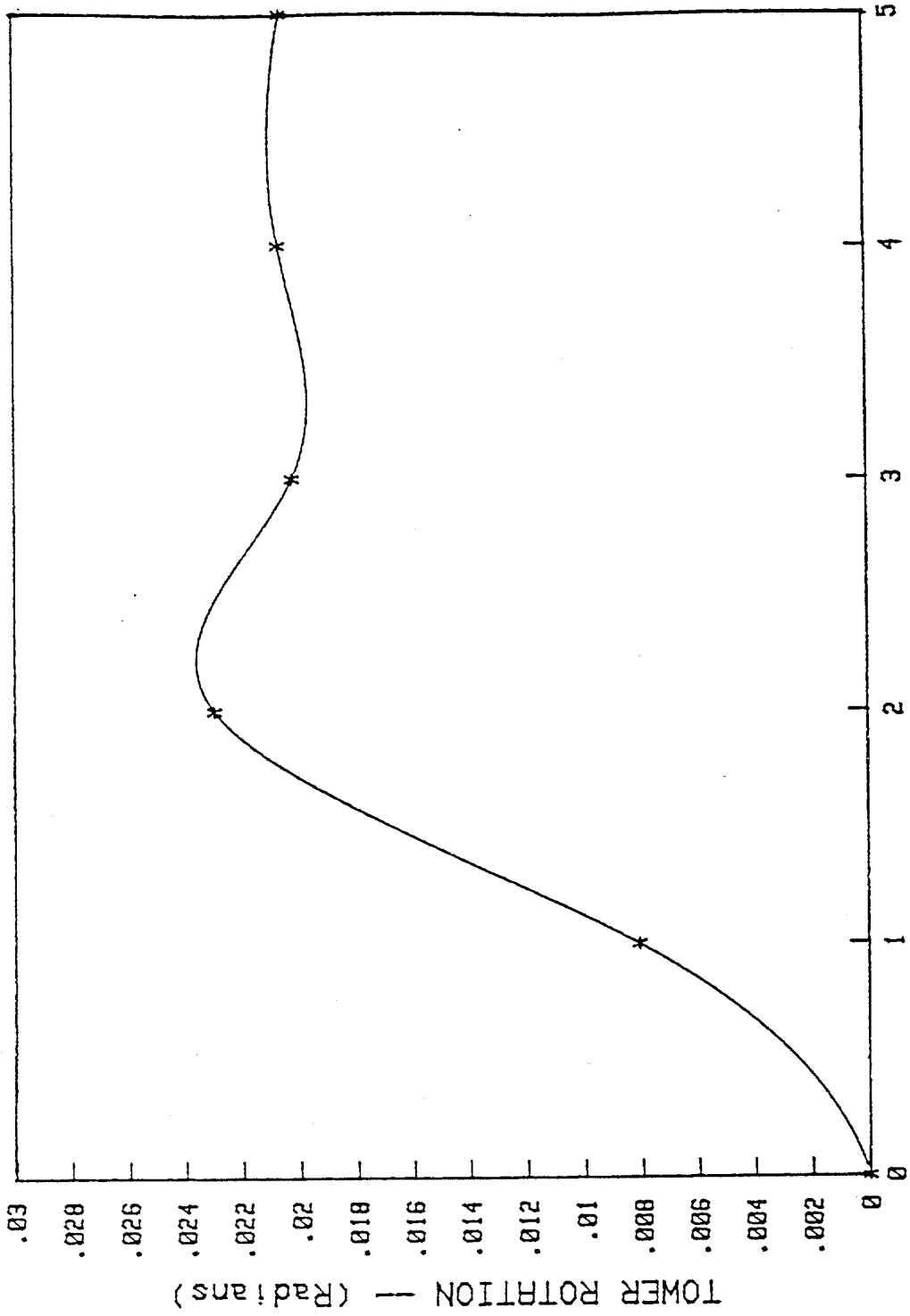

Figure 4.5-2 Viscous relaxation solution performance for an articulated tower

Element Lengths	280.0 ft
Total Cable Length	280.0 ft
E * A Value	1.92×10^5 lb
Drag Coefficient	1.5

Spherical Body Data

Diameter	1.0 ft
Submerged Weight	580.9 lb
Drag Coefficient	0.23

The problem was started with the cable suspended vertically and again viscous relaxation was used. The convergence tolerance was 0.01, the initial artificial damping constant was 6860 lb/ft, and the damping and decrement parameters were 0.001 and 0.05 respectively. Convergence was reached in eleven iterations. The final configuration at a speed of 10.5 knots is plotted in Figure 4.6-1. Also shown are the results of Webster and the experimental results of Gibbons and Walton. The present results compare favorably with the experimental curve. The viscous relaxation solution convergence in eleven iterations compares favorably to the 91 iterations to convergence required by the Webster solution in which viscous relaxation was not used.

4.7 Problem 7: Articulated Tower in Waves

To test the dynamic solution algorithm of the program with hydrodynamic loads acting on a structure, the articulated tower of Section 4.5 was subjected to a 30-meter, 17-second wave. All parameters were as in Section 4.5 except the drag coefficient which was

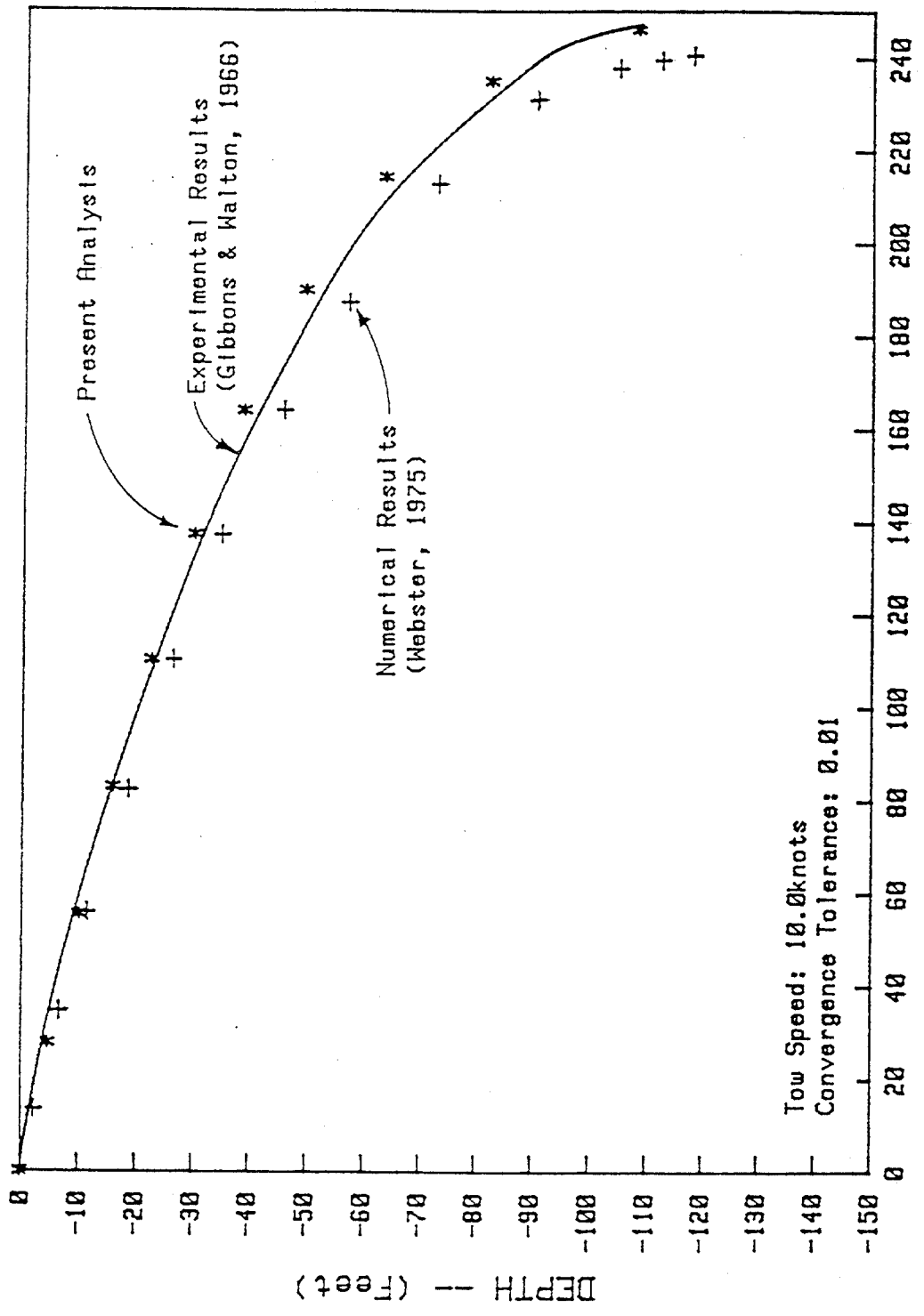

Figure 4.6-1 Steady tow of a cable with a spherical end mass

set to 1.0. The Newmark beta parameters α and ζ were set to 0.25 and 0.5, respectively. The time increment was 1.75 seconds and the convergence tolerance was 0.01.

The response is shown in Figure 4.7-1. Also plotted in the figure is the response obtained by Kirk and Jain, 1977. There is a large difference in the form of the initial response although the solutions appear to approach each other in the steady-state. Kirk and Jain indicate that they required no special starting procedure in their solution, and that the solution was sufficiently damped to give steady state response almost immediately. They used an explicit, fourth-order two-point block integration method for solving the equation of motion as opposed to the implicit Newmark method used in this work. It is not known what the precise reason for the discrepancy is, but it is suspected to be in the difference in the integration methods used. The question is which one better represents the tower motion. Explicit methods are conditionally stable; implicit methods are known to be unconditionally stable for the linear problem (Bathe 1981).

To obtain an idea of the dynamic response of the tower, it was leaned over to the maximum amplitude of excursion from the previous problem and released. The convergence tolerance was again 0.01. The dynamic response is shown in Figure 4.7-2. Since only a few cycles were available for analysis, the log decrement was measured for each half cycle and the effective damping parameter was calculated. The results are tabulated below.

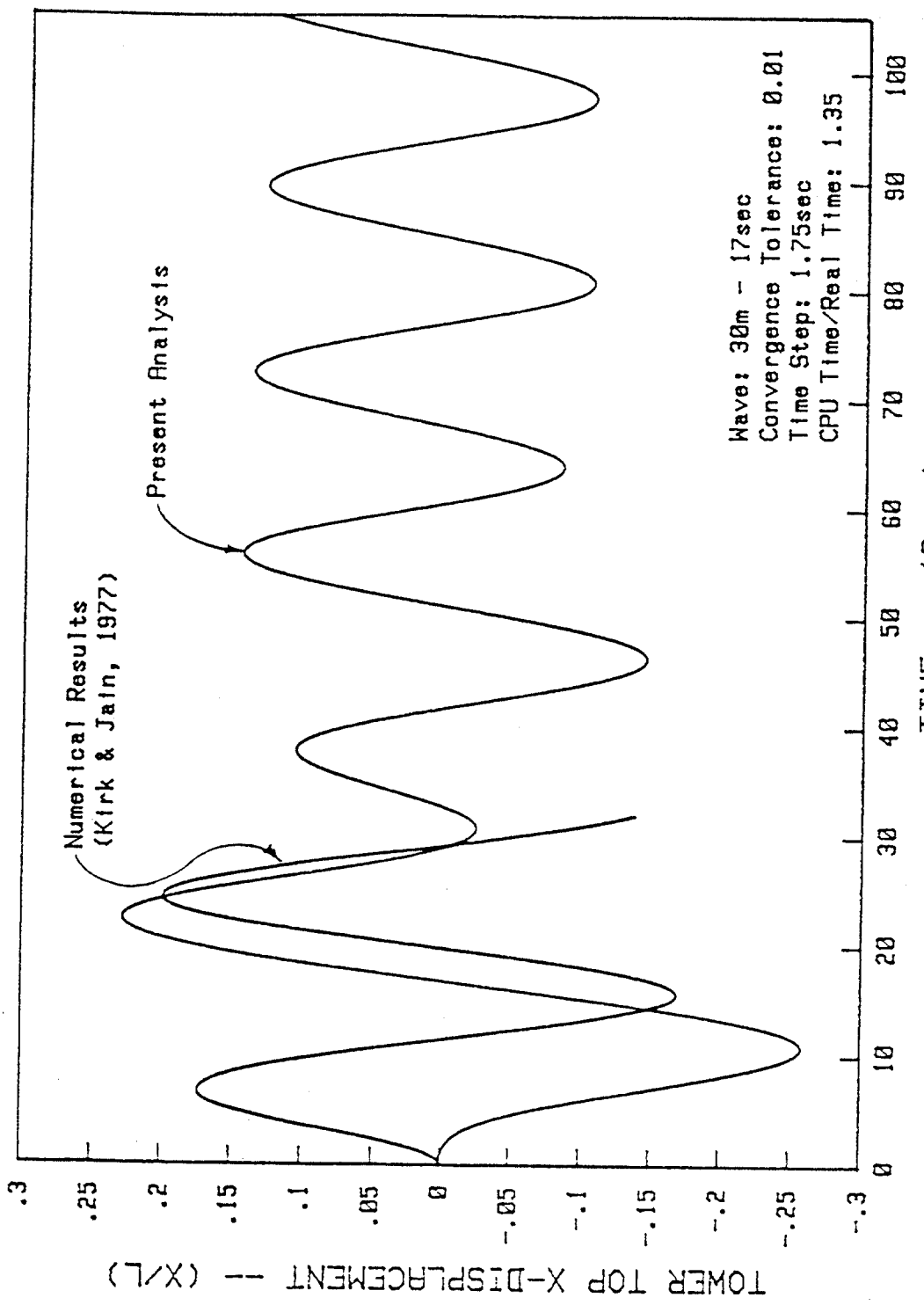

Figure 4.7-1 Motion of an articulated tower in waves only

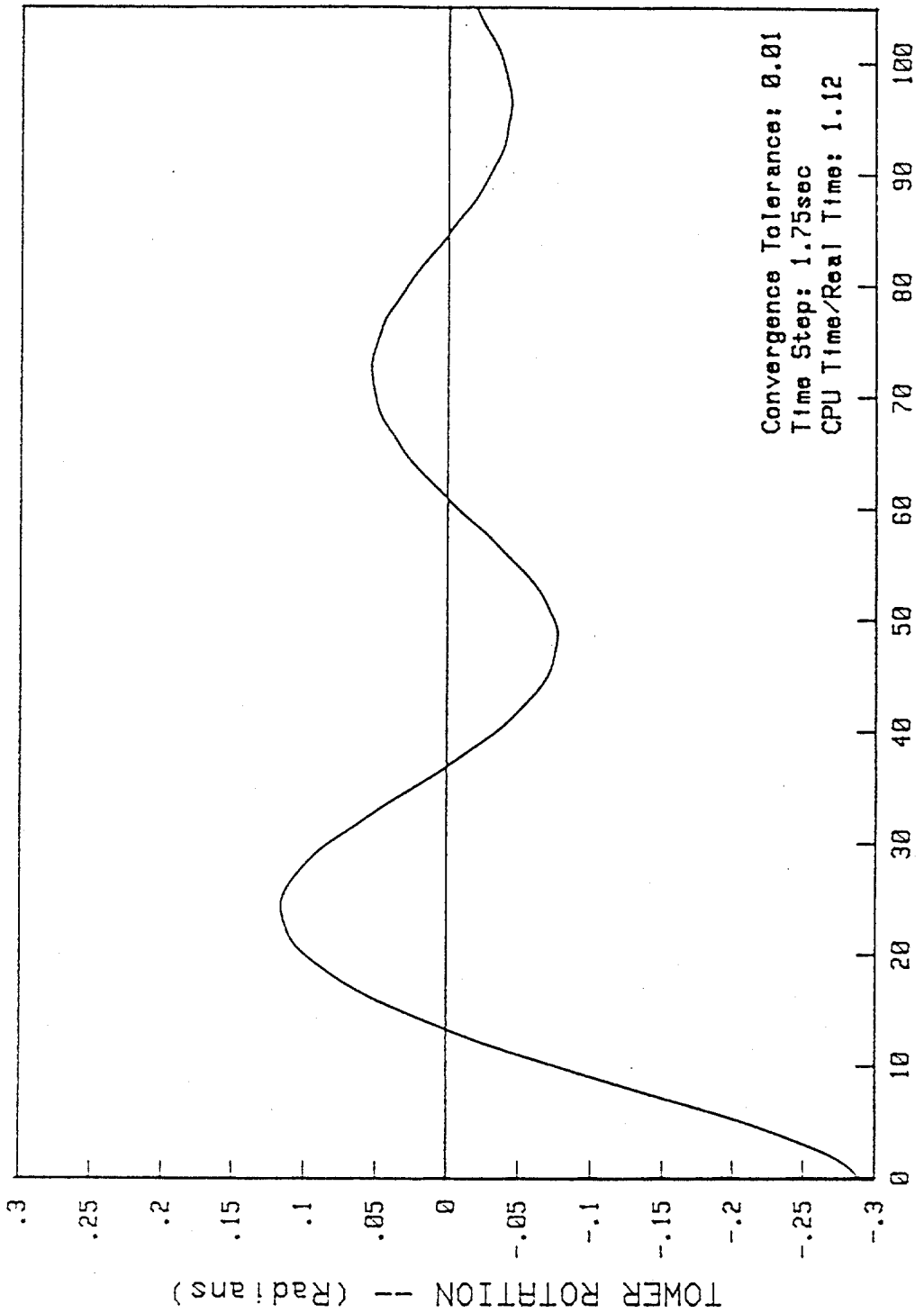

Figure 4.7-2 Free oscillation of an articulated tower in still water

Half Cycle	Damping Factor, ξ
1	-
2	0.17
3	0.09
4	0.08
5	0.06

These results indicate a system that is not heavily damped as would be implied by the results of Kirk and Jain, 1977. The present results were determined, however, using the Newmark integration scheme, so the results are not independent. When the forced results are compared with the free oscillation results, the undulation of the forced results fit well with the undulation of the free oscillation results as would be expected leading one to believe that the algorithm is functioning properly. Whether the block integration or Newmark integration best describes the motion of a real tower needs to be determined from laboratory data. That data is not available for inclusion in this work.

The articulated tower was subjected to a 30 meter, 17 second wave plus a 0.9125 m/s current moving at 90 degrees to the wave direction to see if the program results are similar to Kirk and Jain's 1977 results. A plot of the calculated x-y motion of the tower top and the Kirk and Jain results are shown in Figure 4.7-3. Again the initial amplitudes are large, but the motion of the tower predicted by the present algorithm is otherwise very similar to the results of Kirk and Jain.

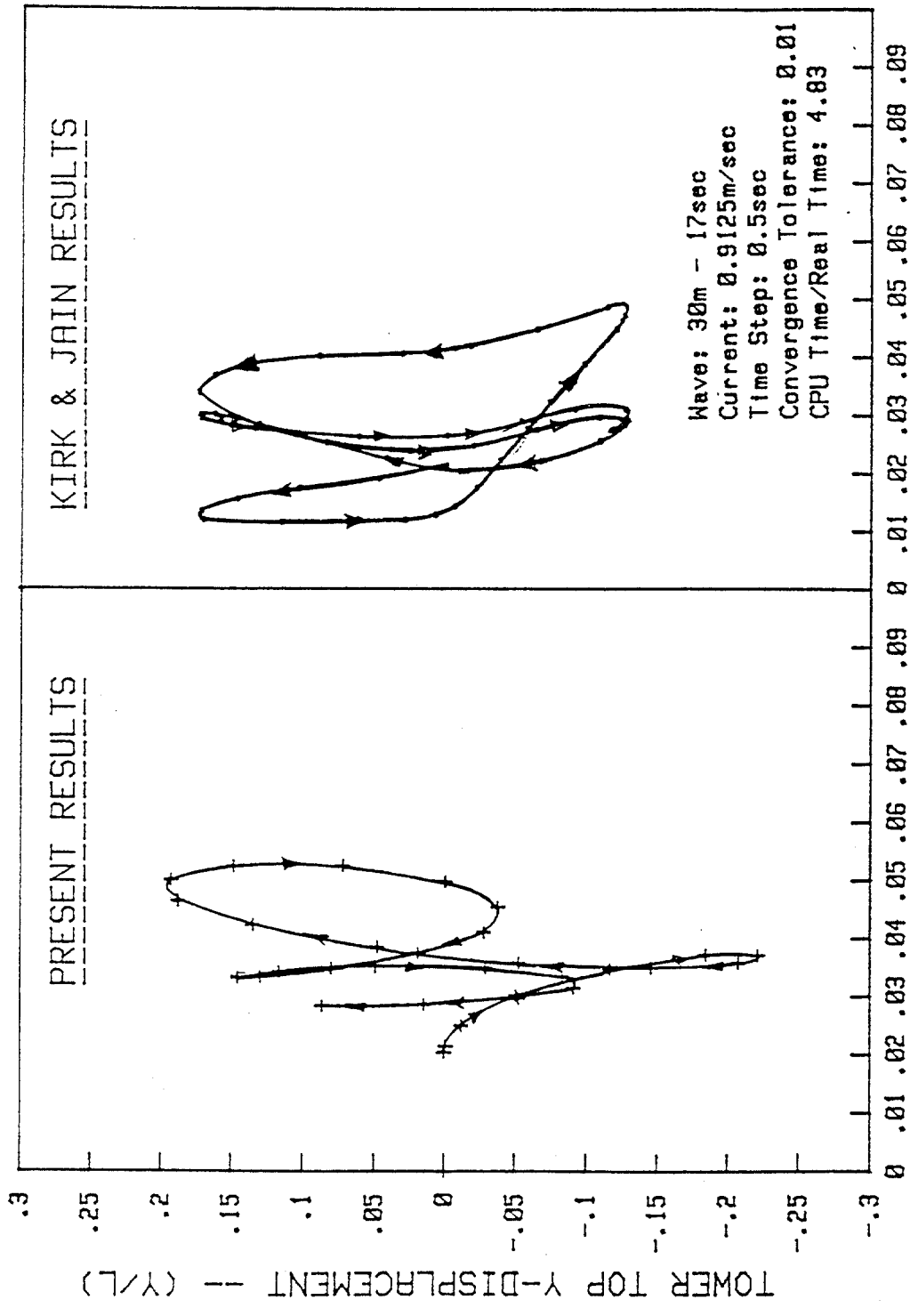

Figure 4.7-3 Motion of an articulated tower in waves and transverse current

4.8 Problem 8: Two Dimensional Guyed Tower in Waves

A two dimensional model of a guyed tower was formulated to demonstrate the use of beam, cable, and foundation elements in a single problem and to demonstrate the ability to obtain solutions in which some of the elements are assumed to participate in a quasi-static manner. A definition sketch of the model is shown in Figure 4.8-1. The tower was modelled as two beam elements, one extending from the pinned base to the guy connection and one from the point of guy connection to the deck mass. The two guys were each modelled as three cable elements terminated at the seafloor by a foundation spring whose horizontal stiffness was equivalent to that of the length of cable which usually extends from the clump weight to the guy anchor. The physical properties of the model used in the analysis are as follows

Environment

Water Depth	1500 ft
Wave Period	10 sec
Wave Height	30 ft

Deck

Mass	466.4 k slugs
Rotational Inertia	0

Column

Mass Density	.00249 k slug/ft^3
Weight Density	.0160 kip/ft^3
Elastic Modulus	4.176 x 10^6 kip/ft^2

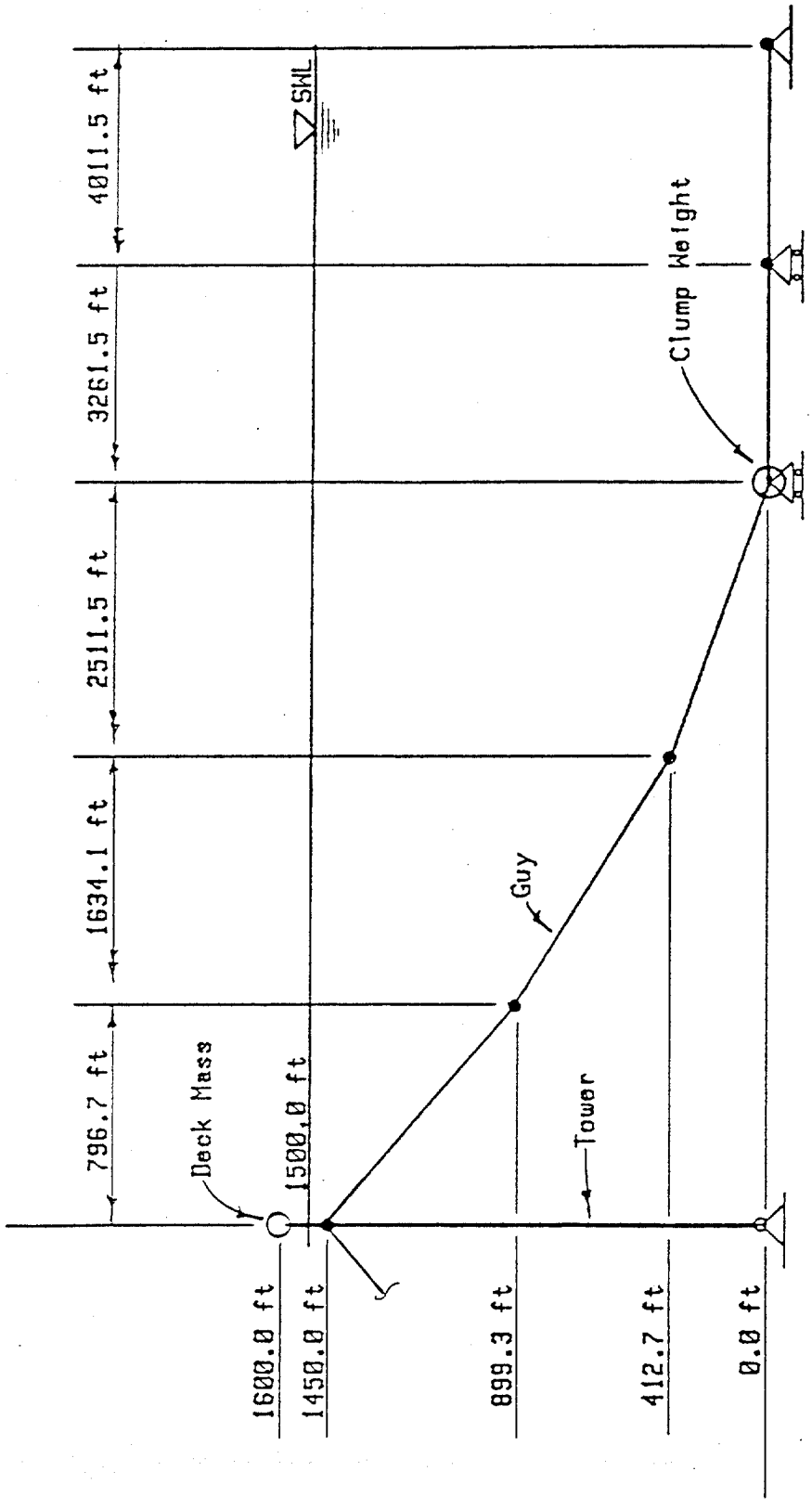

Figure 4.8-1 Elevation of guyed tower model

Cross-sectional Area	62.8 ft^2
Second Moment of the Area (about $x_2' - x_2'$ and $x_3' - x_3'$ axes)	1.571×10^5 ft^4
Torsional Constant	3.142×10^4 ft^4
Displaced Volume	312.5 ft^3/ft
Drag Width	115.0 ft
Drag Coefficient	0.7
Inertia Coefficient	1.814

Guys

Mass Density	.01524 k slugs/ft^3
Weight Density	.426 kip/ft^3
Elastic Modulus	$.43 \times 10^7$ kip/ft^2
Cross-sectional Area	.3341 ft^2
Displaced Volume	.3341 ft^3/ft
Drag Width	1.458 ft
Drag Coefficient	0.7
Inertia Coefficient	2.0
Initial Tension at Tower	1250 kip

Foundation Springs

Horizontal Stiffness	957.7 kip/ft
Vertical Stiffness	1×10^{14} kip/ft

For the solution in which quasi-static cables were assumed, the mass density, drag coefficient and inertia coefficient of the cables were set equal to zero so that the cables performed as static catenary springs. The time step selected was 0.5 sec and a convergence tolerance of 0.01 was used.

Plots of the horizontal displacement of the deck for both the dynamic and the quasi-static solutions are shown in Figure 4.8-2. The quasi-static solution is seen to overpredict the amplitude of deck movement by 20 to 100 percent in the 45 seconds of data plotted. These results imply that the deck accelerations are overpredicted when the guys are modelled as springs.

In Figure 4.8-3 are plotted the guy tensions calculated at the point of guy connection for the dynamic and the quasi-static cable solutions. It is seen that the quasi-static cable solution overpredicts the peak guyline tension and that the times at which peak loadings occur are significantly different. The unusual shape of the dynamic load trace is attributable to the spatial dependence of hydrodynamic loading on the guys.

4.9 Problem 9: Tension Leg Structure in Waves

A simplified tension-leg structure was subjected to waves as an additional demonstration of the versatility of the solution techniques employed in this work. A surface piercing cylindrical buoy was moored to the bottom by a single cable. A definition sketch is shown in Figure 4.9-1. The particulars are as follows:

Environment

Water Depth	450 m
Wave Period	15 sec
Wave Height	15 m

Column

Mass Density	.2529 kg/m^3

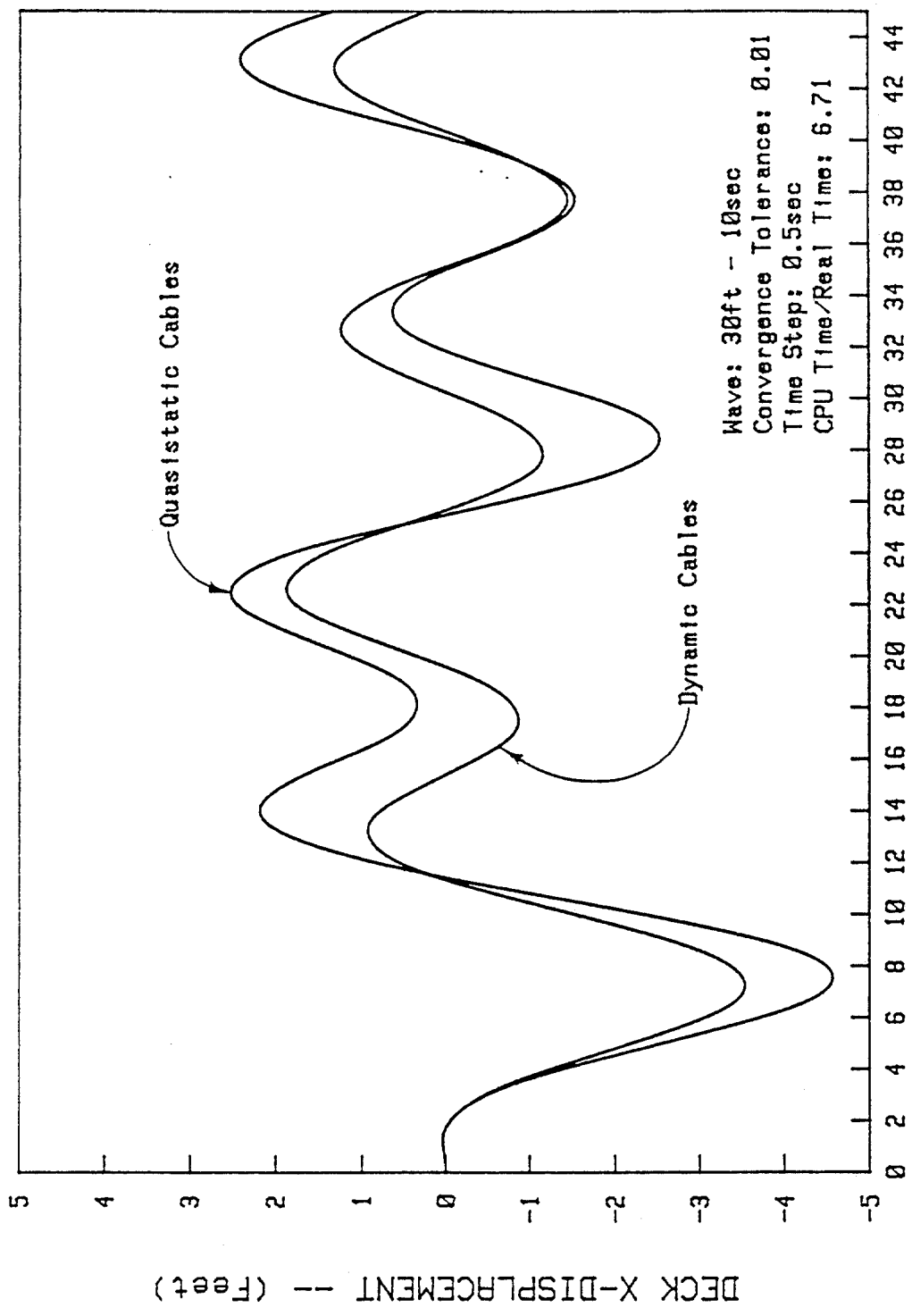

Figure 4.8-2 Transverse displacement of guyed tower deck vs. time

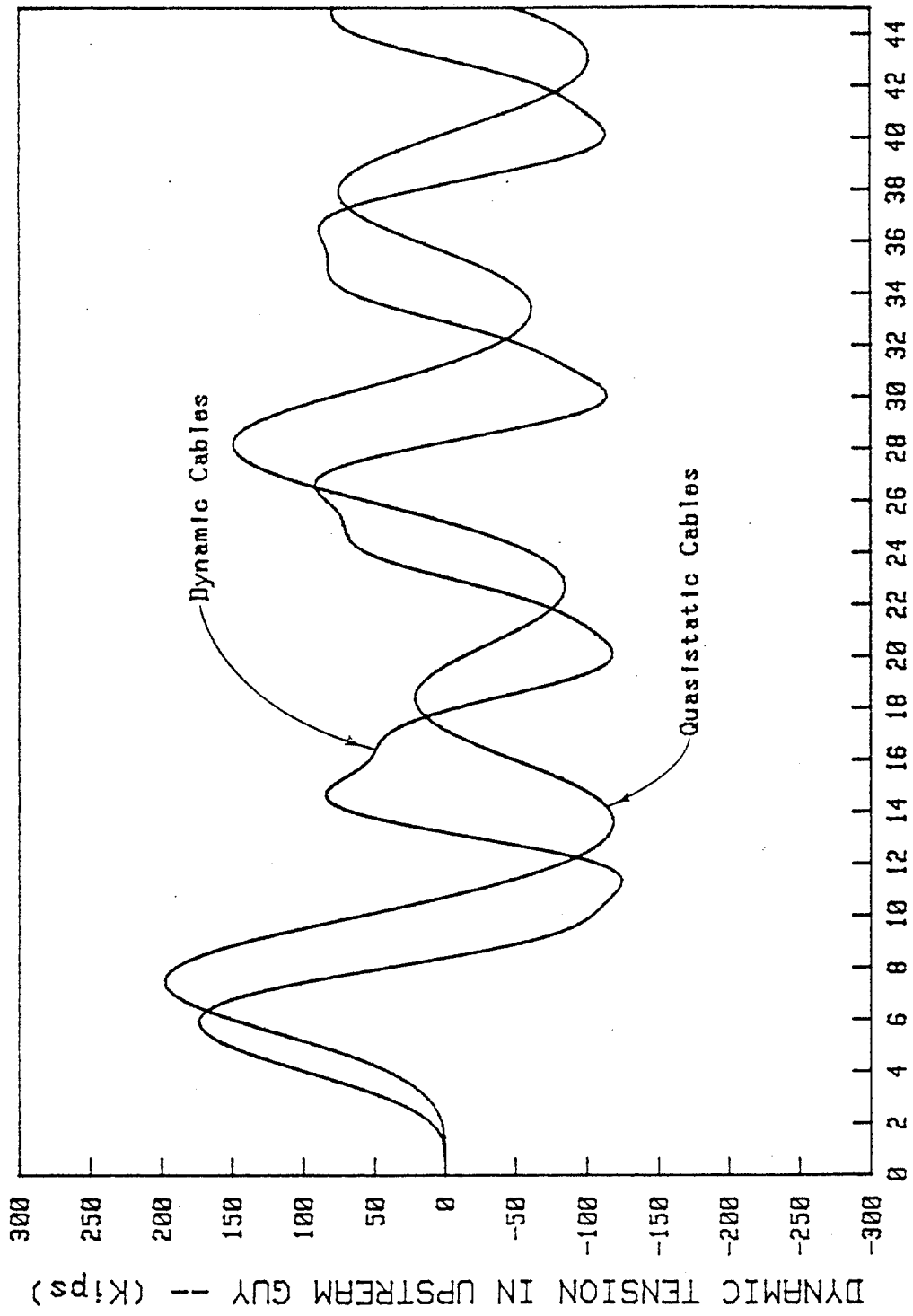

Figure 4.8-3 Guy tension vs. time

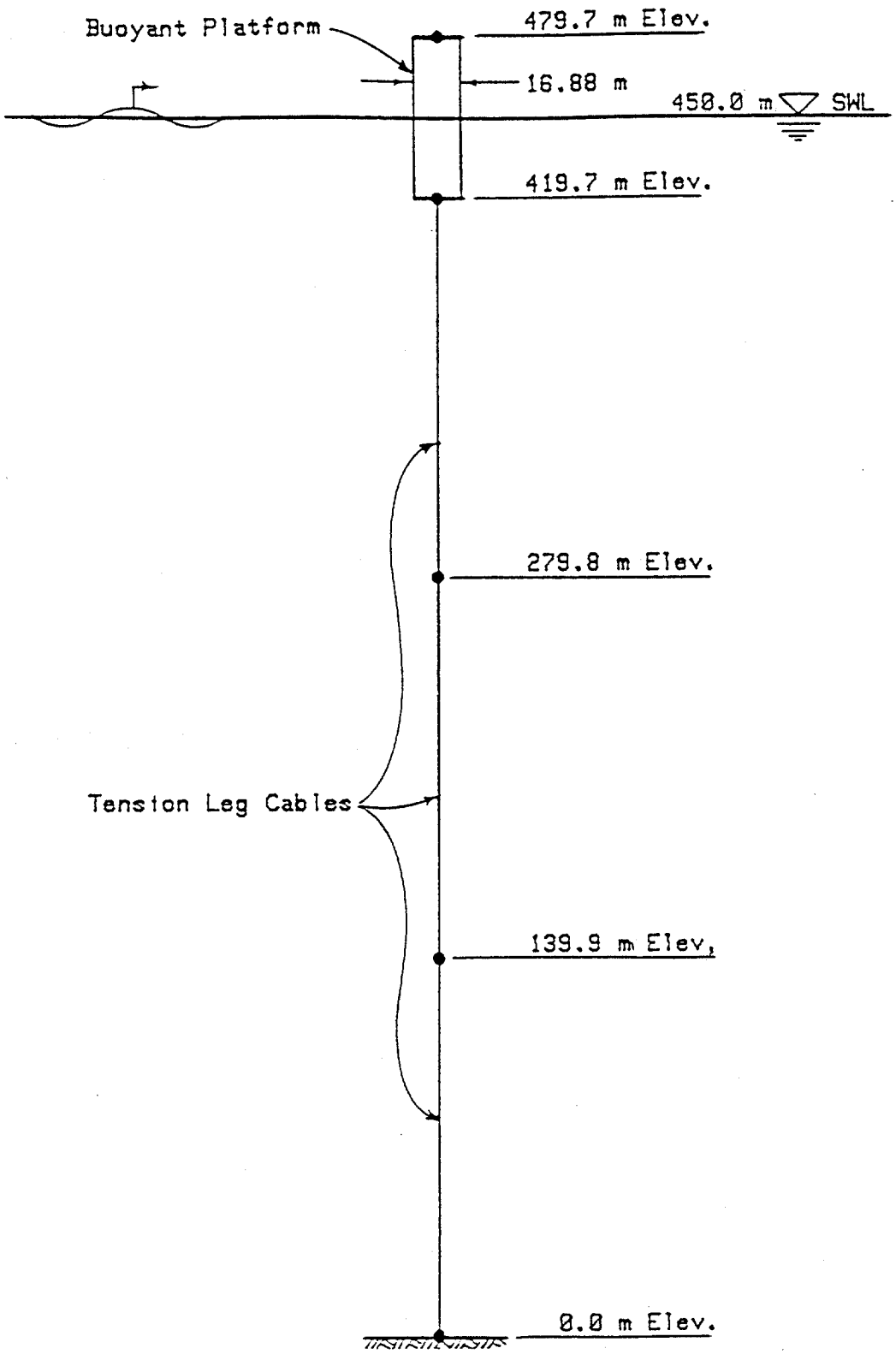

Figure 4.9-1 Tension leg structure

Weight Density	1.229 N/m^3
Elastic Modulus	2.1×10^8 N/m^3
Cross-sectional Area	2.066 m^2
Second Moment of the Area	75.55 m^4
Torsional Constant	151.3 m^4
Displaced Volume	223.8 m^3/m
Drag Width	16.88 m
Drag Coefficient	0.7
Inertia Coefficient	2.0

Cables

Mass Density	1.023 kg/m^3
Weight Density	10.03 N/m^3
Elastic Modulus	2.1×10^8 N/m^2
Cross-sectional Area	.397 m^2
Displaced Volume	.397 m^3/m
Drag Width	1.422 m
Drag Coefficient	.7
Inertia Coefficient	2.0

Viscous relaxation was used to obtain the inertial equilibrium position of the structure. The parameters used were:

Initial Artificial Damping Constant	596139 nt/m/sec
Damping Factor	1.0
Decrement Factor	0.05

The time step selected was 0.5 sec. and the convergence tolerance was 0.01.

The horizontal displacement of the cylinder top and bottom are plotted versus time in Figure 4.9-2. One can observe the pitch response of the cylinder as well as the long period response in the surge mode. The bottom of the cylinder, being restrained by the tether, shows a more attenuated response at the wave frequency than the top of the cylinder shows. The response appears stable and appears to be approaching steady state at the conclusion of the time record.

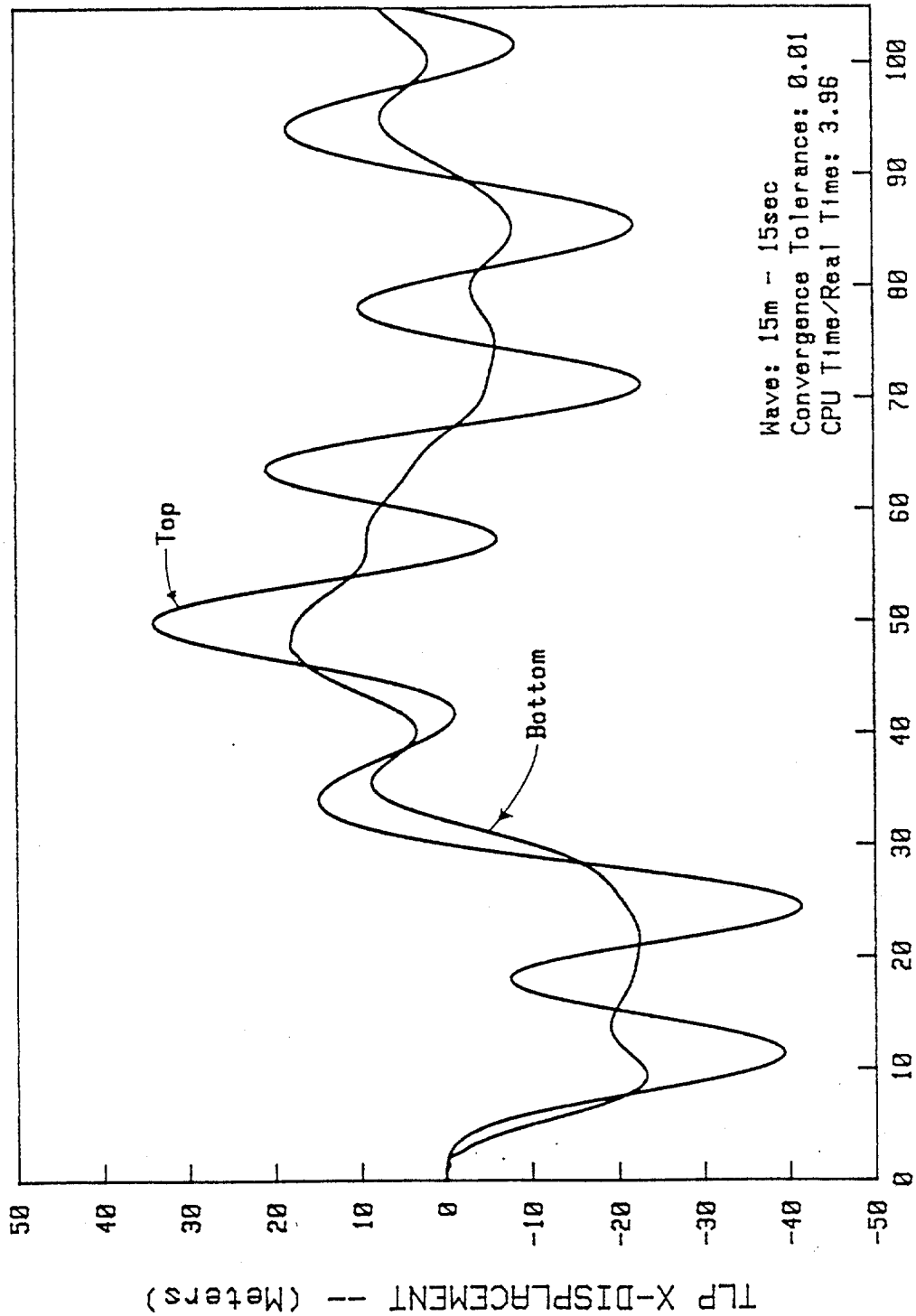

Figure 4.9-2 Transverse displacement of tension leg structure vs. time

5.0 Summary and Recommendations

A three-dimensional, large-deflection finite element program has been developed which is capable of simulating the static and dynamic behavior of large compliant ocean structures. The structures are assumed to be in the Morison regime and to be composed of cable and beam-column elements. No vortex shedding, diffraction effects, nor material nonlinearities are considered. Linear wave theory is used and multidirectional irregular seas may be simulated by a series of regular waves. Current may be included as an arbitrary current profile varying in magnitude and direction with depth. Concentrated masses and loads as well as foundation properties may also be modelled.

The use of updated Lagrangian coordinates and a residual feedback solution scheme has been shown to be a valid technique for solving the geometrically nonlinear problem. Static test problems 1 and 3 indicate that the scheme yields excellent results in comparison to available theoretical solutions. Furthermore, these results were obtained with liberal convergence tolerances and large element discretizations.

It has been confirmed that the viscous relaxation method is an excellent method to start the static solution of hardening nonlinear problems with little or no initial stiffness in one or more degrees of freedom. It has been demonstrated that the method is particularly efficient when used on articulated structures which use buoyancy for stability. More iterations are required when the

method is used on cable problems and on problems using both cables and beams, but the technique is still superior to dynamic relaxation (Webster, 1980) for the examples considered in this work.

The selection of the coefficients used in the relaxation process depends largely upon the experience of the analyst. However, some observations can be made to determine if the selected coefficients are adequate and if they can be improved. If insufficient initial stiffness is added to the nodes, the structure remains unstable and this instability will be exhibited in the first iteration by a zero or negative pivot during Gauss reduction of the set of equilibrium equations. If the decrement factor is too small, a similar situation will occur during subsequent iteration. Conversely, if the decrement factor is large and the initial stiffness is large, the convergence plot will appear like the dynamic free response of an overdamped system subject to a step load and the solution will converge monotonically to the proper values. An optimum solution appears like the dynamic free response of an underdamped system and exhibits some overshoot as in Figure 4.5-2, but a heavily damped solution resulting from large initial artificial stiffness and a large decrement factor will permit a solution to be obtained only at the expense of additional iteration cycles.

The iterative Newmark method has been shown to provide good time domain solutions to nonlinear dynamic problems even at time steps and convergence tolerances which are large compared to those

often suggested in the literature. The solution algorithm has been shown to give reasonable results for hydrodynamic solutions. However, although these results are similar to published results, there is enough disparity to warrant investigation of the performance of this and other algorithms compared to experimental results.

The starting procedure of assuming zero initial velocity and acceleration has been shown to be an acceptable method for problems in which the steady state dynamic response is sought. In fact, it is actually a superior method for those problems in which some of the response periods of the structure are much smaller than the selected time step of the numerical integration. When an initial acceleration vector is calculated for the system, the system responds as it would respond to an impact load. If this response has high accelerations at a period shorter than the time step, the inertial loads overpower the other loads in the system and convergence is hampered. When a solution is started from zero velocity and acceleration, the net effect of the constant average acceleration scheme of Newmark is to apply the load as a ramp function over one time step. For the higher frequencies, the loading appears as a static load and the high structure accelerations at high frequencies are not present. The convergence of the iterative solution is smoother and more rapid in this case.

Results of the guyed tower test problems show that for the examples presented, the use of static spring models of the guys,

the quasistatic cables, leads to an overprediction of the tower motion and also of the guy tensions. There is also a large difference in the time phase of the cable tensions and in the form of the tension versus time plots.

The tension leg structure problem demonstrates that the algorithms developed in this work are capable of handling tension-leg structures and that the solution is stable over a long time history.

In general the algorithms selected and used in this work perform in a manner which is satisfactory for their intended function. The techniques require a considerable amount of computer time to obtain solutions compared to the computer time usually required by linear analyses. As the nonlinearities increase in strength, the computer time for similar problems increases greatly but there is no apparent degradation in the accuracy of the results for the test problems considered. Because of the relatively long solution times, the analysis of this work is not recommended as a tool for the detailed design of structures. Its best roles are probably as 1) an analytic tool used on simplified models to study the motion characteristics of various structure concepts, 2) as a verification tool for use on simplified models to study the motion characteristics of various concepts, 3) as a verification tool for simplified design techniques, and 4) as a final design check on complicated models.

The algorithms and methodologies developed in this work are adequate to study a large variety of problems but there is still additional work which will enhance the capabilities of the present computer program. Following is a list of recommendations for future additions or improvements:

1) Include the effects of a finite free surface profile to the buoyancy, wave, and current loads.
2) Add nonlinear elastic and viscoelastic material properties to the cable element to better model synthetic hawser materials.
3) Improve the cable element from a simple two node element to a multinoded isoparametric element to allow the use of larger elements and consequently decrease problem size.
4) Change the beam element to an isoparametric element to eliminate the rigid body rotation problem in calculating internal loads and to allow the use of large curved beam elements.
5) Implement a dynamic wind loading package so that the effect on the structure of this dynamic loading combined with hydrodynamic loading can be studied.
6) Implement a loading package which will permit the modelling of vortex shedding loads.

The list could be extended of course but these few modifications appear to be of more immediate concern.

It is also desirable to execute a simple experimental study of a scale model to resolve the questions raised by comparing the dynamic solutions of the program developed in this work with the dynamic solutions of the program developed by Kirk and Jain, 1977. A laboratory model test of an articulated tower would provide an independent check on the performance of the dynamic solution algorithm.

References

Albrecht, H.G., D. Koenig and K. Kokkinowrachos, 1978, "Nonlinear Analysis of Tension Leg Platforms for Medium and Greater Depths," Proceedings, Offshore Technology Conference, Paper No. 3044.

Anagnostopoulos, S.W., 1982, "Dynamic Response of Offshore Platforms to Extreme Waves Including Fluid-Structure Interaction," Engineering Structures, v. 4, July, pp 179-185.

Ansari, K.A., 1980, "Mooring with Multicomponent Cable Systems," ASME Jour. of Energy Resource Tech., v. 102, n2.

Ashford, R.A. and W.L. Wood, 1978, "Numerical Integration of the Motions of a Tethered Buoyant Platform," Int. Jour. for Numerical Methods in Engineering, v. 13.

Bathe, K., Ramm, E., Wilson, E.L., 1975, "Finite Element Formulations for Large Deformation Dynamic Analysis," Int. Jour. for Numerical Methods in Engineering, v. 9, pp 353-386.

Bathe, K., 1982, Finite Element Procedures in Engineering Analysis, Prentice-Hall, Inc.

Belytschko, T. and Schoeberle, D.F., 1975, "On the Unconditional Stability of an Implicit Algorithm for Nonlinear Structural Dynamics," Jour. of Applied Mechanics, v. 97, pp 865-869.

Berteaux, H.O., 1976, Buoy Engineering, John Wiley and Sons.

Biesel, F., 1950, "Etude Theoretique de La Houle en Eau Courante," La Houille Blanche, v. 5A, pp 279-285.

Chakrabarti, S.K. and D.C. Cotter, 1980, "Transverse Motion of Articulated Tower," ASCE Jour. of the Waterways Port, Coastal and Ocean Div., v. 106, n1.

Chakrabarti, S.K., 1980, "Steady and Oscillating Drift Forces on Floating Objects," ASCE Jour. of the Waterways, Port, Coastal and Ocean Div., v. 106, n2.

Cook, R.D., 1981, Concepts and Applications of Finite Element Analysis, 2nd Ed., John Wiley and Sons.

Dalrymple, R.A., 1974, "Models for Nonlinear Water Waves on Shear Currents," Proceedings, Offshore Technology Conference, Paper No. 2114.

De Zoysa, 1978, "Steady State Analysis of Undersea Cables," Ocean Engineering, v. 5, n3.

Ellers, F.S., 1982, "Advanced Offshore Oil Platforms," Scientific American, v. 246, n4.

Finn, L.D., 1976, "A New Deepwater Offshore Platform - The Guyed Tower," Proceedings, Offshore Technology Conference, Paper No. 2688.

Finn, L.D. and Young, K.E., 1978, "Field Test of a Guyed Tower," Proceedings, Offshore Technology Conference, Paper No. 3131.

Fish, P.R., R.B. Dean and N.J. Heaf, 1980, "Fluid-Structure Interaction in Morison's Equation for the Design of Offshore Structures," Engineering Structures, v. 2, n1.

Fish, P.R. and R. Rainey, 1979, "The Importance of Structural Motion in the Calculation of Wave Loads on an Offshore Structure," Proceedings, BOSS 76, v. 2.

Frisch-Fay, R., 1962, Flexible Bars, Butterworth & Co., (Publishers) Ltd., London.

Gibbons, T. and Walton, C.O., 1966, "Evaluation of Two Methods for Predicting Tensions and Configurations of a Towed Body System Using Bare Cable," David Taylor Model Basin Report 2313.

Gie, T.S. and W.C. de Boom, 1981, "The Wave Induced Motions of a Tension Leg Platform in Deep Water," Proceedings, Offshore Technology Conference, Paper No. 4074.

Jain, R.K. and C.L. Kirk, 1981, "Dynamic Response of a Double Articulated Offshore Loading Structure to Noncollinear Wave and Current," ASME Jour. of Energy Resource Tech., v. 103, n1.

Jefferys, E.R. and M.H. Patel, 1981, "Dynamic Analysis Models of the Tension Leg Platform," Proceedings, Offshore Technology Conference, Paper No. 4075.

Kirk, C.L. and R.K. Jain, 1977, "Response of Articulated Towers to Waves and Current," Proceedings, Offshore Technology Conference, Paper No. 2798.

Kitami, E.K. Ninomiya, M. Katayama and K. Unoki, 1982, "Response Characteristics of Tension Leg Platform with Mechanical Damping Systems in Waves," Proceedings, Offshore Technology Conference, Paper No. 4393.

Leonard, J.W. and Hudspeth, R.T., 1979, "Loads on Sea-Based Structures," Structural Technology in the Ocean, ASCE Nat'l. Convention, Atlanta, GA.

Lewis, R.E., 1982, "An Overview of Deepwater Compliant Structures," Petroleum Engineer International, v. 54, n6, May, pp 92-114.

Lo, A., 1982, "Nonlinear Dynamic Analysis of Cable and Membrane Structures," Ph.D. Thesis, Oregon State University, Corvallis, OR.

MacDonald, R.D., 1974, "The Design and Field Testing of the 'Triton' Tension Leg Fixed Platform and its Future Application of Petroleum Production and Processing in Deep Water," Proceedings, Offshore Technology Conference, Paper No. 2104.

McGuire, W. and Gallagher, R.H., 1979, Matrix Structural Analysis, John Wiley and Sons.

McIver, D.B., 1981, "The Static Offset of Tension Leg Platforms," Proceedings, Offshore Technology Conference, Paper No. 4070.

Mercier, J.A., 1982, "Evolution of Tension Leg Platform Technology," Proceedings, BOSS 1982, MIT, Cambridge, MA.

Mercier, J.A., R.G. Goldsmith and L.B. Curtis, 1980, "The Hutton TLP: A Preliminary Design," Proceedings, European Offshore Petroleum Conference and Exhibition, paper EUR 264, London, England.

Mercier, J.A. and R.W. Marshall, 1981, "Design of a Tension Leg Platform," Proceedings, Symposium on Offshore Engineering, Royal Institute of Naval Architects, London, England.

Mes, M.J. 1981-82, "Guyed Tower Design and Analysis, Parts 1-5," Petroleum Engineering International, v. 53, n13.

Morison, J.R., O'Brien, M.P., Johnson, J.W., Schaff, S.A., 1950, "The Force Exerted by Surface Waves on Piles," Petroleum Trans., AIME, v. 189, pp 149-154.

Nair, D. and Duval, P.S., 1982, "Design Concepts and Strategies for Guyed Tower Platforms," Proceedings, BOSS 1982, MIT, Cambridge, MA.

Natvig, B.J. and J.W. Pendered, 1977, "Nonlinear Motion Response of Floating Structures to Wave Excitation," Proceedings, Offshore Technology Conference, Paper No. 2796.

Pauling, J.R. and E.E. Horton, 1970, "Analysis of Tension Leg Stable Platform," Proceedings, Offshore Technology Conference, Paper No. 1263.

Pauling, J.R., 1979, "Frequency Domain Analysis of OTEC CWP and Platform Dynamics," Proceedings, Offshore Technology Conference, Paper No. 3543.

Penzien, J., 1976, "Structural Dynamics of Fixed Offshore Structures," Behavior of Offshore Structures, Proceedings, 1st Int'l Conf., v. 1.

Peyrot, A.H., 1980, "Marine Cable Structures," ASCE Jour. Structural Div., v. 106, n12.

Rainey, R.C.T., 1978, "The Dynamics of Tethered Platforms," Transactions, Royal Institute of Naval Architects, v. 120, London, England.

Rainey, R.C.T., 1980, "Parasitic Motions of Offshore Structures," Transactions, Royal Institute of Naval Architects, v. 122, London, England.

Sarpkaya, T. and Isaacson, M., 1981, Mechanics of Wave Forces on Structures, Van Nostrand Reinhold Co., NY.

Sergev, S.S. and W.D. Iwan, 1981, "The Natural Frequencies and Mode Shapes of Cables with Attached Masses," ASME Jour. of Energy Resource Tech., v. 103, n3.

Smith, E., A. Aas-Jakobsen and R. Sigbornsson, 1980, "Nonlinear Stochastic Analysis of Compliant Platforms," Proceedings, Offshore Technology Conference, Paper No. 3801.

Suhara, T., Koterayama, W., Tasai, F., Hiyama, H., Sao, K., Watanabe, K., 1981, "Dynamic Behavior and Tension of Oscillating Mooring Chain," Proceedings, Offshore Technology Conference, Paper No. 4053.

Taudin, P., 1978, "Dynamic Response of Flexible Offshore Structures to Regular Waves," Proceedings, Offshore Technology Conference, Paper No. 3160.

Tetlow, J.H. and Leece, M.J., 1982, "Hutton TLP Mooring System," Proceedings, Offshore Technology Conference, Paper No. 4428.

Triantafyllou, G. Kardomateas and A. Blick, 1982, "The Statics and Dynamics of the Mooring Lines of a Guyed Tower for Design Applications," Proceedings, BOSS '82, v. 1, pp. 546-564.

Tuah, H., 1982, "Cable Dynamics in an Ocean Environment," Ph.D. Thesis, Oregon State University, Corvallis, OR.

U.S. Army Coastal Engineering Research Center, 1977, Shore Protection Manual, U.S. Govt. Printing Office.

Volterra, E. and Zachmanoglou, E.C., 1965, Dynamics of Vibrations, Charles E. Merrill Books, Inc., Columbus, Ohio.

Wade, B.G. and Dwyer, M., 1976, "On the Application of Morison's Equation to Fixed Offshore Platforms," Proceedings, Offshore Technology Conference, Paper No. 2723.

Webster, R.L., 1975, "Nonlinear Static and Dynamic Response of Underwater Cable Structures Using the Finite Element Method," Proceedings, Offshore Technology Conference, Paper No. 2322.

Webster, R.L., 1980, "On the Static Analysis of Structures with Strong Geometric Nonlinearity," Computers and Structures, v. 11, pp 137-145.

Wilhelmy, V., Fjeld, S., and Schneider, S., 1981, "Non-linear Response Analysis of Anchorage Systems for Compliant Deep Water Platforms," Proceedings, Offshore Technology Conference, Paper No. 4051.

Yoshida, K., T. Koneya, N. Oka and M. Ozaki, 1981, "Motions and Leg Tensions of Tension Leg Platforms," Proceedings, Offshore Technology Conference, Paper No. 4073.

Zienkiewicz, O.C., 1977, The Finite Element Method, 3rd Ed., McGraw Hill Book Co., London.

APPENDIX B

DYNAMIC WAVE-PLATFORM-RESTRAINT INTERACTION FOR TENSION LEG PLATFORMS

by

Robert T. Hudspeth, Associate Professor, Ocean Engineering Program, Dept. of Civil Engineering, Oregon State University, Corvallis, Oregon 97331 USA

John W. Leonard, Professor, Ocean Engineering Program, Dept. of Civil Engineering, Oregon State University, Corvallis, Oregon 97331 USA.

Abstract

In the design of a tension leg platform, the variation in tether tension should be minimized in order to inhibit fatigue failure. In addition, a stable platform must be maintained with small motions. The tension legs serve to inhibit roll, pitch and heave in shallower waters. However, in deep water, the tether elongations may lead to significant values of these motions. TLP's are extremely compliant systems when the horizontal plane motions are considered. The legs provide nonlinear restoring forces because of the interactions of the prestress with the surge and sway motions.

For fixed structures such as gravity platforms and tension leg platforms which have characteristic member dimensions that are no longer negligible compared to the incident wave length, the Morison equation assumption that the structure has no observable effect on the incident wave field is no longer valid. A diffraction theory is needed to account for the additional pressure field that is developed around a large structure due to the no longer negligible wave-structure interaction.

For the case of a large floating vessel such as a TLP, the wave-induced motion of the floating structure creates an additional reaction force of the water on the structure. The wave-induced pressure forces on the structure are linearly decomposed into two components: a diffraction force on a fixed structure; and a reaction force on an oscillating structure in otherwise still water.

Numerical computer algorithms have been developed from a Green's function solution for fixed structures of arbitrary shape. This approach can be significantly improved computationally for axisymmetric bodies by using an eigenfunction expansion of the Green's function. That approach is extended to include radiation damping and added mass matrices and buoyancy and tether stiffness matrices. The option of

using a hydroelastic Morison's equation for selected member elements is included. The equations are transformed (with phase lag) from the center of gravity of the total platform and solved for the dynamic degrees of freedom of the TLP.

Introduction

Tension leg platforms (TLPs) are a type of semi-submerged platform being considered for use in deep-water operations. A representative TLP design is depicted in Fig. 1. The TLP is similar to conventional semi-submersible platforms in that a deck is mounted above the waterline on a structural framework supported by several vertical buoyant members. The buoyancy of these vertical and horizontal members is such that it exceeds the total platform's weight and thus pretensions several tether elements anchored to the ocean bottom. These tether elements comprise the "tension legs" and maintain the TLP in position.

In the design of a TLP, the variation in tether tension should be minimized to inhibit fatigue failure. Also a stable platform must be maintained with small roll, pitch and heave motions as well as surge, sway and yaw. The tension legs inhibit roll, pitch and heave in shallower waters. However, in deep water, the tether elongations may lead to significant values of these motions.

The platform horizontal plane motions of surge, sway and yaw are of primary importance. TLPs are extremely compliant systems when the horizontal plane motions are considered. The legs provide nonlinear restoring forces because of the interaction of the prestress with the surge and sway motions.

Pressure forces on fixed and floating structures result from the interaction of the structure with the weakly nonlinear and slightly non-Gaussian surface water waves. For fixed space frame structures with structural members that are small compared to the dimensions of the incident wave length, the Morison equation is used to provide a static-equivalent wave force loading. For fixed, but compliant, space-frame structures, a wave-structure interaction type of Morison equation has been developed that employs the relative motion between the compliant structure and the water particles in the oscillatory wave field. The Morison equation method assumes that the effect of the structure on the

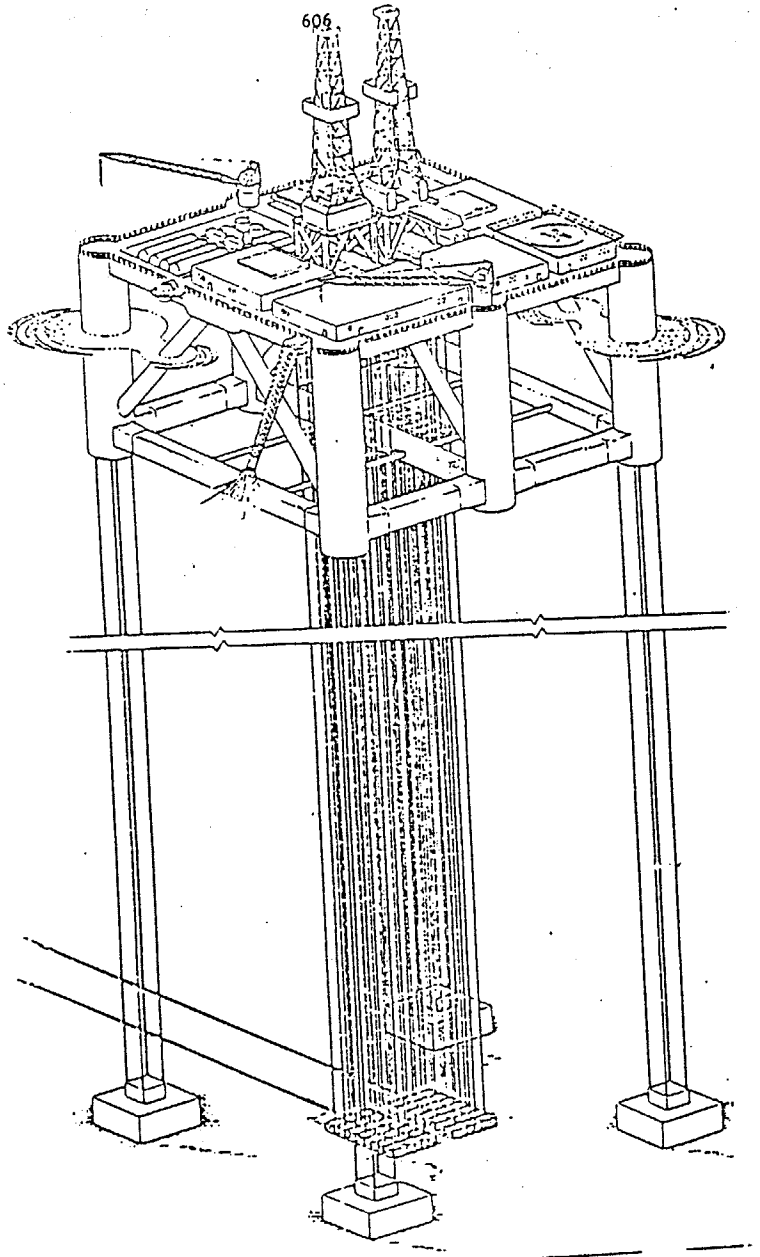

Fig. 1 Representative Tension Leg Platform

wave field is negligible and that no waves may be observed radiating away from the structure despite the motions that result from the wave-structure interaction.

For fixed structures such as the gravity platforms in the North Sea which have characteristic member dimensions that are no longer negligible compared to the incident wave length, the Morison equation assumption that the structure has no observable effect on the incident wave field is no longer valid. A linear diffraction theory has been developed to account for the additional pressure field that is developed around a large structure due to the no longer negligible wave-structure interaction. Because this theory is a linear approximation, it is not capable of including in a rigorous manner the nonlinear drag force effects which dominate the wave force loading when the ratio of pile diameter/wave length becomes small.

For the case of a large floating vessel such as a TLP, the wave-induced motion of the floating structure creates an additional reaction force of the water on the structure. The present method of analyzing this interaction is to linearly decompose the wave-induced pressure forces on the structure into two components: a diffraction force on a fixed structure that is termed an exciting force; and a reaction force on an oscillating structure in otherwise still water that is termed a restoring force.

A computationally efficient algorithm was developed for the DOT TLP shown in Fig. 2. This one-third scale model consists of a triangular shaped deck with three vertically axisymmetric circular cylinders, one at each corner of the deck. Smaller diameter circular cylinders connect each of these three vertical buoyant legs. Because of the vertical axes of symmetry in the three vertical legs and because there are no larger horizontal buoyant members between these three vertical members, a computationally efficient numerical algorithm was developed which incorporated an eigenfunction expansion for the Green's function for axisymmetric bodies of revolution and a linearized hydroelastic Morison equation for the hydrodynamic pressure forces on the small member cross bracing (vide, Fig. 2). A sample calculation and comparison with experimental results from the DOT TLP are also included.

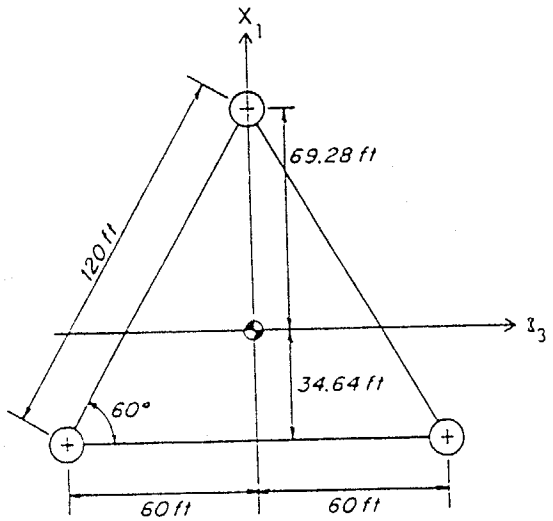

DECK PLAN VIEW

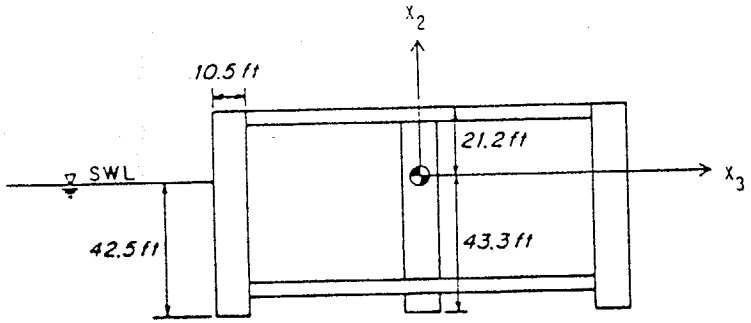

ELEVATION

FIG. 2 Definition Sketch for DOT TLP

Theoretical Modeling Assumptions

The DOT TLP algorithm solves for the dynamic response of a TLP having vertically axisymmetric buoyant members and small member cross bracing. The dynamic response of the TLP in the global coordinate axes shown in Fig. 2 is obtained by solving for the hydrodynamic pressure forces on each member in local member coordinates and then transforming these local forces back into the global coordinate axes by simple coordinate transformations. Interaction between the large buoyant members or small member cross bracings is considered to be negligible and is not included in the analysis.

Global Platform Coordinate Axis

The global coordinate axis for a platform having N vertically axisymmetric buoyant members is shown in Fig. 3. The X-Z plane lies parallel to the horizontal still-water plane with the vertical Y axis positive up. Each buoyant member is rigidly connected to the platform deck. The origin of the global coordinate axis {X,Y,Z} is located at the platform center of gravity (vide, Fig. 2).

Local Body Coordinate Axes

A local body coordinate system for each of the N vertically axisymmetric buoyant body is aligned parallel to the global coordinate system with each of the axes origins located at the center of gravity for each axisymmetric buoyant local body (vide, Fig. 2). A local body coordinate system for each of the N' hydroelastic Morison members is shown in Fig. 3. A position vector $\vec{R}_n$ defines the distance from the global coordinate axes at the TLP center of gravity to the n^{th} local body coordinate axes at the local body center of gravity for both the vertically axisymmetric buoyant bodies and the hydroelastic Morison members according to

$$\vec{R}_n = X_n \vec{e}_x + Y_n \vec{e}_y + Z_n \vec{e}_z \qquad (1)$$

Wave Coordinate Axis

Monochromatic, long-crested, linear waves are assumed to be propagating without change of form at a constant angle of attack, ψ, shown in

Fig. 3. Hydrodynamic interaction is neglected between either the large vertically axisymmetric buoyant diffraction bodies or the hydroelastic Morison member cross bracings. Consequently, neither the scattered wave field from the buoyant diffraction bodies nor the shielding effect from the hydroelastic Morison member cross bracings are included in the determination of the local hydrodynamic pressure forces. This assumption appears to be experimentally justified by the DOT TLP data comparisons.

Local to Global Coordinate Transformations

The TLP is assumed to have six degrees of freedom in dynamic response to the waves; viz., three translational modes $\{X_1, X_2, X_3\}$ and three rotational modes $\{\Omega_4, \Omega_5, \Omega_6\}$ (vide, Fig. 2). The n^{th} local body translational displacements may be expressed in terms of the global coordinates according to

$$\vec{x}_n = \vec{X} - \vec{R}_n \times \vec{\Omega} \tag{2}$$

$$= \{x, y, z\}$$

and the n^{th} local rotational displacements by

$$\vec{\omega}_n = \vec{\Omega} \tag{3}$$

The velocity and acceleration of the n^{th} local body are obtained from the temporal derivatives of Eqs. (2) and (3), respectively; i.e.,

$$\vec{u}_n = \dot{\vec{X}} - \vec{R}_n \times \dot{\vec{\Omega}} \tag{4a}$$

$$\dot{\vec{\omega}}_n = \dot{\vec{\Omega}} \tag{4b}$$

$$\vec{a}_n = \ddot{\vec{X}} - \vec{R}_n \times \ddot{\vec{\Omega}} \tag{5a}$$

$$\ddot{\vec{\omega}}_n = \ddot{\vec{\Omega}} \tag{5b}$$

Hydrodynamic Pressure Forces on n^{th} Local Body

The hydrodynamic pressure forces on the n^{th} local body due to long crested, linear waves propagating at an angle, ψ, to the global coordinate axes are assumed to be linearly decomposed into three separate components: viz., 1) hydrostatic restoring force; 2) wave-induced exciting force on a fixed body; and 3) wave-induced restoring force on a body oscillating in otherwise still water (wavemaker force).

Efficient TLP Vessel Response Computations

Numerical computer algorithms have been developed[1,2,3] which are derived from a Green's function solution to the problem of diffraction of linear progressive waves by a fixed structure of arbitrary shape. A more computationally efficient numerical solution to the linear wave diffraction problem has been developed[4] based on the eigenfunction solutions and a variational principle for fixed and floating structures whose geometry is not arbitrary, but is separable in either Cartesian or polar coordinates. Although the latter method exhibits significant computational savings over the Green's function algorithm for arbitrary structural geometry, the structural geometric restrictions imposed by the latter method severely limits its usefulness for many ocean engineering applications.

Recently, it has been demonstrated[5] that the computational aspects of the Green's function method could be significantly improved for structures with vertical axes of symmetry by expanding the Green's function in an eigenfunction expansion. It has been noted[6] that the eigenfunction expansion of the Green's function resulted in computer savings of three orders of magnitude over the surface area integrations required by the original Green's function method. This extremely computationally efficient, yet versatile, eigenfunction expansion of the Green's function will be employed in this application.

Equations of Motion

The problems under consideration is represented schematically in Fig. 3. A small amplitude regular wave train of wave height H is considered to progress in water of depth h and interact with the semi-constrained floating body. The mean position of the center of mass of

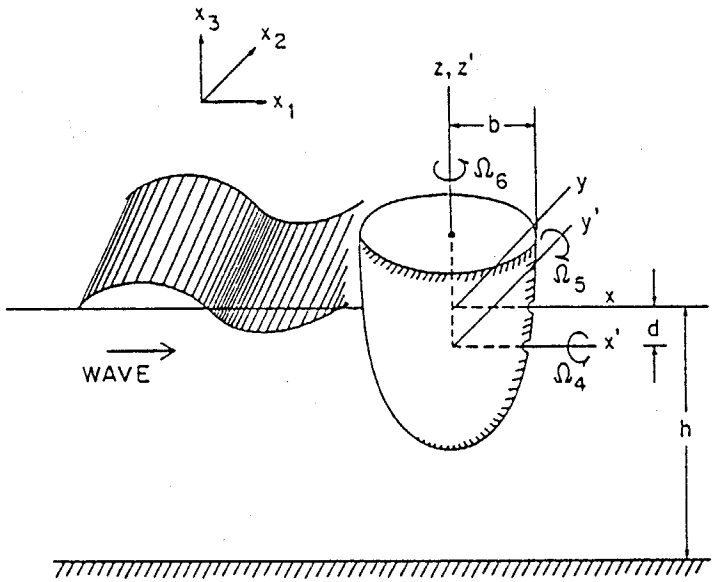

Fig. 3 Definition sketch for vertically axisymmetric buoyant TLP member

the body is located at distance d beneath the mean free surface and a coordinate system x', y', z', is attached to the body with origin at the mass center (c.g.) and is aligned with the wave coordinate system (x,y,z) at the still-water level. The small amplitude displacement of the body center of mass with respect to its mean position (C.G.) in the global reference frame (X_1,X_2,X_3) of the assemblage is described by the three coordinates $U_1(t)$, $U_2(t)$ and $U_3(t)$ which are referred to as surge, sway and heave, respectively. The small angular displacements of the body about the X_1, X_2, X_3 axes are denoted by U_4, U_5 and U_6 and are referred to as roll, pitch and yaw, respectively. The corresponding kinematic degrees of freedom in the individual body coordinates will be denoted by lower case u_n, n = 1, 6.

The equations of motion for the individual body linearized with respect to the small angular displacements of the body may now be written at the bodies c.g. as follows:

$$f_1^T(t) = m_{11}\ddot{u}_1(t)$$

$$f_2^T(t) = m_{22}\ddot{u}_2(t)$$

$$f_3^T(t) = m_{33}\ddot{u}_3(t) \qquad (6a)$$

$$f_4^T(t) = m_{44}\ddot{u}_4 - m_{45}\ddot{u}_5 - m_{46}\ddot{u}_6$$

$$f_5^T(t) = m_{55}\ddot{u}_5 - m_{56}\ddot{u}_6 - m_{54}\ddot{u}_4$$

$$f_6^T(t) = m_{66}\ddot{u}_6 - m_{64}\ddot{u}_4 - m_{65}\ddot{u}_5 \qquad (6b)$$

where $f_1^T(t)$, $f_2^T(t)$ and $f_3^T(t)$ denote the three components of the total external force acting on the body and $f_4^T(t)$, $f_5^T(t)$ and $f_6^T(t)$ denote the three components of the total external moment about the c.g. The symbol m denotes the body mass which equals the displaced mass for freely floating bodies: $m = m_{11} = m_{22} = m_{33}$. The moments of inertia are defined, typically as

$$m_{45} = m_{54} = \int x'\, y'\, dm \qquad (6c)$$

where the integration is to be carried out over the complete mass of the individual body. For bodies having symmetry with respect to the (x' - y') and (y' - z') planes, all of the products of inertia vanish. Although this type of symmetry is common to most ocean structures, there is no need to apply the limitation at this point since the inclusion of the product of inertia terms do not, in principle, complicate the development. In a later section the forces and kinematic degrees of freedom will be transformed to the total platform CG for assemblage.

For free-floating bodies $f_n^T(t)$ represent the contributions from the surrounding fluid only and are generally considered to be composed of three parts: a) the wave excitation forces and moments, b) the dynamic forces and moments caused by the responsive motion of the body, and c) the hydrostatic forces and moments caused by body displacements. For the linear problem these three contributions may be determined separately and superimposed (n = 1 to 6 and repeated subscripts denote summation over range 1 to 6).

$$f_n^T(t) = C_n(t) \qquad \text{(part a)}$$

$$- M_{nj}\ddot{u}_j(t) - N_{nj}\omega\dot{u}_j \qquad \text{(part b)} \qquad (7)$$

$$- K_{nj}u_j \qquad \text{(part c)}$$

For partially restrained bodies such as TLPs, a tension leg restoring force must be added (considered later).

Exciting Force

The generalized force coefficient $C_n(t)$ may be expressed as

$$C_n(t) = \frac{H}{2} \text{Re}\left\{|C_n| \exp\left[-i\left(\omega t - \alpha_n\right)\right]\right\} \qquad (8)$$

where $i = \sqrt{-1}$, H is wave height, the frequency of wave excitation is denoted by ω and α_n denotes the phase shift angle of the n^{th} component of force or moment in relationship to the incident wave. All phase shift angles are measured relative to the incident wave with the t = 0 conditions corresponding to the condition when the crest of the undisturbed incident wave is at the coordinate origin. The magnitude $|C_n|$ of the complex-valued exciting force or moment coefficient occurring in Eq. (8) is to be determined from a wave diffraction problem about an equivalent fixed body and will be discussed subsequently.

Restoring Force

As the body responds to the wave excitation, dynamic pressures arise due to the motion which may be resolved into two components of generalized force, one in-phase and proportional to the acceleration $\ddot{u}_n$ of the body and a second in-phase and proportional to the velocity $\dot{u}_n$ of the body. These two components are characterized by added mass coefficients, M_{nj}, and damping coefficients, N_{nj}. According to the definitions of these parameters, $C_{nj}(t)$ which denotes the n-component force due to the j-component motion is given by

$$C_{nj}(t) = - M_{nj}\ddot{u}_j(t) - \omega N_{nj}\dot{u}_j \qquad (9)$$

The added mass and damping coefficients are dependent on the shape of the body, the water depth and the wave frequency.

Hydrostatic Force

The final contribution to the generalized force resulting from the surrounding fluid comes from the hydrostatic pressure. As the body is displaced from its equilibrium position, forces and moments arise which are proportional to the body displacement. The hydrostatic pressure increases with depth according to $p = -\rho gz$ and, consequently, the n^{th} component of hydrostatic force or moment resulting from this pressure variation and acting on the body are given by the integrals

$$F_n^H = \rho g \iint_S z' g_n \, dS \,, \qquad (10)$$

where g_n (n = 1,2,3) are the direction cosines of the unit normal to the surface area dS. The pseudo direction cosines g_n(n = 4,5,6) represent moment arms of a general surface point about the c.g.:

$$g_4 = g_3y' - g_2z' \,; \quad g_5 = g_1z' - g_3x' \,; \quad g_6 = g_2x' - g_1y' \qquad (11)$$

Moreover, the following linearized relationships exist between the coordinates (x,y,z) of the wave coordinate system and the body coordinates for a given point on the body surface located at x', y', z':

$$x = x' + u_1 + \Omega_5 z' - \Omega_6 y' \tag{12a}$$

$$y = y' + u_2 + \Omega_6 x' - \Omega_4 z' \tag{12b}$$

$$z = z' - d + u_3 + \Omega_4 y' - \Omega_5 x' \tag{12c}$$

Equation (10) represents the hydrostatic force (or moment) acting on the immersed surface including the buoyant force which must, of course, just balance the weight. It is desired, however, to determine the n^{th} component of force associated with a j^{th} ($j = 1,2,\ldots 6$) component of displacement of the body, $j = 1,2,3$ denoting displacement in the x', y', z' directions, respectively and $j = 4,5,6$ denoting angular displacement about the x', y', z' axes, respectively.

For the linearized problem this force (or moment) may be written in Taylor expansion form as:

$$F_n^H = \frac{\partial F_n^H}{\partial u_j} u_j = u_j \frac{\partial}{\partial u_j} \iint_S z' g_n dS = K_{nj} u_j \tag{13}$$

where we have defined a buoyant stiffness K_{nj} as

$$K_{nj} = \iint_S \frac{\partial}{\partial u_j} (z' g_n)\, dS \tag{14}$$

To the buoyant stiffness must be added the tether stiffness $\overline{K}_{nj}$. Assuming the tension leg is connected to the body at the c.g., we find

$$\overline{K}_{nj} = \left[\frac{AE}{L} \delta_{nj} + \frac{T}{L} \theta_n \theta_j\right] \text{ if } n, j < 3.$$

$$\overline{K}_{nj} = 0 \text{ otherwise}$$

where δ_{nj} = Kronecker delta; and for each tether T = tension, L = length, A = cross-sectional area, E = modulus of elasticity, θ_j = direction cosines of the tension leg.

The equations of motion for a tethered floating body are therefore

$$(m_{nj} + M_{nj})\, \ddot{u}_j + N_{nj}\, \omega \dot{u}_j + (K_{nj} + \overline{K}_{nj})\, u_j = \mathrm{Re}\{|C_n| \exp[-i(\omega t - \alpha_n)]\} \tag{15}$$

Furthermore, the body response in the n^{th} degree of freedom may be expressed in the form

$$u_n(t) = u_n^o \,\mathrm{Re}[\exp(i\psi_n)\exp(-i\omega t)] \tag{16}$$

which, when substituted into Eq. (15), yields the complex-valued equations of motion,

$$\left[-(m_{nj} + M_{nj}) - iN_{nj} + \frac{(K_{nj} + \overline{K}_{nj})}{\omega^2}\right] \frac{2u_n^o}{H} \exp(i\psi_n) = \frac{|C_n|}{\omega^2} \exp(i\alpha_n) \tag{17}$$

Equation (17) represents six equations corresponding to $n = 1,2\ldots 6$. The repeated j index denotes, as usual, the summation over the six degrees of freedom. The amplitude ratio $2u_n^o/H$ denotes the ratio of the amplitude of the motion to the amplitude of the incident wave and ψ_n denotes the phase angle of the motion in relation to the reference condition of the crest of the incident wave being located at the coordinate origin.

It will be recalled that for bodies possessing x' - y' and y' - z' plane symmetry, $m_{nj} = 0$ for $n \neq j$ in Eq. (17). Also, M_{nj} and N_{nj} denote the 36-element added mass and damping tensors. It can be shown, however that

$$K_{nj} = K_{jn},\ M_{nj} = M_{jn},\ N_{nj} = N_{jn} \tag{18}$$

Hydrodynamic Exciting Forces and Moments

The wave-induced exciting forces and moments on a floating vessel in Eq. (8) may be computed from a solution to the wave diffraction problem on a fixed body. The wave train has amplitude a (wave height = H), wavelength λ, wave number $k = 2\pi/\lambda$, and wave frequency $\omega = 2\pi/T$, where T is the period. Using irrotational flow theory and the linearized wave approximation, we have the following equations for a body of arbitrary shape.

A velocity potential Φ exists:

$$\Phi = \mathrm{Re}\{\phi(x,y,z)\exp(-i\omega t)\} , \tag{19}$$

where t is time and ϕ is a complex variable which may be split into incident and scattered parts

$$\phi = \phi_i + \phi_s , \tag{20}$$

where the incident term is well known from linear wave theory,

$$\phi_i = \frac{-gH}{2\omega}\frac{\cosh k(z+h)}{\cosh kh}\exp(ikx) \tag{21a}$$

in which g is the gravitational acceleration and provided that

$$\omega^2 = gk \tanh kh . \tag{21b}$$

The scattered potential, as yet unknown, may be assumed to be generated by a distribution of sources with strength f(X,Y,Z) over the immersed surface of the body:

$$\phi_s(x,y,z) = \frac{1}{4\pi}\int_A f(X,Y,Z)\, G\,(x,y,z|X,Y,Z)dA , \tag{22}$$

where the variables of integration (X,Y,Z) are the coordinates of points on the wetted surface of the body, denoted by A.

The unknown source strength distribution f(X,Y,Z) must be such as to satisfy the boundary condition on the body surface, that no fluid passes through the surface. Combining Eqs. (20)-(20) and differentiating with respect to n, the local outwardly directed normal to the surface, to obtain the normal fluid velocity, we have

$$-2\pi f(x,y,z) + \frac{\partial}{\partial n}\int_A f(X,Y,Z)G(x,y,z|X,Y,Z)dA(X,Y,Z) - 4\pi\frac{\partial\phi_i}{\partial n}(x,y,z) = 0 . \tag{23}$$

Equation (23) is to be satisfied at all points on the wetted body surface A (x,y,z). Once this integral equation has been solved for f, this is substituted into Eq. (22) to give $\phi_s(x,y,z)$. From this, other physical quantities are easily calculated:

$$p/\rho = \partial\Phi/\partial t = \mathrm{Re}\{-i\omega(\phi_i + \phi_s)\exp(-i\omega t)\} , \tag{24}$$

where p is the pressure at any point and ρ is fluid density;

$$\eta = \mathrm{Re}\{(-i\omega/g)(\phi_i + \phi_s)\exp(-i\omega t)\} \quad \text{on } z = 0 , \tag{25}$$

where η is the free-surface elevation relative to the undisturbed level. Fluid velocities v are given by

$$v = -\nabla\Phi = \mathrm{Re}\{-\nabla(\phi_i + \phi_s)\exp(-i\omega t)\} . \tag{26}$$

The total exciting force exerted on the body F and the moment of this force M are given by

$$F(t) = -\int_A p\hat{n}dA , \tag{27}$$

$$M(t) = -\int_A p(\hat{r} \times \hat{n})\, dA , \tag{28}$$

where $\hat{n}$ is a unit outward normal vector on A and $\hat{r}$ is the vector from the point about which moments are taken.

Introducing horizontal cylindrical coordinates as

$$r^2 = x^2 + y^2 ; \; R^2 = X^2 + Y^2 ; \; \tan\theta = Y/x ; \; \tan\Theta = Y/X ;$$

then $q^2 = R^2 + r^2 - 2Rr\cos(\theta - \Theta)$. Making use of Graf's addition theorem gives

$$J_o(kq) = \sum_{j=-\infty}^{\infty} J_j(kR)J_j(kr)\cos j(\theta-\Theta) ,$$

$$Y_o(kq) = \sum_{j=-\infty}^{\infty} Y_j(k_R^r)J_j(k_r^R)\cos j(\theta-\Theta) , \qquad (29)$$

$$K_o(\mu_m q) = \sum_{j=-\infty}^{\infty} K_j(\mu_m {}^{r}_{R})I_j(\mu_m {}^{R}_{r})\cos j(\theta - \Theta) ,$$

where the upper of the alternative arguments is used if $r > R$ and the lower otherwise. In each of the three series the $-j^{th}$ term is equal to the j^{th} term. Introducing a Kronecker delta we may write

$$J_o(kq) = \sum_{j=0}^{\infty} (2 - \delta_{jo})J_j(kR)J_j(kr)\cos j(\theta - \Theta) , \qquad (30)$$

the other two expressions being transformed in the same way.

The Green's function, $G(r,\vartheta,z|R,\Theta,Z)$, (or resolvent kernel) in Eq. (22) is given by the following orthonormal eigenfunction expansion:

$$G(r,\vartheta,z|R,\Theta,Z) = i\pi \sum_{n=1}^{\infty} Q_n(\kappa_n z)Q_n(\kappa_n Z) \sum_{j=0}^{\infty} (2-\delta_{jo})$$
$$J_j(\kappa_n \{{}^{R}_{r}\})H_j^{(1)}(\kappa_n \{{}^{r}_{R}\})\cos j(\theta - \Theta) \qquad (31)$$

in which the orthonormal eigenfunctions, $Q_n(\cdot)$, are defined by

$$Q_n(k_n \{{}^{z}_{Z}\}) = N_n^{-1} \cosh \kappa_n (z + h) \qquad (32a)$$

$$N_n^2 = (4\kappa_n)^{-1}\{2\kappa_n h + \sinh 2\kappa_n h\} \qquad (32b)$$

and the eigenvalues computed from Eq. (21b) are

$$\kappa_n = \begin{cases} k & ; \quad n = 1 \\ i\kappa_n & ; \quad n > 2 \end{cases} \qquad (32c)$$

and $H_\ell^{(1)}(\cdot)$ = Hankel function of the first kind of order ℓ and the upper argument is to be used in the Bessel functions if $r > R$ and the lower argument otherwise. Since only the Hankel function of the first kind will be used in the following, superscript (1) for the Hankel function will be omitted hereafter.

Defining

$$G_{j1} = Q_1(kz)Q_1(kZ)J_j(k_r^R)(Y_j(k_R^r) - iJ_j(k_R^r)) \qquad (33a)$$

and

$$G_{jm} = Q_m(k_m z)Q_m(k_m Z)(\mu_m {}^{r}_{R})I_j(\mu_m {}^{R}_{r}) . \qquad (33b)$$

permits Eq. (31) to be rewritten as

$$G(r,\theta,z|R,\Theta,Z) = \sum_{j=0}^{\infty} (G_{j1} + \sum_{m=2}^{\infty} G_{jm})(2-\delta_{j0})\cos j(\theta-\Theta) . \qquad (33c)$$

We use the integral equation (23) together with the Fourier expansion of the Green's function in Eqs. (33) to obtain a Fourier series. Subsequently, it is shown that only the zeroth and first terms need be solved to give the exciting forces and moments on the body.

The source strength f is a function of position on the body and may be written as $f(s,\theta)$, where the coordinate $s(r,z)$ specifies a point on the body surface. As the problem is symmetrical about the x axis, we may expand f in a cosine series:

$$f(s,\theta) = \sum_{p=0}^{\infty} f_p(s)\cos p\theta . \qquad (34)$$

Substituting Eqs. (34) and (33) into (33) we have

$$-2\pi \sum_{p=0}^{\infty} f_p(s)\cos p\Theta + \frac{\partial}{\partial n}\int_A \Big[\sum_{p=0}^{\infty} f_p(S)\cos p\Theta\Big]$$
$$\times \Big[\sum_{j=0}^{\infty} (2-\delta_{j0})(G_{j1} + \sum_{m=2}^{\infty} G_{jm})\cos j(\theta-\Theta)\Big]dA + 4\pi \frac{\partial \phi_i}{\partial n} = 0 . \qquad (35)$$

Eq. (21a) for ϕ_i may be written in cylindrical coordinates as the following:

$$\phi_i = -\frac{gH}{2\omega}\frac{\cosh k(z+h)}{\cosh kh}\exp(ikr\cos\theta)$$

It is easily shown that the operator $\partial/\partial n$ for an axisymmetric body traced anticlockwise is

$$\partial/\partial n \equiv z'\partial/\partial r - r'\partial/\partial z ,$$

where $z' = dz/ds$ and $r' = dr/ds$. Performing the operation we have

$$\frac{\partial\phi_i}{\partial n} = \frac{gHk\exp(ikr\cos\theta)}{2\omega\cosh kh}\{r'\sinh k(z+h) - iz'\cos\theta\cosh k(z+h)\}$$

$$= \frac{gHk}{2\omega\cosh kh}(r'\sinh k(z+h) - iz'\cos\theta\cosh k(z+h)\sum_{p=0}^{\infty}(2-\delta_{10})i^pJ_1(kr)\cos p\theta$$

$$= \frac{gHk}{2\omega\cosh kh}\sum_{p=0}^{\infty}(2-\delta_{p0})i^p[r'\sinh(kz+h)J_1kr) - z'\cosh(kz+h)J_1'(kr)]\cos p\theta \qquad (36)$$

which shows that the incident velocity field has been expressed as a Fourier series with coefficients that are functions of r and z.

Now we can rewrite the integral in the second term in Eq. (35) with $dA = Rd\theta dS$, where dS is an element of AA', so that it becomes

$$\frac{\partial}{\partial n}\int_S\sum_{p=0}^{\infty}f_p(S)\sum_{j=0}^{\infty}\left[\left(G_{j1}+\sum_{m=2}^{\infty}G_{jm}\right)(2-\delta_{j0})R\int_{-\pi}^{\pi}\cos p\theta\cos j(\theta-\theta)\right]d\theta dS \qquad (37)$$

Integrating with respect to θ we have

$$2\pi\sum_{p=0}^{\infty}\left[\frac{\partial}{\partial n}\int_S f_p(S)R\left(G_{p0}+\sum_{m=1}^{\infty}G_{pm}\right)dS\right]\cos p\theta \qquad (38)$$

From Eqs. (34)-(36) and (32) we see that the integral equation can be expressed as a Fourier series, with each term satisfying the equation. Thus, for each term we can write

$$-f_p(s) + \int_S f_p(S)R\left(z'\frac{\partial}{\partial r} - r'\frac{\partial}{\partial z}\right)\left(G_{p1}+\sum_{m=2}^{\infty}G_{pm}\right)dS$$
$$+\frac{(2-\delta_{p0})ghki^p}{\omega\cosh kh}\{r'\sinh k(z+h)\,J_p(kr)$$
$$- z'\cosh k(z+h)\,J_p'(kr)\} = 0,\ p = 0,1,2... \qquad (39)$$

and we now have a series of one-dimensional integral equations in place of the original surface integral equation. The line integral can be evaluated numerically by the trapezoidal rule. The problem reduces to the solution of a set of linear algebraic equations for f at the center of each of N straight line segments.

Hydroelastic Morison Force/Moment

The small member cross bracings shown in Fig. 2 do not lie in the diffraction force regime as do the large vertically axisymmetric corner members. Forces on these small members must be computed by a linearized hydroelastic Morison equation. The coordinate system used for the small member hydroelastc Morison force is shown in Fig. 4.

By generalizing the one-dimensional form of the Morison equation, the three-dimensional form of the hydrodynamic force acting normally to the n^{th} hydroelastic Mosion small member element is given by

$$\vec{F}_n^S = (C_m-1)\rho V(\vec{a}_n - \ddot{\vec{x}}_n) + C_D\frac{\rho}{2}A|\vec{V}_n-\dot{\vec{x}}_n|(\vec{V}_n-\dot{\vec{x}}_n) + \rho V\vec{a}_n \qquad (40)$$

in which C_m, C_D = inertia and drag coefficients, respectively; $\vec{a}_n, \vec{v}_n$ = local water particle acceleration and velocity normal to the member at the center of the n^{th} small member element, respectively; $\ddot{\vec{x}}_n, \dot{\vec{x}}_n$ = motion-induced member acceleration and velocity normal to the member at the center of the n^{th} small member element, respectivly; ρ = fluid mass density; and V, A = volume and normal area projection of the n^{th} small member element, respectively. Equation (40) may be linearly decomposed into a wave-induced exciting force for a fixed body and a motion-induced restoring force on a body oscillating in otherwise still water according to

$$\vec{F}_n^S = \vec{F}_n^e - \vec{F}_n^R = \vec{F}_n^e - \vec{F}_n^I - \vec{F}_n^v \qquad (41)$$

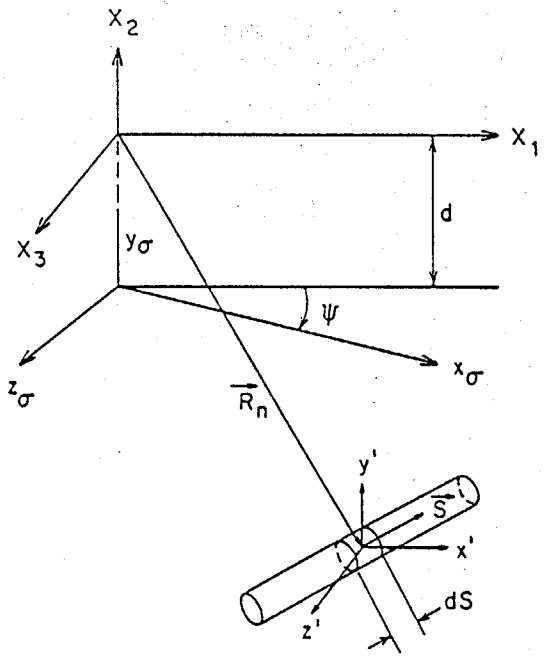

Fig. 4 Definition sketch for global, local and wave coordinate axes for Morison members

The corresponding hydrodynamic pressure moment induced on the global structure by Eq. (18) on the n^{th} local member may be expressed as

$$\vec{M}_n^S = \vec{R}_n \times \vec{F}_n^e - \vec{R}_n \times \{\vec{F}_n^I + \vec{F}_n^V\} \tag{42}$$

Equation of Motion for TLP

The preceding forces/moments on the N individual buoyant diffraction members plus the n' individual segments of the hydroelastic Morison member cross bracing are assembled to give the dynamic equations of motion for the TLP in the global coordinates according to

$$\sum_{n=1}^{N} \{\vec{F}_n^I + \vec{F}_n^D + \vec{F}_n^H + \vec{F}_n^M\} + \sum_{n=1}^{N'} \{\vec{F}_n^I + \vec{F}_n^V\} + \vec{F}^G = \sum_{n=1}^{N} \vec{F}_n^e + \sum_{n=1}^{N'} \vec{F}_n^e \tag{43a}$$

$$\sum_{n=1}^{N} \{\vec{M}_n^I + \vec{M}_n^D + \vec{M}_n^H + \vec{M}_n^M\} + \vec{M}^G + \sum_{n=1}^{N} \vec{R}_n \times \{\vec{F}_n^I + \vec{F}_n^D + \vec{F}_n^H + \vec{F}_n^M\} + \sum_{n=1}^{N'} \vec{R}_n \times \{\vec{F}_n^I + \vec{F}_n^V\} = \sum_{n=1}^{N} \vec{M}_n^e + \sum_{n=1}^{N} \vec{R}_n \times \vec{F}_n^e + \sum_{n=1}^{N'} \vec{R}_n \times \vec{F}_n^e \tag{43b}$$

in which N = total number of large vertically axisymmetric buoyant members and N' = total number of small member elements.

Example Problem for DOT TLP

Experimental response data recorded for the DOT TLP were compared with the present algorithm results. The moments of inertia for each local member were computed and compared with the DOT values. The local members analyzed are identified on the DOT TLP in Fig. 5. The 1:3 scale model DOT TLP shown in Fig. 2 consists of 3 vertically axisymmetric buoyant caissons located at each apex of the triangular shaped lock structure (denoted as #1a, b, c in Fig. 5); 3 each exterior and interior horizontal cross bracing members (#2, 7 in Fig. 5); 3 vertical small member columns (#4 in Fig. 5); 6 diagonal interior struts (#5 in Fig. 5); and 3 main deck cross braces (#6 in Fig. 5). Forces and moments on the 3 vertically axisymmetric buoyant caissons were computed by the

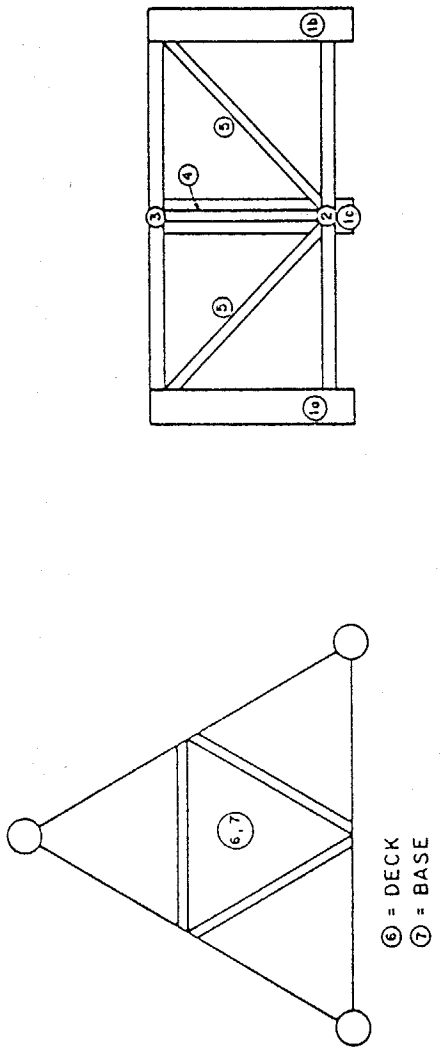

FIG. 5 Summary of DOT TLP inertia calculations

Green's function diffraction method while the forces and moments on all of the remaining small members were computed by the linearized hydroelastic Morison equation method.

The discretization scheme used to compute the forces/moments on the DOT TLP is shown in Fig. 6. Each vertically axisymmetric buoyant pontoon was discretized into 8 nodal points beginning at the submerged centerline of the vertically axisymmetric member (0, - 42.6) and ending at the stillwater level (5.25,0). Each of the 3 horizontal exterior cross bracing members were discretized into 10 equal segments for analyses by the linearized hydroelastic Morison equation (vide Fig. 4). Each of the 3 vertical small member columns and each of the 6 diagonal small member interior struts were discretized into 5 equal segments for analyses by the linearized hydroelastic Morison equation (vide Fig. 4).

Table 1 summarizes the inertia computations bases on the member dimensions. Table 2 compares the present calculations with the DOT values.

TABLE 2. Comparison of Present & DOT Inertia Values

INERTIA ($slug\text{-}ft^2 \times 10^{-7}$)	Present	DOT	$\frac{\text{Present}}{\text{DOT}}$ (%)
I_{xx}	3.111	4.136	75
I_{yy}	3.826	5.291	72
I_{zz}	3.111	4.136	75

It was originally proposed to represent the hydrodynamic pressure on the 1:3 scale model DOT TLP by only the vertically axisymmetric buoyant caissons (i.e., members 1a, b, and c). The comparison of these inertia values are summarized in Table 3.

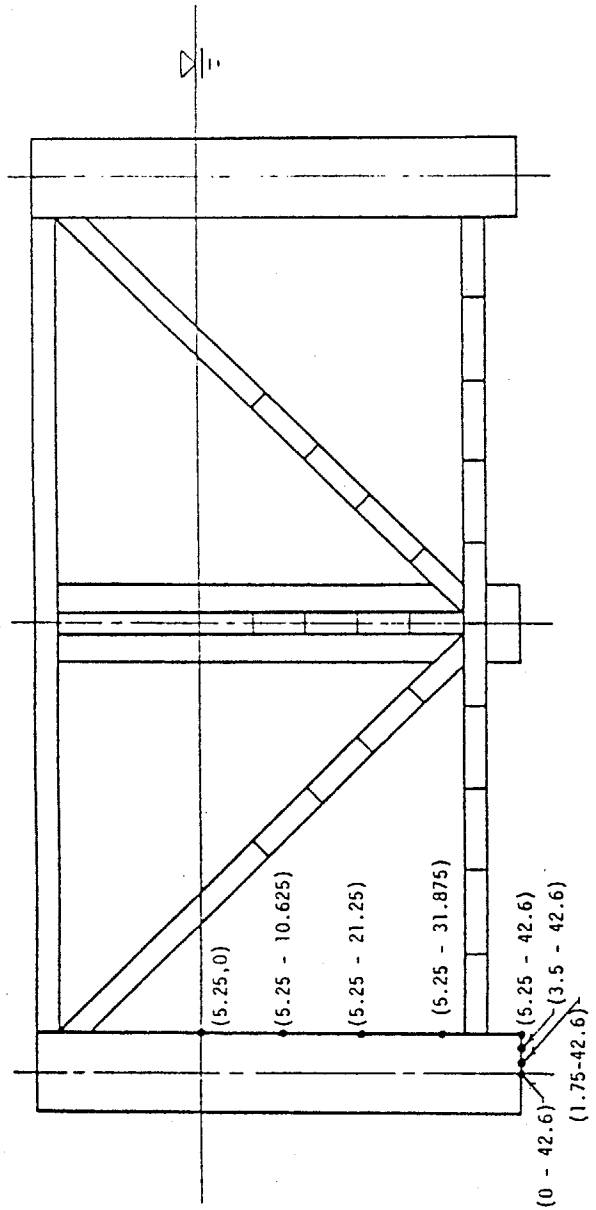

Fig. 6 Discretization of DOT TLP

TABLE 3. Summary of Vertically Axisymmetric Buoyant Caissons Only

INERTIA (slug-ft^{2}x10^{-7})	Present	DOT	$\frac{\text{Present}}{\text{DOT}}$ (%)
I_{xx}	2.816	3.416	82
I_{yy}	3.683	4.370	84
I_{zz}	2.816	3.416	82

Comparing Table 3 with Table 2 demonstrates that the large buoyant caissons represent very well the inertia of the 1:3 scale model DOT TLP. However, the hydrodynamic pressure forces on these caissons are only marginally inertially dominated (i.e., diffraction regime).

The dynamic response of the DOT TLP in the surge mode is compared in Fig. 7 with the results of the present TLP algorithm for various combinations of diffraction and Morison forces and moments. It can be seen that as more members are included in the model the surge results converge on both the accelerometer and microwave measured results. The results which include the Morison equation are better than the results for diffraction only. This is because the vertically axisymmetric buoyant members are only marginally large enough to consider diffraction effects. The prototype TLP results are expected to be more inertially dominated. The 5 frequencies used to compute the surge mode RAO in Fig. 7 were taken from the DOT WAVE-2 spectrum for 0° angle of attack in the global coordinate axis.

Summary

The dynamic equations of motion for the dynamic response of a floating vessel have been formulated for a linear six degree of freedom oscillating vessel. The wave-induced forces and moments on the vessel have been linearly decomposed into: 1) an exciting force on a fixed vessel in waves, and 2) a restoring force on an oscillating vessel that is being harmonically forced in otherwise calm water. The exciting force is computed by the more computationally efficient eigenfunction expansion of the Green's function for axisymmetric bodies. The exciting force may also be used to compute wave diffraction forces on fixed gravity structures.

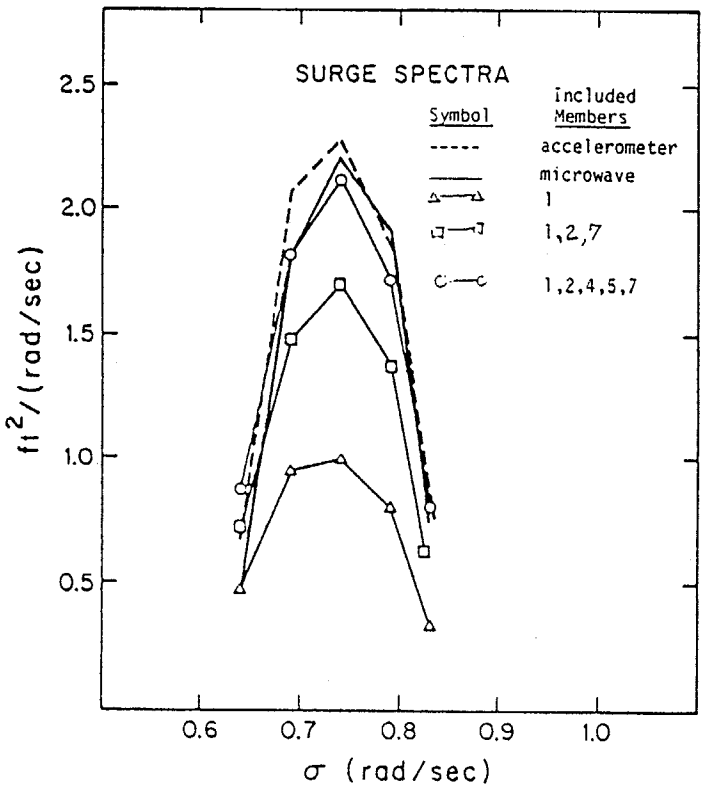

FIG. 7 Surge spectra for DOT TLP

References

1. Garrison, C.J., "Hydrodynamics of Large Objects in the Sea, Part I: Hydrodynamic Analysis," J. Hydronautics, Vol. 8, No. 1, January 1974, pp. 5-12.
2. Garrison, C.J., "Hydrodynamics of Large Objects in the Sea, Part II: Motion of Free-Floating Bodies," J. Hydronautics, Vol. 9, No. 2, April 1975, pp. 58-63.
3. Hogben, N. and R.G. Standing, "Experience in Computing Wave Loads on Large Bodies," Proc. 1975 Offshore Technology Conf., Vol. 1, Paper No. OTC 2189, 1975, pp. 413-431.
4. Black, J.L. and C.C. Mei, "Scattering and Radiation of Water Waves," Report No. 121, Water Resources and Hydrodynamics Lab., M.I.T., April 1970, 248 p.
5. Black, J.L., "Wave Forces on Vertical Axisymmetric Bodies," Journal Fluid Mechanics, Vol. 67, part 2, 1975, pp. 369-376.
6. Fenton, J.D., "Wave Forces on Vertical Bodies of Revolution," Journal of Fluid Mechanics, Vol. 85, March 1978, pp. 241-255.